USE OF GANGUE KAOLIN FROM COAL DEPOSITS IN SYNTHETIC ZEOLITE PRODUCTION

A THESIS SUBMITTED TO
THE GRADUATE SCHOOL OF NATURAL AND APPLIED SCIENCES
OF
MIDDLE EAST TECHNICAL UNIVERSITY

BY

BURAK TEMEL KUTLU

IN PARTIAL FULFILLMENT OF THE REQUIREMENTS
FOR
THE DEGREE OF MASTER OF SCIENCE
IN
GEOLOGICAL ENGINEERING

AUGUST 2022

Approval of the thesis:

USE OF GANGUE KAOLINS FROM COAL DEPOSITS IN SYNTHETIC ZEOLITE PRODUCTION

submitted by **BURAK TEMEL KUTLU** in partial fulfillment of the requirements for the degree of **Master of Science** i**n Geological Engineering, Middle East Technical University** by,

Prof. Dr. Halil Kalıpçılar
Dean, Graduate School of **Natural and Applied Sciences** _____

Prof. Dr. Erdin Bozkurt
Head of the Department, **Geological Engineering Dept.** _____

Assoc. Prof. Dr. Fatma Toksoy Köksal
Supervisor, **Geological Engineering Dept., METU** _____

Prof. Dr. Burcu Akata Kurç
Co-Supervisor, **Micro and Nanotechnology Dept., METU** _____

Examining Committee Members:

Prof. Dr. Semih Gürsu
Dept. of Geological Eng., Muğla Sıtkı Koçman University _____

Assoc. Prof. Dr. Fatma Toksoy Köksal
Dept. of Geological Eng., METU _____

Assoc. Prof. Dr. Hüseyin Evren Çubukçu
Dept. of Geological Eng., Hacettepe University _____

Assoc. Prof. Dr. Kaan Sayıt
Dept. of Geological Eng., METU _____

Asst. Prof. Ali İmer
Dept. of Geological Eng., METU _____

Date: ...

I hereby declare that all information in this document has been obtained and presented in accordance with academic rules and ethical conduct. I also declare that, as required by these rules and conduct, I have fully cited and referenced all material and results that are not original to this work.

Name Last name : Burak Temel Kutlu

Signature :

ABSTRACT

USE OF GANGUE KAOLINS FROM COAL DEPOSITS IN SYNTHETIC ZEOLITE PRODUCTION

Kutlu, Burak Temel
Master of Science, Geological Engineering
Supervisor: Assoc. Prof. Dr. Fatma Toksoy Köksal
Co-Supervisor: Prof. Dr. Burcu Akata Kurç

August 2022, 119 pages

Kaolin is a mineral with industrial value and can be used as a raw material in different areas. In most uses, pure quality kaolin is required. However, not all the kaolin occurrences are pure as much as needed and additional processes are applied before use. Nevertheless, some occurrences are accepted as gangue material due to their poor quality and low reserve. Kaolin-rich layers are widespread in coal deposits, but their quality is low. The presence of clay-rich layers with kaolin content in coal deposits is accepted as a problem in coal mines worldwide. In Turkey, it is also a common problem.

Zeolite is another widely used and commercially valuable industrial raw material, with applications in desiccants, molecular sieves, catalysts, water softeners, and warm mix asphalt additives. However, natural zeolites are limited in purity, color, quality of the zeolite crystals, and reserve, and synthetic ones are produced to use in end products. In the production of synthetic zeolite like zeolite 4A, kaolin is a unique source due to its similar silicon and aluminum contents, and structures. Even the

economically valuable kaolin used for zeolite production is generally pre-treated to have unique high quality. This brings an additional expense in production.

In this study, samples from kaolin-rich clay layers that are in assemblage with coal layers within the Thrace basin of Turkey and accepted as gangue material in coal mines were tested to synthesize zeolite 4A. The samples are composed of montmorillonite and illite as well. Three different activation methods were applied to the samples for the first time, and the synthesis of zeolites was successfully fulfilled.

The study showed that commercially invaluable, clay and kaolin-rich gangue from coal deposits within the Thrace region of Turkey can be converted into zeolites, as a value-added product for the market which can be used in various applications in industry. In that way, the wastes that are considered gangue minerals from coal mines could be aimed to be brought back into the economy.

Keywords: Kaolin, Zeolite, Synthesis, Gangue, Applications

ÖZ

KÖMÜR YATAKLARINDAKİ GANG KAOLİNLERİN SENTETİK ZEOLİT ÜRETİMİNDE KULLANIMI

Kutlu, Burak Temel
Yüksek Lisans, Jeoloji Mühendisliği
Tez Yöneticisi: Doç. Dr. Fatma Toksoy Köksal
Ortak Tez Yöneticisi: Prof. Dr. Burcu Akata Kurç

Ağustos 2022, 119 sayfa

Kaolin, endüstriyel değeri olan ve farklı alanlarda hammadde olarak kullanılabilen bir mineraldir. Kullanım alanlarının çoğunda saf ve kaliteli kaolin gereklidir. Ancak tüm kaolin oluşumları gerektiği kadar saf değildir ve kullanımdan önce ek işlemler uygulanır. Bununla birlikte, bazı oluşumlar düşük kalite ve rezerv nedeniyle gang malzemesi olarak kabul edilmektedir. Kömür yataklarında kaolince zengin katmanlar yaygındır, ancak kaliteleri düşüktür. Kömür yataklarında kaolin içerikli kilce zengin tabakaların varlığı, dünya çapında kömür madenlerinde bir sorun olarak kabul edilmektedir ve bu sorun Türkiye'de de yaygındır.

Zeolit, kurutucular, moleküler elekler, katalizörler, su yumuşatıcılar ve sıcak karışım asfalt katkı maddelerindeki uygulamalarla yaygın olarak kullanılan ve ticari olarak değerli bir başka endüstriyel hammaddedir. Ancak doğal zeolitlerin saflığı, rengi, zeolit kristallerinin kalitesi ve rezervi sınırlıdır ve nihai ürünlerde kullanılmak üzere sentetik olanlar üretilir. Zeolit 4A gibi sentetik zeolit üretiminde kaolin, benzer silikon ve alüminyum içerikleri ve yapıları nedeniyle eşsiz bir kaynaktır. Zeolit üretimi için kullanılan ekonomik açıdan değerli kaolin bile,

benzersiz yüksek kaliteye sahip olması için genellikle ön işleme tabi tutulur. Bu da üretimde ek bir masrafı beraberinde getirmektedir.

Bu çalışmada, Türkiye Trakya havzasında kömür tabakaları ile birleşen ve kömür madenlerinde gang malzemesi olarak kabul edilen kaolince zengin kil tabakalarından alınan numunelerin zeolit 4A sentezlenmesi için test edilmiştir. Örneklerde montmorillonit ve illitte bulunmaktadır. Örneklere ilk kez üç farklı aktivasyon yöntemi uygulanmış ve zeolitlerin sentezi başarıyla gerçekleştirilmiştir.

Bu çalışma, Türkiye'nin Trakya bölgesindeki kömür yataklarından elde edilen ticari açıdan değersiz, kil ve kaolince zengin gang malzemenin, endüstride çeşitli uygulamalarda kullanılabilecek, pazar için katma değerli bir ürün olan zeolite dönüştürülebileceğini göstermiştir. Böylece kömür madenlerinden çıkanve gang minerali sayılan atıkların ekonomiye kazandırılması hedeflenmektedir.

Anahtar Kelimeler: Kaolin, Zeolit, Sentez, Gang, Uygulama

To Miracles

ACKNOWLEDGMENTS

I wish to express my greatest gratitude to my supervisor Associate Professor Doctor Fatma Toksoy Köksal, and co-supervisor Professor Doctor Burcu Akata Kurç for their guidance throughout the research and during the preparation and writing of this work.

I would like to extend my gratitude to my beloved parents Nilgün Caner Kutlu, and Mahmut Kutlu, and my beloved grandparents Nebahat Parlatan Caner, and Temel Caner for their endless support during my studentship.

I would like to recognize the assistance and patience I received from my friends Ali Güzel, and Pelin Paşabeyoğlu from METU Central Laboratory during my studies, and I'm deeply indebted to Salih Kaan Kirdeciler for his critical support and close friendship.

My deepest and special thanks to Professor Doctor Aydan Erkmen for giving me the spirit to continue to pursue my life purpose.

The jungler friends of mine, Zühtü Can Soysal, Linda Barış, Esen Özyurt, and Tunç Güven Kaya are gratefully acknowledged. I would like to thank the close friends of mine, Pelin Akça, Muhteşem Akif Korkmaz, Özgün Güzel, Burak Fidancı, Berk Nezir Gün, Marat Magomedov, Alican Arkan, Deniz Vidinli, Deniz Küçüközdemir, Cenk Özkurt, Şükrü Botan Işık, Alişan Balkoca, Arman Besler, Akın Çil, Devin Aykasım, Gencehan Topsakal, Ayhan Üsküdar, Duygu Kuzyaka, Süleyman Şener Akın, İbrahim Uluçay, Serkan Ertuş, Özge Ertuş, Fırat Timur, Ogün Demir, and Erman Kaya.

This work is partially funded by the Scientific and Technological Research Council of Turkey under grant number METU DAP_309-2018-2729, and TÜBİTAK 118M631.

TABLE OF CONTENTS

LIST OF TABLES

TABLES

LIST OF FIGURES

FIGURES

LIST OF ABBREVIATIONS

ABBREVIATIONS

Ilt: Illite

Kln: Kaolin

C-Kln: Calcined Kaolin

Smc: Smectite

Qtz: Quartz

ZA: Zeolite 4A

ZP: Zeolite P

ZX: Zeolite 13X

CHAPTER 1

INTRODUCTION

Coal is one of the most common energy sources for civilizations for centuries. With the advances in technology, more coal mines are opened in recent years worldwide. According to the studies done by the Turkish Coal Association (TKİ), it is estimated in recent investigations that there are 1.138 billion tonnes of coal in the Thrace region of Turkey. Although the coal-bearing basins mostly occurred in the Paleozoic (Oskay et al., 2013) and Cenozoic (Toprak, 2009) eras, the Mesozoic era coal formation is also available in the country (Oskay et al., 2013). In the Cenozoic era, the Eocene deposits have a higher value industrially than the Miocene and Pliocene coal deposits, however, the Eocene deposits are found less in the country (Oskay et al., 2013).

The coal deposits within the Thrace basin, Oligocene-Miocene in age (Şengüler, 1982), are dominated by clastic sedimentary units intercalating with coal as investigated in the other coal deposits in the world. The sedimentary layers that contain coal show different thicknesses, they are thinner at the edges of the Thrace region and the coal of that thin sedimentary region is closer to the surface, while the sedimentary layers are thicker at the center of the region but the coal in those layers are found at relatively greater depths (Kantarcı, 2017).

Clay intercalations of sedimentary depositions are common in coal mines in the Thrace basin like other coal deposits in the country. These kinds of clay-rich intercalations are commonly kaolin abundant as inferred from coal beds within different geological environments (Dill et al., 2008). These clay-rich intercalations are usually considered gangue material and are mostly used as waste-filling materials and dumped into the sea. The kaolin-rich clay samples used in this study are from this type of waste material and its economic recyclability has been investigated.

In industry, kaolin is frequently used in the production of ceramic, paper, zeolite, etc. However, kaolins found near coal mines are considered gangue material due to the impurities such as heavy metal contents like Fe_2O_3 and quartz that they contain and are accepted as waste in coal mining areas (Liu et al., 2017). The solid waste discharged from the coal mining and washing operation is known as gangue (Ma et al., 2019). Thus, there is a high potential for kaolin-rich gangue material in the coal deposit areas.

In this study, the usability of gangue kaolin from the coal beds within the Thrace basin was investigated in the production of synthetic zeolite having many industrial uses. To understand the usability, zeolite 4A synthesis from the kaolin-rich gangue samples with different methods was carried out. At the beginning of the study, four different kaolin-rich samples used as raw materials were examined in terms of their chemical and mineral contents using X-ray fluorescence spectroscopy (XRF), X-ray diffraction (XRD), and scanning electron microscopy (SEM). Later, the characterized kaolin-rich samples were treated at high temperatures with two different methods. With the first method, they were heated alone and converted into metakaolin, and then zeolite 4A synthesis was carried out by hydrothermal method by mixing these meta-kaolin samples with laboratory chemicals. With the second method, the kaolin samples were first mixed with laboratory chemicals before heat treatment, and the synthesis of zeolite 4A was carried out by hydrothermal method. The produced zeolites were characterized by XRD and information about their crystal structures was obtained, as well as their particle morphologies were observed by visualizing them with SEM. The zeolite 4A was successfully produced from those

kaolin-rich samples, which are considered waste material due to the high impurities it contains. Besides those impurities, some different clay materials were also observed in the gangue kaolin samples and their effect on the final product was also investigated.

1.1 Purpose and Scope

In this study, the kaolin-rich gangue samples are used as raw material to produce synthetic zeolite 4A in laboratory conditions, and their usability is evaluated in this concern. The possibility of synthetic zeolite 4A production from the kaolin-rich gangue clay materials from coal mines could result regain of this gangue material in industry instead of getting thrown off to the seas. The importance of this objective is to confirm a cheap new raw material for synthesizing an industrially important zeolite 4A that is an essential material used in detergents and asphalt. Despite its common use and need, it is not produced in Turkey and is imported from abroad. The scope is to investigate the possibility of regaining these gangue kaolin samples to the economy.

1.2 Geographic Setting

The kaolin-rich gangue samples are coming from the Thrace region, the northwest part of Turkey. The formation of this gangue kaolin material is with the coal of the region as intercalation material. The gangue kaolin samples used in this study are obtained from coal fields in the Akpınar district of Istanbul (Figure 1.1).

According to the Turkish General Directorate of Mineral Research and Exploration (MTA), the clayey coal of Eyüp - Çiftealan - Kısırmandıra field, which is located at Akpınar district, in the Thrace region has a weight content of 25.6-41% Al_2O_3, and 1-5 % Fe_2O_3% which matches the kaolin samples used in this study (Üzer, 2001), and the coal deposits found in the area formed during the Oligocene period (Oskay et al., 2013; Şengüler, 1982).

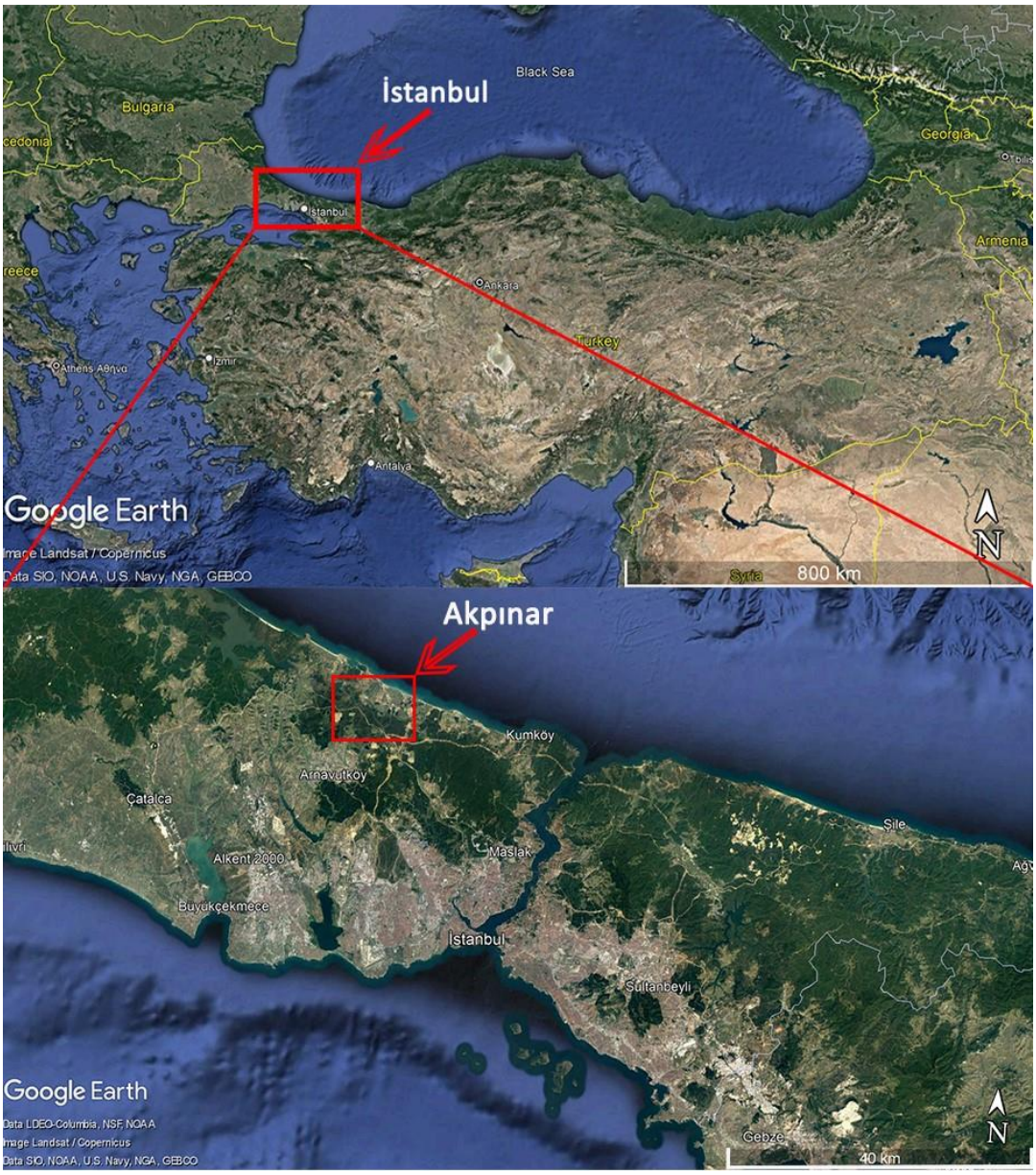

Figure 1.1. Location of İstanbul and Akpınar district

1.3 Methods of Study

In this study, 4 different kaolin-rich coal gangue samples, which are named kaolin samples, were used as a raw material to produce Zeolite 4A crystals with two different methods, which are metakaolinization (Otieno et al., 2019), and one-pot fusion (Kirdeciler & Akata, 2020). Both methods include 4 main steps which are

high temperature heating, aging, reaction, and lastly washing-drying the samples. All the steps were used in the same way in both methods, however, different temperature levels were applied in high temperature heating step. In the metakaolinization, the chemical additives are added to the kaolin samples after the high temperature heat treatment, while in the one-pot fusion the chemical additives are added and mixed with the kaolin samples before heating the materials. Besides that, two different chemicals are used as a sodium source and compared with each other in the one-pot fusion method. Moreover, the effect of high temperature heat treatment with different levels was examined.

CHAPTER 2

LITERATURE REVIEW

In the mining industry, gangue minerals are always encountered. Among these gangue minerals, coal gangue is one of the most which is investigated by scientists. Although it has no industrial value, many studies show that the coal gangue can be used in some applications. Coal gangue is a type of solid waste that is related to the formation of coal, and it is separated from the coal during mining (Li et al., 2021). The coal gangue can be used in brick making, concrete, calcined kaolin, refractory material preparation, filling material, road construction, and mullite production (Hao et al., 2022; Li et al., 2021; Liu et al., 2020; Zhou et al., 2014; Zhu et al., 2021). In the coal gangue, some of the most common materials that can be found are quartz, carbonaceous materials, and clay minerals like kaolinite (Li & Wang, 2019). Several studies are showing that gangue kaolin can be used in different applications. It can be used as a cement replacement in concrete for strengthening the cement compound (Liu & Ling, 2018), a functional filler for rubber to increase mechanical properties (Zhang et al., 2021), and can be used for improving the preparation of coal gangue based geopolymers (Li et al., 2021), producing low-cost adsorption materials (Jin et al., 2022), producing materials for soil remediation (Ge et al., 2022), and producing low-cost zeolite synthesis (Jin et al., 2021). Moreover, if the gangue kaolin is treated and separated from its impurities, it can be used as a coating pigment in paper applications and as a filler in paints, ceramics, and paper (Yildirm et al., 2009).

In this chapter, mineralogical information about kaolin and zeolites is given, including the industrial applications and history of both minerals. Additionally, information about gangue kaolin and its utilization, synthetic zeolites, and the relation between gangue kaolin and synthetic zeolites are also given.

2.1 Kaolin

Kaolin has attracted considerable interest since people started to use it first in the third century BC in China (Adamis et al., 2005). It is a mineral group having a cation-exchange capacity in the classification of clay minerals, which takes its name from the most significant mineral kaolinite, and it indicates the group of four polymorphs of kaolinite (Kloprogge, 2018). If a clay sample contains 85-95% of kaolinite it is called kaolin, however, clay samples having more than 10% kaolinite can also be called kaolin (Adamis et al., 2005). Kaolin group minerals other than kaolinite are dickite, nacrite, and halloysite while kaolin usually includes minerals of quartz, mica, feldspar, montmorillonite, iron oxides, titanium oxides, magnesium oxides, calcium oxides, sulfides and carbonates in their content as impurities (Ramaswamy & Raghavan, 2011; Survey, 2002; Weaver & Pollard, 1973).

The kaolin group minerals are phyllosilicates having a 1:1 layer structure and consist of continuous tetrahedral and octahedral sheets. The tetrahedrons of kaolin are made up of a silicon atom that is linked to four oxygen atoms by sharing three corners to generate an infinite two-dimensional hexagonal mesh pattern. This forms an infinite two-dimensional hexagonal mash pattern. The octahedron consists of an aluminum atom or an empty space and it is coordinated by six oxygen atoms, and it is linked to neighboring octahedrons by sharing edges (Kloprogge, 2018; Velde & Meunier, 2008). Kaolinite type of kaolin is made up of small sheets of triclinic crystals having hexagonal or pseudohexagonal morphology, and the structure of it is a tetrahedral silica sheet alternating with an octahedral alumina sheet (Figure 2.1) (Kloprogge, 2018).

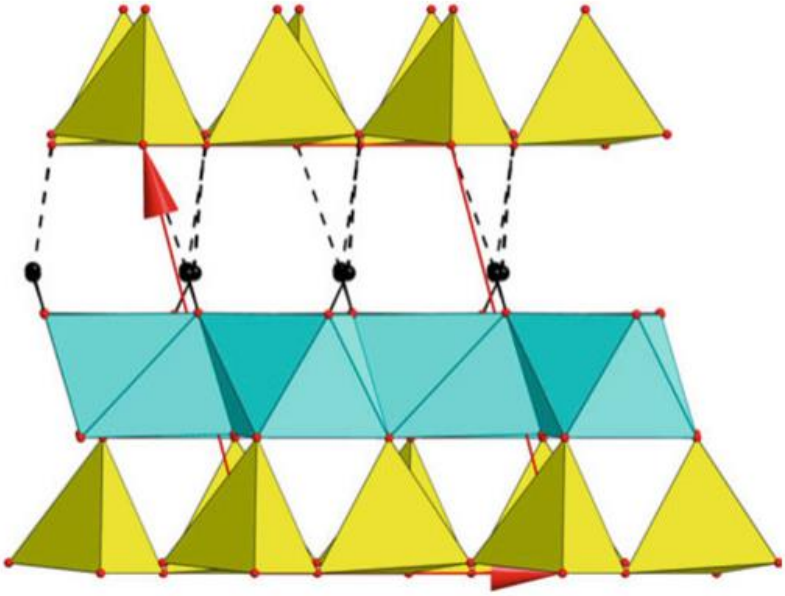

Figure 2.1. Crystal structure of kaolinite, 1:1 layer with the adjacent tetrahedral net on the top (Kloprogge, 2018)

The formation of kaolin can occur mainly in two ways, and the formation of it is called kaolinization. The first way is related to physical effects like crumbling and transformation of parent rocks due to surficial processes. The second way is related to the chemical alteration of the parent rocks due to hydrothermal effects. The kaolin deposits are also categorized as primary deposits and secondary deposits. The primary kaolin deposits are formed by the in-situ minerals, which means the formation occurs where the parent rock is based at. The secondary kaolin deposits are formed during the transportation of the parent rock due to physical effects like wind and water (Bloodworth et al., 1993).

Among these types, the formation of kaolin is mostly related to granitic rocks in which the feldspar in the granitic rock reacts with water and produces kaolinite with the reaction:

$2\ KAlSi_3O_8 + 3\ H_2O = Al_2Si_2O_5(OH)_4 + 4\ SiO_2 + 2\ K(OH)$

K-Feldspar Water Kaolinite Silica Potash

where the formula of kaolin is $Al_2Si_2O_5(OH)_4$. The product of this formation is classified as primary residual deposits (Kloprogge, 2018).

For industrial use, desired kaolin sources should have a minimum amount of impurities like Fe_2O_3 and K_2O in source content, and the quality of kaolin is determined by its Si/Al ratio, whiteness, and fine particle size. Additionally, having lamellar particle shape, soft and non-abrasive texture, and its chemical inertness over a wide range of pH are kaolin's other important properties that determine the area of use. The quality of the raw material is the determining factor defining if this material can be used as it is in that application field or not. Most of these high purity sources are used in industrial applications such as paper, ceramics, porcelain, plastic, synthetic rubber, paint, cosmetics, and pharmaceutical industries and as an adsorbent (Bloodworth et al., 1993; El-Sabbagh et al., 2012; Ibrahim et al., 2012; Roy et al., 2015; Wood, 2021).

2.1.1 Industrial Uses of Kaolin

Kaolin has a wide range of industrial uses. Kaolin's whiteness and fine particle size are the most valuable characteristics of it for its industrial use. The fine particle size of kaolin, which can be less than 2 microns (Bloodworth et al., 1993; Pabst et al., 2000), plays a role in its viscosity, color, abrasiveness, and ease of dispersion. Additionally, having a lamellar particle shape making it opaque, having a soft and non-abrasive texture and its wide range of pH are also some of the important properties of kaolin for industrial use (Bloodworth et al., 1993). The main use of kaolin is for coating paper. Dispersion, viscosity, brightness, whiteness, and smoothness are some of the most important properties which are demanded by the paper industry (Bloodworth et al., 1993; Murray, 2000). For the ceramics and porcelain industry, chemical content is the most important factor, the Fe_2O_3 content of the kaolin is around 0.6-1.5%, TiO_2 content of the source should be between 0.6-1.2%, CaO should be less than 0.8%, and Al_2O_3 should be higher than 30% in weight (Gajic et al., 2014), and the physical properties like color, translucency, resistance to

heat and porosity are also important for the source to be commercially available to use (Wilson & Hart, 2019). The structural characteristics, stability, and high specific area of kaolin make it useful as an adsorbent for purifying wastewater containing sulfate ions (Hudaib, 2021). In the paint, rubber, and plastic industry, kaolin is used as a functional filler with the help of its attributes such as shape, size, and surface properties (Bloodworth et al., 1993). In the paint industry, the high oil absorption of kaolin makes it useful for undercoats and water-based paints (Bloodworth et al., 1993). Kaolin's high covering power and being a good plasticizer provide smoother surfaces and give a better finish and dimensional stability while reducing the cost of producing paper (Bloodworth et al., 1993; Roy et al., 2015). In the rubber industry, the essential properties of kaolin are particle shape, particle-size distribution, and surface properties. These properties can be used to influence the mechanical properties of rubber like tensile strength, elongation at break, hardness, and heat-aging properties (Bloodworth et al., 1993; Wu & Tian, 2013). In pharmaceutical and cosmetics applications, kaolin can be used as an additive ingredient in which, whiteness is the most important property of kaolin when used as a tablet and capsule diluent. The second most important property is its fine particle size which must be between 0.6 and 0.8 micrometers (Hernández et al., 2019).

In nature, kaolin is not always found in an industrially useful quality, and that kind of kaolin is treated as waste material. However, there are ways for making that waste kaolin become an industrially useful material.

2.1.2 Gangue Kaolin and Its Utilization

Kaolin is an abundant mineral worldwide that can be found in both industrially favorable conditions and as a useless material having insignificant properties with impurities which are called gangue kaolin. The solid waste discharged from the coal mining and washing operation is known as gangue (Ma et al., 2019), they are minerals that have no value economically but are a part of ore and cannot be avoided with the ore. The mining of high-quality kaolin is common in the world, while the

gangue kaolin gets thrown away when found as a secondary mineral in the mining of some other materials such as coal. Due to the invaluable source utilization being favorable for eliminating the use or generation of hazardous substances, there is an interest in research for taking the gangue kaolin and making it useful for industrial applications. Kaolinite is the main component of the kaolin mineral, but the impurities like quartz, graphite, iron oxides, and titanium oxides make it a gangue material when those impurities are high in the content of kaolin, and there are some ways to reduce these impurities.

The gravity separation method is one of the methods for purifying kaolin. This method uses the density difference between the impurities and the kaolin. With this method, kaolin can be separated from impurities like carbon, iron, and titanium which results in obtaining purer kaolin having better whiteness (Yaoli et al., 2017).

Magnetic separation is another method that uses the magnetic difference between kaolin and the impurities contained. Almost all kaolin minerals contain small amounts of iron which sometimes cause discoloration. With the magnetic separation method, the impurities in kaolin can be removed without any chemical application which makes it an environment-friendly technique (Iannicelli & Pechin, 1997).

The flotation method is another one for separating the impurities from kaolin. Both chemical and physical differences between kaolin and impurities are used for this method. Impurities like iron, titanium, quartz, and carbon can be separated from kaolin by this method. Although it is an effective method for purifying kaolin, it needs a chemical reagent, which results in an extra cost for the treatment and can cause pollution (Bu et al., 2017; Luz et al., 2000; Mathur, 2002; Yoon et al., 1992).

Some impurities can be specifically dissolved from kaolin by chemical leaching, which is another method for purifying. Sulfuric acid (Panda et al., 2010; Tuncuk et al., 2013; Veglio', 1997), hydrochloric acid (Bhattacharyya & Behera, 2017), and nitric acid (Lima et al., 2018) are commonly used for this application, while oxalic acid (Martínez-Luévanos et al., 2011), sodium dithionite (Gougazeh, 2018) and other reagents can also be used. By this method, usually, iron and titanium impurities are

targeted for purifying. Although chemical leaching is an effective way of dissolving impurities, it is an expensive technique and can cause the dissolution of some important ingredients like aluminum (Panda et al., 2010).

In the synthesis applications, kaolin-rich coal gangue (gangue kaolin) can be used as a raw material with the help of high-temperature heating treatment. The high-temperature heating treatment for kaolin is called metakaolinization. With metakaolinization, the crystal structure of the material is disturbed and becomes amorphous and more reactive. Additionally, gangue kaolin can be used in synthesizing new materials in the laboratory such as synthetic zeolites with metakaolinization (Ge et al., 2022; Jin et al., 2021; Xie et al., 2021).

2.2 Zeolites

Zeolites are crystalline, porous aluminosilicate minerals including water molecules in their structure. Their primary building unit is a three-dimensional TO_4 tetrahedron where T is usually an aluminum (Al^{3+}) or silicon (Si^{4+}) atom which has four oxygen atoms surrounding them to form subunits, and it repeats to form an infinite lattice. They also include alkali elements such as sodium and magnesium. Frameworks are open structures with cations positioned within the material's pores. The cation neutralizes the negative charge of the lattice.

The main framework of zeolites is aluminosilicate tetrahedra, in which the aluminum (Al^{3+}) and silicon (Si^{4+}) are connected by the surrounding oxygen atoms. The bonding of oxygen with aluminum and silicon creates the three-dimensional framework, and the unit blocks are $(AlO_4)^{5-}$ and $(SiO_4)^{4-}$ (Figure 2.2) (Moshoeshoe et al., 2017).

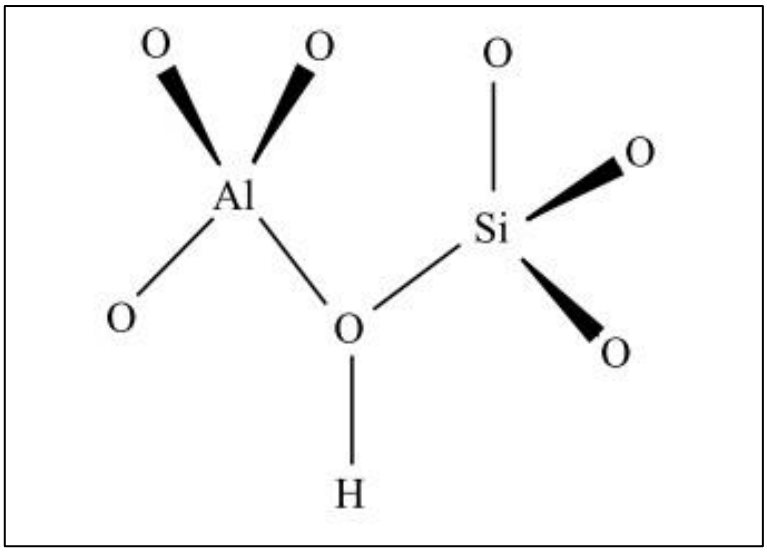

Figure 2.2. The tetrahedral arrangement of zeolites (Moshoeshoe et al., 2017)

The formula of zeolites, in general, is represented as $Me_{y/mn}+[(SiO_2)_x.(AlO_2^-)_y].zH_2O$, where Me mostly represents some alkaline or alkaline earth elements such as K^+, Na^+, Ca^+, Mg^{2+}, Sr^{2+}, Li^+, or Ba^{2+}. Those alkaline elements balance the negative charge created by the differences in formal valency between $(AlO_4)^{5-}$ and $(SiO_4)^{4-}$ when the Si^{4+} and Al^{3+} are substituted (Figure 2.3) (Moshoeshoe et al., 2017). The presence of these neutralizing cations within the framework can influence the diffusion, adsorption, and catalytic properties of zeolites. These properties make zeolites have sensing behavior where the number of cations and hydrophilicity of the material are controlled by the Si/Al ratio so that zeolites can be used in selective adsorption applications (Y. Zheng et al., 2012).

The porous structure of the zeolites is one of the most important properties of this unique material since it increases enormously the surface area which results in the usage of zeolites in catalysis fields. Moreover, the ordered and structured pores, introduce zeolites' important properties of selective gas adsorption and molecular sieving.

The framework structure of zeolites includes primary and secondary building units. The primary building units are common in all zeolites which are corner-sharing TO_4 tetrahedra having 4-connected three-dimensional frameworks (Čejka et al., 2007).

The framework structure also contains more complex units like single rings, double rings, and polyhedra which are called secondary building units. Furthermore, with the linking of the secondary building units in a specific way, more complex units like channels, cages, chains, and sheets are formed which are called composite building units (Figure 2.4) (Moshoeshoe et al., 2017). The specific arrangement of the building units creates different types of a framework which results in different types of zeolites (Figure 2.4). According to the International Zeolite Association (IZA), there are 237 main types of frameworks of zeolites (Figure 2.5).

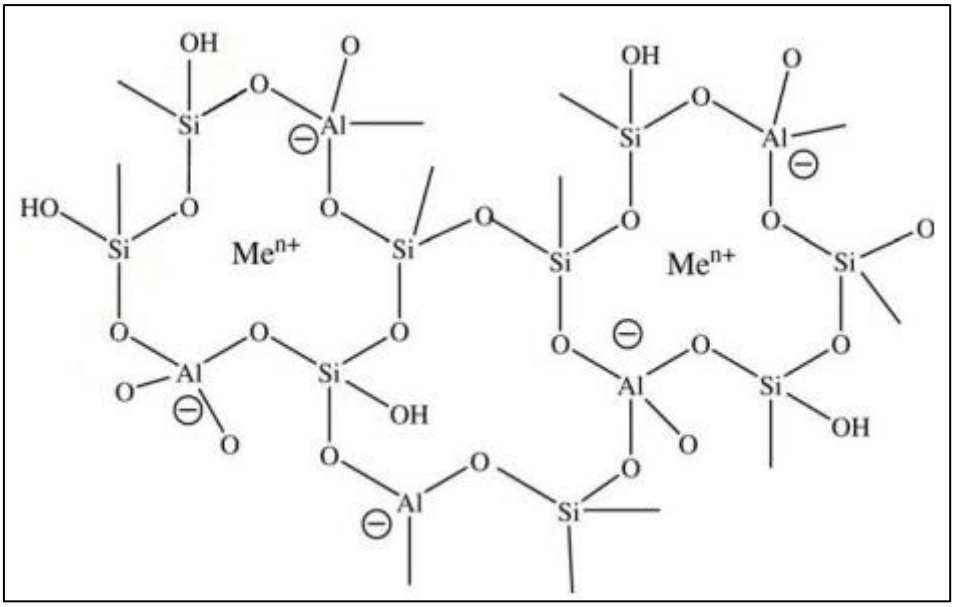

Figure 2.3. The framework structure of zeolites, Me^{n+} represents cations (Moshoeshoe et al., 2017)

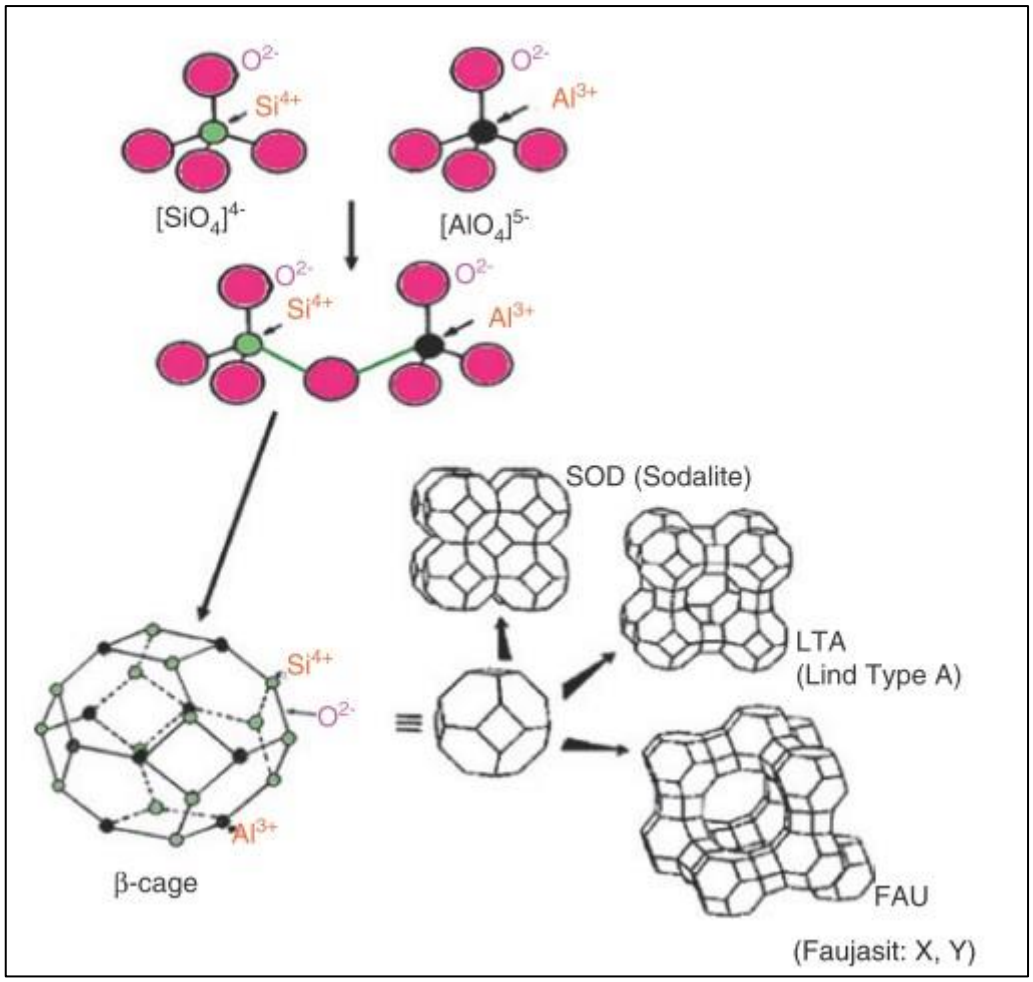

Figure 2.4. Examples of secondary building units of zeolites (Ahmed, 2014)

Zeolites are known for their ability to act as catalysts, molecular sieves, adsorbents, and ion exchangers and can be applied in many fields related to pollution control, wastewater treatment, gas purification, agriculture, and others (Čejka et al., 2007). While zeolites can be synthesized in a laboratory, they can be found as natural sources too, and there are some differences between natural and synthetic zeolites which are important for their area of use.

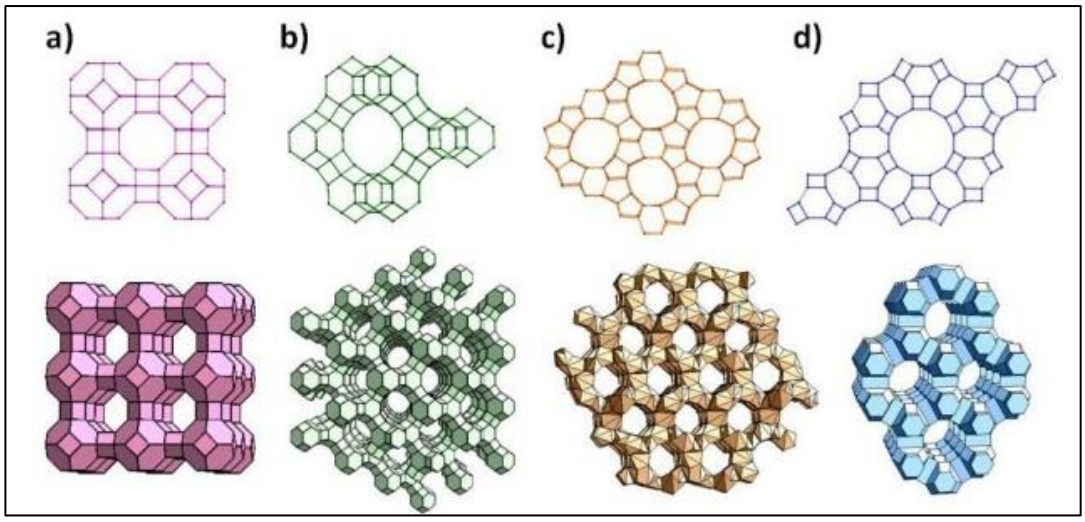

Figure 2.5. Examples of different frameworks of zeolites, a) Zeolite A, b) Zeolite Y, c) Zeolite L, d) ZSM-5 zeolite (Y. Zheng et al., 2012)

2.2.1 History and Industrial Uses of Zeolite

Zeolites are first named by a Swedish scientist Axel F. Cronstedt in 1796 from the combination of Greek words “zeo” meaning to boil, and “lithos” meaning stone, which means “boiling stone” because he realized that when he heated the stone, it created vapor by losing its water (Čejka et al., 2007). After his discovery, natural zeolites took scientists' attention and new types of natural zeolites were discovered such as stilbite, chabazite, analcime, harmotome, and laumontite until 1785. The discoveries of new species of zeolites continued, while some other properties of zeolites started to take attention of the scientists. In the 1800s, the adsorption and ion exchange capacity of zeolites were the point of interest for scientists. After the invention of XRD in the 1930s, studies about zeolites enhanced in quality (Colella & Wise, 2014; Yang, 2003). The first attempt of synthesizing zeolites dates to 1862 done by St. Claire Deville, and in the 1940s, Richard M. Barrer started the first systematic studies of zeolites, but the most influential early reported synthesis of zeolites comes from R. M. Milton and D. W. Breck (Reed & Breck, 1956) in the 1950s (Yang, 2003; Zimmermann & Haranczyk, 2016). Since then, studies about

synthesizing zeolites advanced, and more detailed information about synthetic zeolites achieved.

The main industrial uses of zeolites are catalysis, adsorption, and ion exchange. Their large surface area, unique pore size, crystallinity, and thermal stability are properties of them for being catalysts in petroleum cracking, isomerization, and alkylation reactions (Moshoeshoe et al., 2017). Additionally, they are used for the production of fine chemicals, dyestuffs, detergents, and scents (Cardoso et al., 2015; Kithome et al., 1999; Rožić et al., 2000). Adsorption is another main use of zeolites which can be used to adsorb a variety of materials. Zeolites are good adsorbents for molecules such as H_2O, NH_3, H_2S, NO, NO_2, SO_2, and CO_2 (Moshoeshoe et al., 2017; Roque-Malherbe, 2000). This property gives zeolites use in applications like drying, purification, and separation. Water purification is one of the most common uses of zeolites with its adsorption property. They can be used in the treatment of natural, industrial, agricultural, municipal, and even nuclear wastewater. Wastewaters may contain metallic ions such as stibium, chromium, copper, lead, zinc, cobalt, and nickel and can be purified with the help of zeolites (Li et al., 2015; Visa, 2016). Zeolites are also used for gas separations due to their adsorption capacity with other properties like their uniform system of pores with molecule-sized dimensions, high porosity, and good thermal and chemical stability (Caro et al., 2000; Kosinov et al., 2016). They can be used in the separation of H_2O, CO_2, CH_4, and N_2 in industrial applications like natural gas purification and CO_2 capture (Choi & Hong, 2021; Q. Shi, 2021). The other main use of zeolites comes from their ion-exchange capacity. The hydrated cations in the zeolite are weakly bonded to the framework and can be replaced with other cations when in an aqueous media. This ion-exchange capacity of zeolites makes them mostly used in water softening devices and detergents (Koohsaryan et al., 2020; Rozhkovskaya et al., 2021), but it is also used in other applications like antibacterial applications, medicine, heavy metal removal and wastewater treatments (Morante-Carballo et al., 2021; Torkian et al., 2021). Other than that, zeolites are used in agriculture, horticulture, aquaculture, household odor control, and pet odor control applications.

2.2.2 Synthetic Zeolites

Zeolite synthesis began in the 1940s, and because of how important they are in so many industries, it has continued with growing interest. The synthesized zeolites are mostly used in catalysis, adsorption, and separation processes, and now there are many new applications for synthetic zeolites like in chemical sensors, magnetism, medicine, and electronics (Čejka et al., 2007). With continuous synthesis, there are many new zeolites with new frameworks, compositions, and properties that have evolved. New methods for the synthesis of zeolites are also evolved with continuous work. Hydrothermal synthesis is the most common synthesis method for zeolite synthesis since the beginning but the ultrasonic method (Liu et al., 2020; Yin et al., 2019) and vapor-phase-transport method (Kasneryk et al., n.d.) are also used in recent years. The method used in this study for zeolite synthesis is the hydrothermal method.

Synthesized zeolites are more valuable in the industry than natural ones for some reason. The framework structure of zeolites is one of the most important properties. While natural zeolites can form less than 50 frameworks (Armbruster & Gunter, 2001), synthetic zeolites can reach more than 250 different main frameworks according to International Zeolite Association (IZA). The other advantages of synthetic zeolites are their pure content, higher adsorption capacity for heavy metal ions (eg. lead, zinc, copper), larger pore size, capability to adjust silicon aluminum ratio during synthesis which exhibits a stronger sorption capacity, and having more homogenous surface characteristics (Krol, 2020).

Some of the most common studies on synthetic zeolites include zeolite 4A, zeolite 13X and zeolite P due to their industrial value.

Zeolite 4A is a member of the LTA group zeolites which are mostly used as industrial desiccants (Dyer, 2006; Jaramillo & Chandross, 2004). It has a general formula of $Na_{12}[(AlO_2)_{12}(SiO_2)_{12}]$-$27H_2O$ (Collins et al., 2020) having Si/Al ratio close to 1 (Rahman et al., 2018), and takes its name from having 4 angstrom pore size. They

exhibit strong preferential adsorption of water, as well as several small molecules including oxygen, nitrogen, carbon dioxide and others. Zeolite 4A is an aluminosilicate zeolite with a cubic morphology, and they have a continuous three-dimensional network of channels (Jaramillo & Chandross, 2004). Scanning electron microscopy (SEM) and X-ray diffractogram (XRD) of a reference zeolite 4A is shown in Figure 2.6.

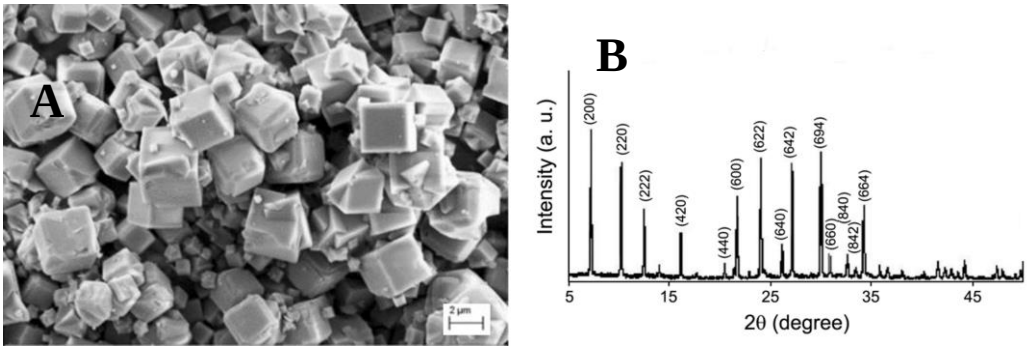

Figure 2.6. Reference zeolite 4A. A) SEM image (Cheng et al., 2020), B) X-ray diffractogram (Zamani et al., 2013)

Zeolite 13X is another industrially valuable aluminosilicate zeolite type. It has a Si/Al ratio of 1.0 to 1.4 (Dyer, 2006), and a chemical formula of Na_2O-Al_2O_3-2.5SiO_2-6H_2O (Y. Shi et al., 2022). It also has regular pores like zeolite 4A which gives it a good ion-exchange and adsorption properties (Cavenati et al., 2004). Zeolite 13X have different morphology than zeolite 4A and have larger pore size of nearly 9 angstroms. It has a selectivity for heavy metals such as lead, cadmium, and copper. The ion-exchange property, selectivity for lead, and regular pore structure makes zeolite 13X a good solid adsorption material (Y. Shi et al., 2022). SEM and XRD images of a reference zeolite 13X are shown in Figure 2.7.

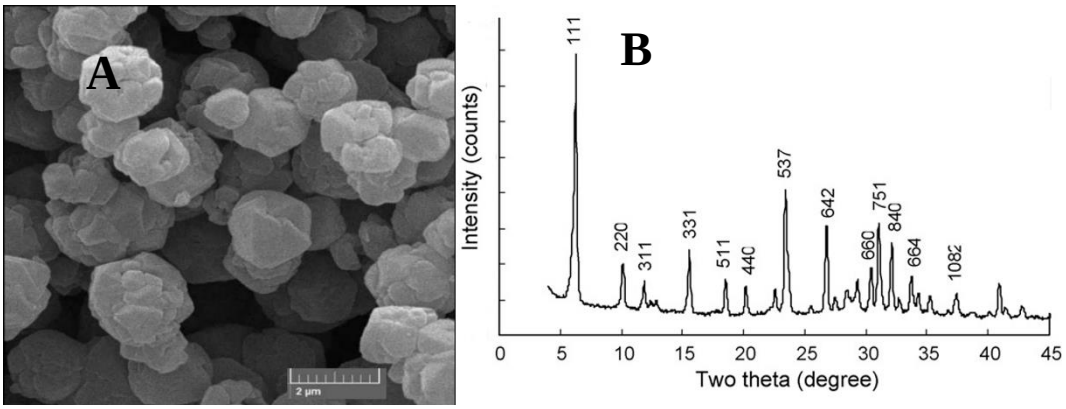

Figure 2.7. Reference zeolite 13X. A) SEM image (Farideh & Mansoor, 2015), B) X-ray diffractogram (H. Zheng et al., 2008)

Zeolite P is not as popular as zeolite 4A and 13X, however it also has industrial uses, such as detergency builders, and gas separation applications (Brown et al., 1989; Novembre et al., 2021). It has a Si/Al ratio of 0.9 to 1.33 (Brown et al., 1989), and the general chemical formula of $M_{2/n}O.Al_2O_3.1.80–5.00SiO_2.5H_2O$ where M is a n-valent cation, such as an alkali metal (Novembre et al., 2021). It has a high calcium exchange capacity (Meftah et al., 2009). They have a tetragonally distorted cubic crystal structure. SEM and XRD images of a reference zeolite P is given in Figure 2.8.

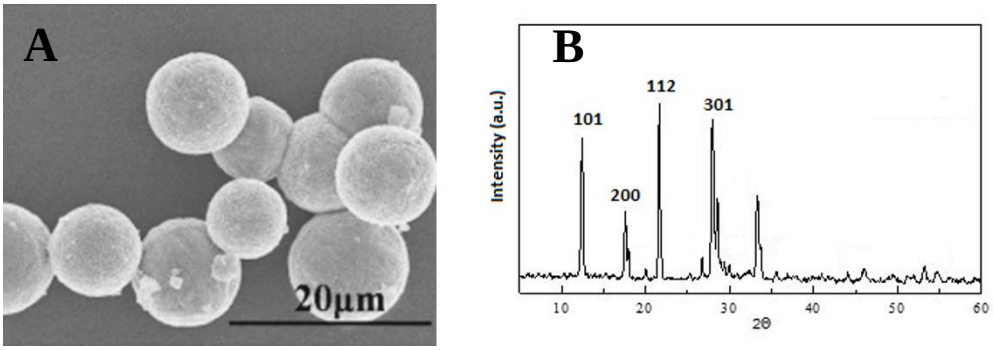

Figure 2.8. Reference zeolite P. A) SEM image (P. Wang et al., 2019), B) X-ray diffractogram (Mostafa et al., 2015)

2.3 Synthetic Zeolite and Kaolin

There are different types of synthetic zeolites as mentioned in the previous section. Zeolite 4A is one of the synthetic types, which is one of the most demanded in industrial uses.

Zeolite 4A is a synthetic zeolite type commonly produced in a laboratory environment by using pure laboratory chemicals. Hydrothermal synthesis is the main method type for producing zeolite 4A by using silicon, aluminum and sodium sources (Čejka et al., 2007; Reed & Breck, 1956). The syntheses done by pure laboratory chemicals give expected results if the required conditions are provided in experiments, however, the cost of using pure chemicals for that kind of guaranteed experiment is usually high. Consequently, scientists have always been in search of alternative raw materials that can be used in laboratory experiments. For zeolite synthesis, there are different raw materials used for many years instead of only using pure laboratory chemicals. There are some commonly used cheap raw materials for zeolite syntheses for many years including kaolin (Kirdeciler & Akata, 2020; Ugal et al., 2010), bentonite (Abukhadra et al., 2019; Hamidi et al., 2021), montmorillonite (Mackinnon et al., 2010), fly ash (Akın et al., 2021; Lin & Chen, 2021), and halloysite (Meftah et al., 2017; Rubtsova et al., 2022).

Kaolin, as a clay mineral, is widely used in producing synthetic zeolites. Having a Si/Al ratio of 1 makes kaolin useful for synthesizing some zeolite types like zeolite 4A (Ayele et al., 2015; Ayele, Pérez-Pariente, Chebude, & Díaz, 2016), zeolite 13X, and zeolite P (Lin et al., 2004). Kaolin has a framework structure of a 1:1 ratio having one layer of silica tetrahedron and one layer of alumina octahedron. This structure needs to be disrupted for the silicon and aluminum components to be integrated into the structure of the created zeolite, to make kaolin useful for zeolite synthesis. High-temperature heating, usually between 600 - 1100 ℃, is a way that is commonly

encountered in the literature for breaking the structure of kaolin so that its silicon and aluminum ingredients of it can be added to the synthesis as raw materials (Kovo et al., 2009). While kaolin can be heated alone to get an amorphous state for synthesis, it can also be heated in a mixture of laboratory chemicals (Kirdeciler & Akata, 2020). In brief, kaolin should be heated first to use it as a raw material.

CHAPTER 3

GEOLOGY OF THE THRACE BASIN, TURKEY

The Thrace Basin of Turkey is an area that geologists studied many times due to its coal potential. While having coal and hydrocarbons, it also includes several industrial mineral mines and metallic mines which makes it a more attractive area. The location of Thrace Basin is in the Marmara Region of Turkey, and it is also called Ergene Basin taking its name from the river in the basin. This basin contains the region which is from the Marmara Region to Europe, having Istanbul at its east and boundaries of Greece and Bulgaria at its west, the Black Sea at its north, and the Marmara Sea at its south (Figure 3.1).

The stratigraphy of the area includes claystone, pebblestone, sandstone, siltstone, mudstone, limestone, marl, shale, lignite, tuff, and agglomerate (Şengüler, 1982). Ophiolithic mélange creates the basement rock of the basin. Eocene deposits follow that ophiolitic mélange with sandstone, siltstone, and silicified tuff called Gaziköy Formation. It is followed by Keşan Formation which includes mostly sandstone, marl, and shale, then continue with Soğucak Formation having micritic and reef limestones, then followed by Ceylan Formation which includes tuff intercalated shale, sandstone, and clayey limestone (Figure 3.2).

After the Eocene deposits, Oligocene deposits continue with the Mezardere Formation having shale, marl, and tuff. Above that, Osmancık Formation stands there with sandstone, pebble stone, limestone, and lignite bands and continues with Danişmen Formation which is defined by Kasar et al. (1983) with claystone, sandstone, pebble stone, tuff, and lignite (Siyako 2005) (Figure 3.2).

The formations continue with the Miocene deposits following the deposition of Oligocene units. At the bottom of the Miocene Deposits, there are Hisarlıdağ Volcanites. Above them, there is Çanakkale Formation with claystone, sandstone,

and siltstone respectively and the Çekmece formation with mudstone, sandstone, marl, and limestone respectively, and lastly Ergene Formation with sandstone, claystone, and siltstone lithology respectively. Pliocene and Quaternary deposits come afterward (Figure 3.2).

The Pliocene Deposits are considered pebblestone, sandstone, and claystone and are called the Thrace Formation. Quaternary Deposits are above all of them with carbonate sandstone and pebble stones (Figure 3.2).

Several studies showed that the main coal formation in the Thrace region is formed during the late Oligocene in Danişmen Formation even in different parts of the region (Çelik et al., 2017; Demir et al., 2012; Ediger et al., 2014; Erarslan et al., 2014; Erarslan & Örgün, 2017; Karayigit et al., 2021). In the region, there occurred a regional regression and resulted in a deltaic environment covering the area at the beginning of the Oligocene after the transgression in the Eocene (Çelik et al., 2017; Erarslan & Örgün, 2017).

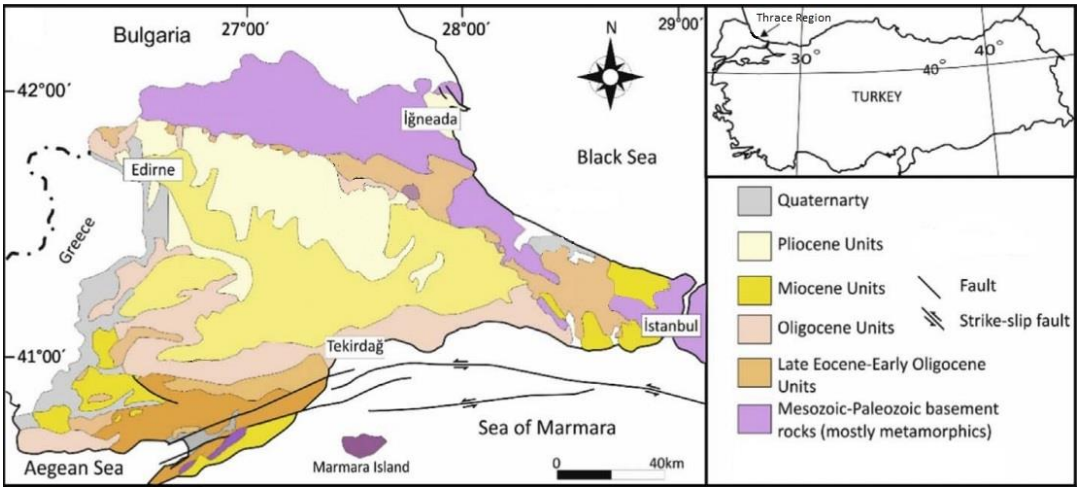

Figure 3.1. Simplified geological map of the Thrace Region (Çelik et al., 2017)

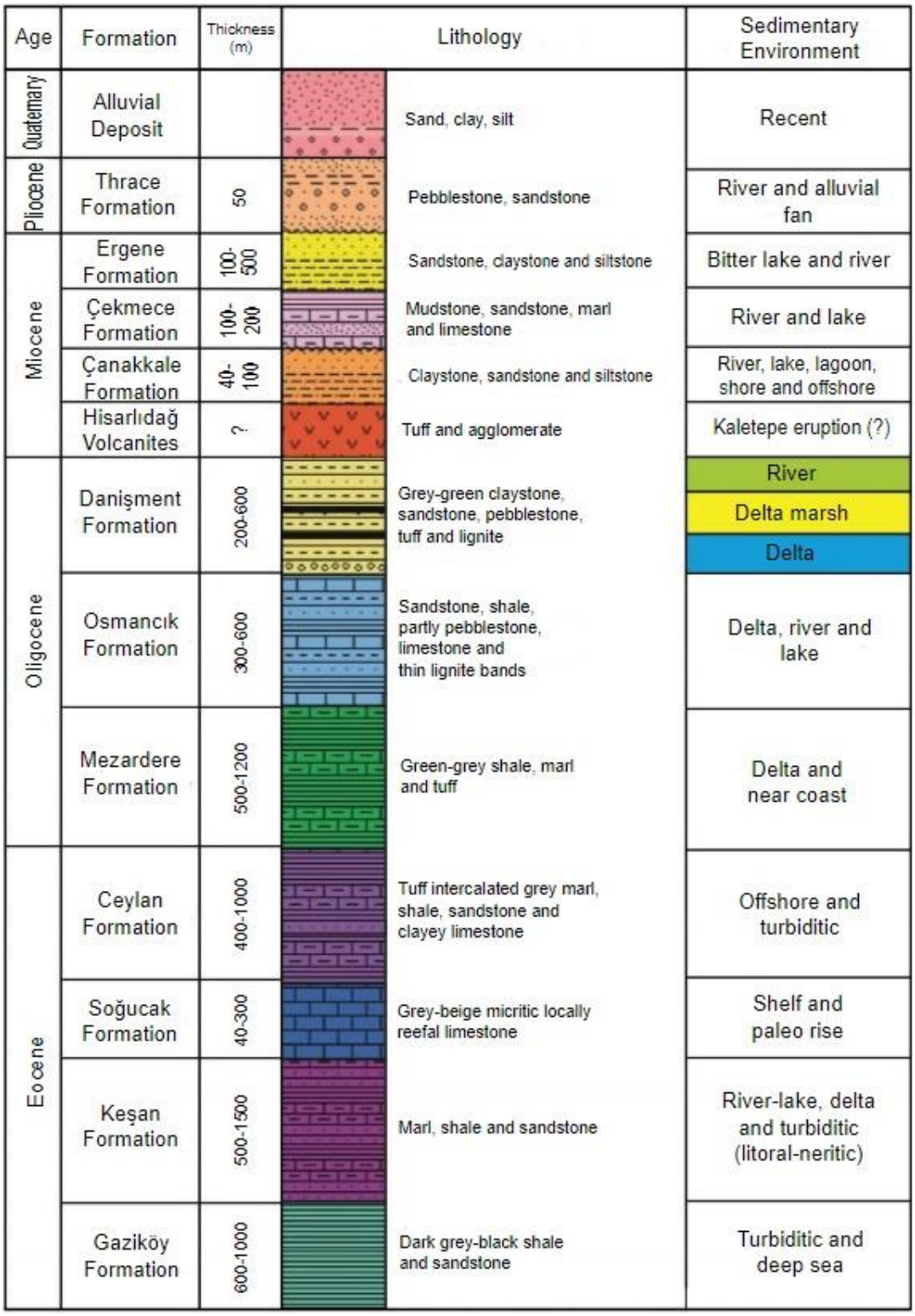

Figure 3.2. Generalized stratigraphic section of Thrace Region (Şengüler, 1982)

In the area, where the samples of this study were provided, Danişmen Formation remains in between Ceylan and Ergene Formations (Figure 3.3). Danişmen Formation is composed of interlaminated claystone, shale, sandstone, and pebblestone at the lower parts. These sequences are followed by plant debris-bearing claystone and coal seams with variable thicknesses having the average thickness of 5.5 meters (Perinçek et al., 2015; Tuncalı, 2002). On top of the coal-bearing sequence, alternation of shale and siltstone are deposited (Atalay, 2002; Çelik et al., 2017) (Figure 3.3). The coal of Danişmen Formation contains high amounts of sulfur and boron (Çelik et al., 2017; Erarslan & Örgün, 2017).

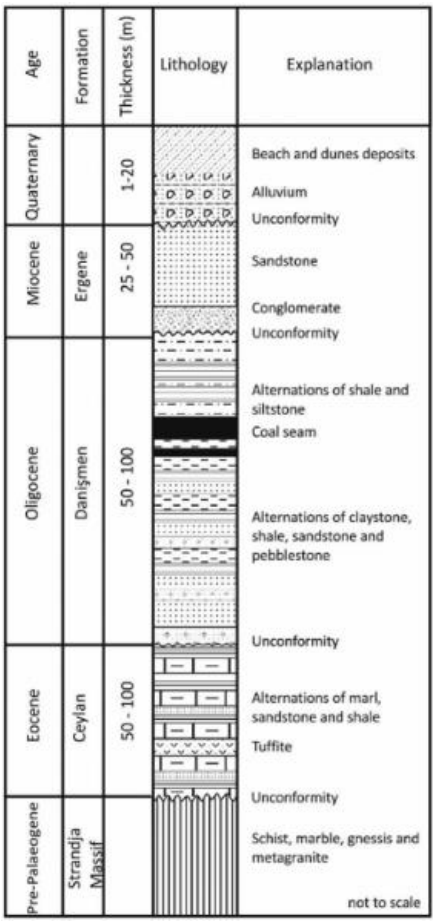

Figure 3.3. Stratigraphy of the coal deposits area (Çelik et al., 2017)

The coal in the area is dark colored and brittle. Most of the coal is xylite-rich indicating the presence of liquid hydrocarbon in crude coal (Çelik et al., 2017). The

ash yield of the coal is low, 13.6% on average, and variable total sulfur content is 2.2% on average on a dry basis, however, it can reach up to 3.7% (Çelik et al., 2017).

In some places, coal beds contain clay and sand bands that are thinner than 1 millimeter and fossilized wood fragments. The coal is in between sandy claystone with intercalations mainly composed of sandstone and claystone (Çelik et al., 2017). In the bulk coal and inorganic sediments, quartz, pyrite, and clay minerals such as illite, smectite, and kaolinite are found, and concentrations of hazardous trace elements are generally low (Çelik et al., 2017). In coal, pyrite is the most common mineral phase, while quartz and clay minerals are enormously present in all sediments. The dominance of clay minerals in the sediments may indicate that clay minerals were transported during flood events as suspended loads by a fluvial system from peripheral rocks. Additionally, kaolinized feldspars found in coal samples might indicate that kaolinites are partly of authigenic origin (Çelik et al., 2017).

The samples called as gangue kaolin used in this study are from the intercalated sediments within this coal (Figure 3.4). All the samples are fine grained, brittle, and moderately weak clay-rich sediments. They are massive rock samples, and silt sized grains are observable in hand specimens. However, their color differs. Sample kaolin 1 (Figure 3.5) is whitish and it has the lightest color in all specimens. Sample kaolin 2 (Figure 3.5) is gray colored and it has the darkest color in all samples. Kaolin 3 (Figure 3.6) also has a light color but it is more yellowish than kaolin 1. Lastly, kaolin 4 (Figure 3.6) has a brownish-yellowish color.

The mineralogy and more detailed investigation of the samples are explained in section 5.1.

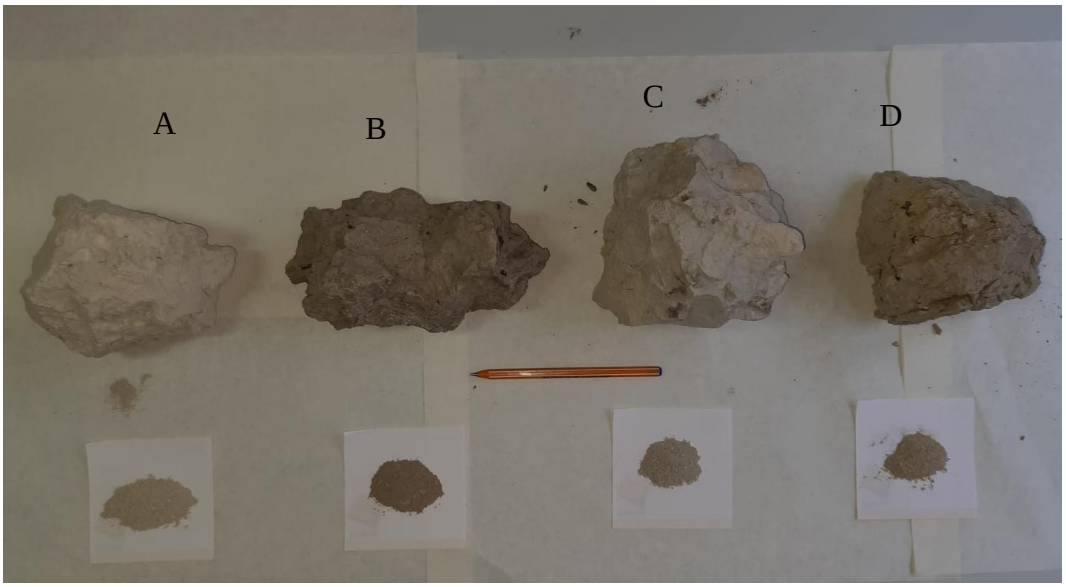

Figure 3.4. Kaolin samples and their powder forms. A: Kaolin 1, B: Kaolin 2, C: Kaolin 3, D: Kaolin 4

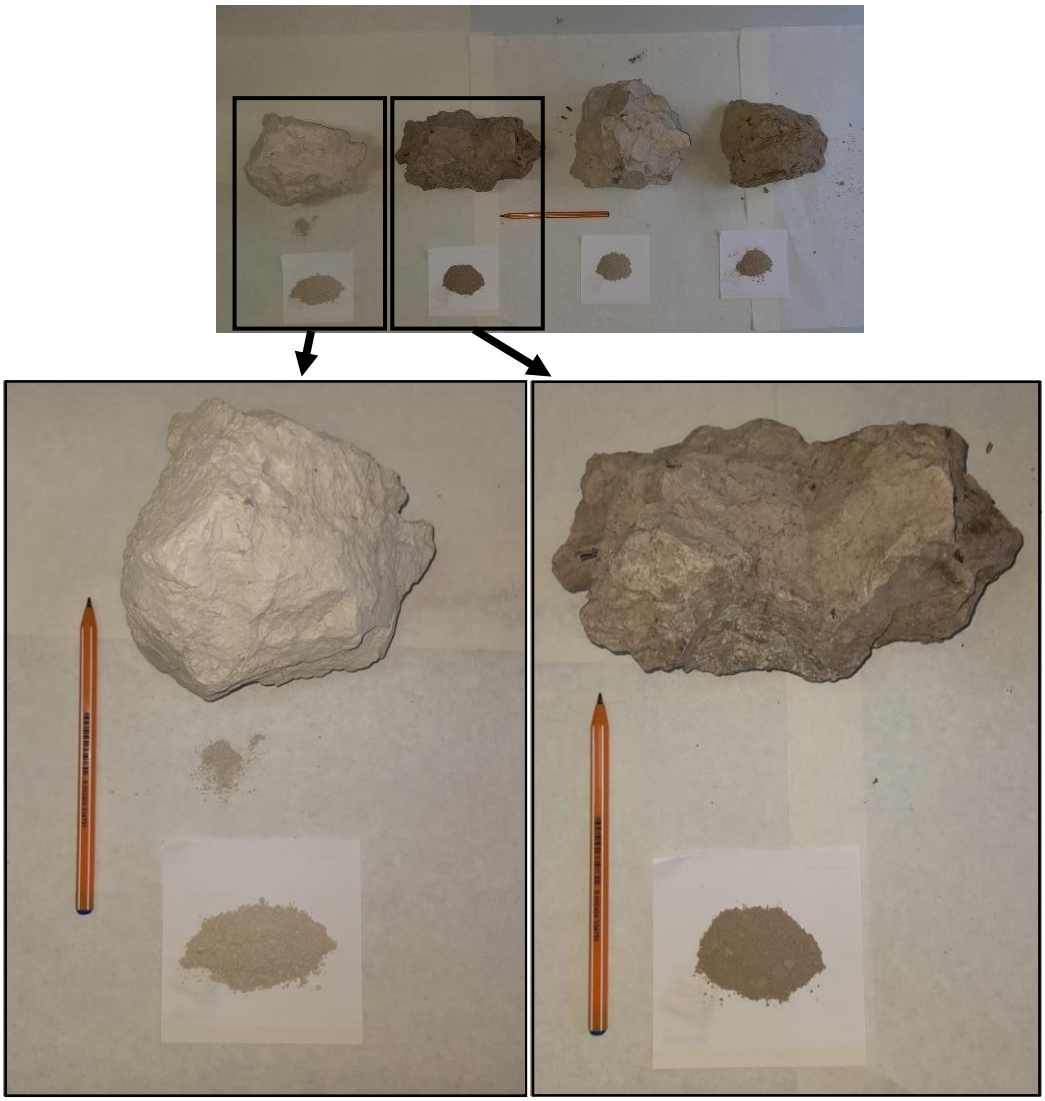

Figure 3.5. Close-up images of kaolin samples. A: Kaolin 1, B: Kaolin 2

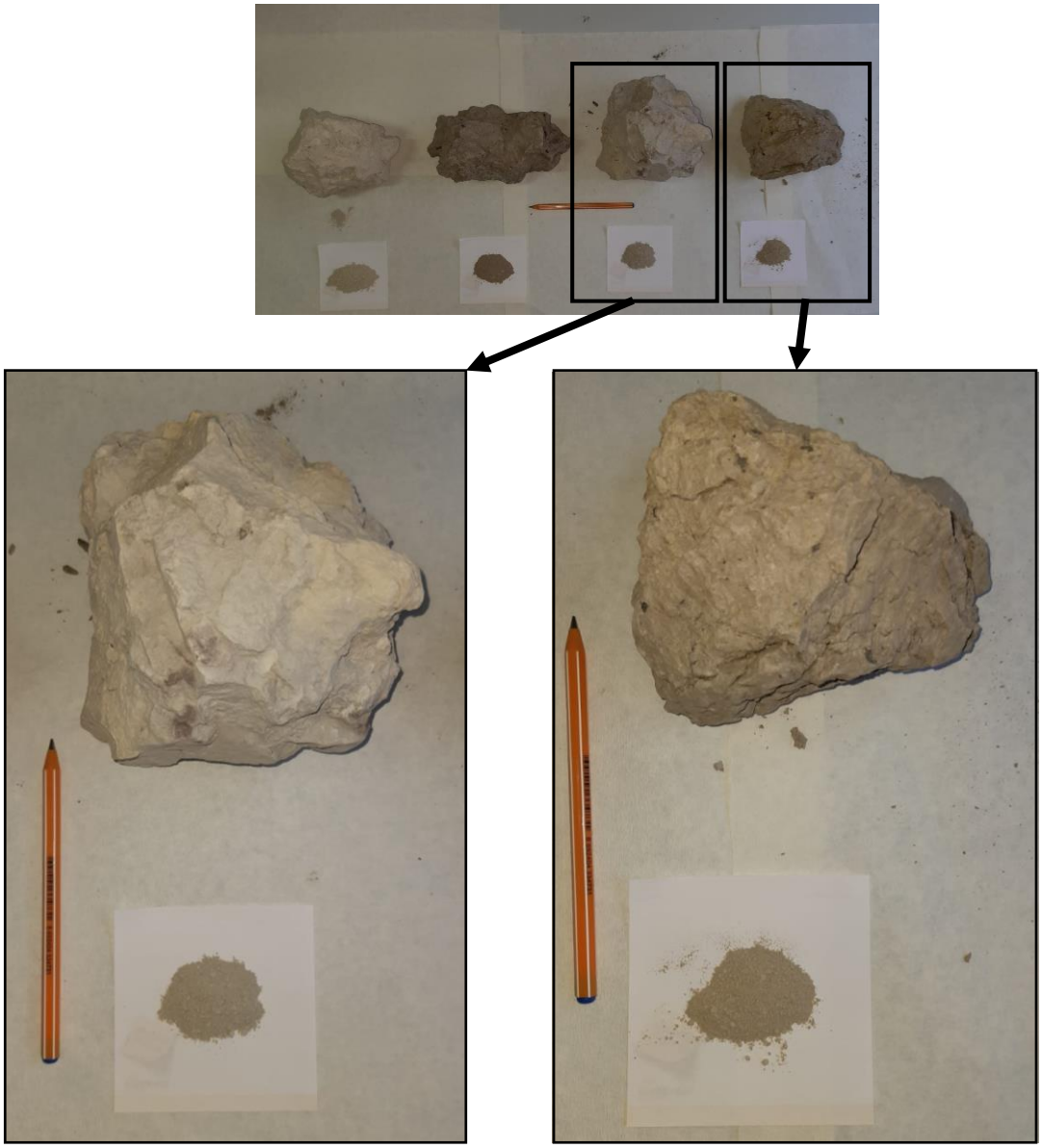

Figure 3.6. Close-up images of kaolin samples. A: Kaolin 3, B: Kaolin 4

CHAPTER 4

MATERIALS AND EXPERIMENTAL PROCEDURE

In this chapter, the materials that are used in the synthesis procedure, the preparation of the gangue kaolin samples for the characterization and the synthesis procedure, the synthesis procedure of zeolite 4A, and the characterization methods are given.

4.1 Materials Selection

Kaolin-rich coal gangue samples were chosen to provide the desired Si/Al ratio for the synthesis of zeolite 4A, and they are named kaolin samples. Although they have proper Si/Al ratios for the zeolite 4A synthesis, the impurity content makes it useless for the industry. Additionally, the quartz content is also critical for the use of silicon in it. To obtain silicon in the quartz, its structure should be broken.

Aluminum-hydroxide was used to balance the silicon/aluminum ratio. The sodium sources are not only used to balance the sodium ratio but also as an alkali agent in the synthesis.

Four kaolin samples (Figure 3.4) that were provided from coal mines in the Thrace region were used as raw materials for the synthesis of zeolite 4A. Aluminum hydroxide powder from Kazan Soda Elektrik Company, Turkey was used as an aluminum source. Sodium hydroxide pellets were obtained from Sigma Aldrich Chemicals. Sodium carbonate powder taken from Kazan Soda Elektrik A.Ş. was used as a different sodium source. As water, double distilled water (DDW) with <18Ω was used in the synthesis.

4.2 Sample Preparation for Raw Material Characterization

Characterization of the raw material is important for the synthesis because the synthesis procedure can be shaped concerning the raw material, and the results of the syntheses can be compared to each other in a more detailed way. The gangue kaolin samples' detailed characterization will result in a gained advantage for the synthesis procedure. For detailed characterization, the gangue kaolin samples should be treated and investigated before the synthesis. The sample preparation for the whole rock characterization, the clay parts of the sample's characterization, and the non-clay parts of the sample's characterization are done with the help of pretreatment steps.

Firstly, massive rock pieces of the kaolin samples are ground in an agate mortar to obtain powder form, then the product was sieved with a 90-micron sieve (ASTM mesh no 170) to obtain small particle-sized material without pellets which is useful for synthesis and characterization. This is necessary for the samples to be in particle size for mixing them with other powder chemicals used in the synthesis of zeolite 4A. After this mechanical treatment, the kaolin samples were analyzed by XRF to understand the elemental composition of each sample. After the XRF, the samples were prepared for further analysis by XRD to investigate the mineral content in more detail.

The powder samples of kaolin are taken by 10 grams of each in different beakers. In the beakers, they were mixed for 3 minutes with 1 liter of distilled water (DI water) and a small amount of sodium polyphosphate powder for preventing flocculation of powdered samples. After mixing, the beakers waited for 8 hours at room temperature. After 8 hours, the non-clay parts of the samples were settled at the bottom of the beaker while the clay parts continue to float in the water. The water containing clay particles was taken by a pipe from deeper than the middle of the beaker without touching the non-clay particles. The first water samples coming from beakers were taken in tubes and centrifuged. The washed samples were taken from the tubes and applied 4 different glass sections for each kaolin sample. One of the glass sections for each kaolin sample was dried at room temperature and labeled as

air-dried. Another glass section of each was waited in an ethylene glycol container in a furnace at 60 ℃ temperature for 4 hours and labeled as ethylene glycol treated samples. The other two glass sections were dried at 300 ℃, and 550 ℃, and labeled as 300 ℃ dried and 550 ℃ dried, respectively. All these oriented glass sections were analyzed by XRD in the interval of 1-40 2θ degrees, and the powder samples were analyzed in the interval of 5-50 2θ degrees.

The samples remaining in the beakers continued to be washed. Each time the water has been removed without taking the settled parts at the bottom, more DI water was added and mixed with 8 hours of waiting. Nearly 800 ml of water was taken by a pipe in the 1 liter of mixture each time. This process is called siphoning and the siphoning for the samples continued until the water seemed clear after 8 hours of waiting each time. After the siphoning is done and the water seemed clear, the settled parts of the clay samples in the beakers were taken by vaporizing the DI water by putting the beaker in a furnace at 50 ℃. The remaining samples were dried and analyzed by XRD which were labeled as the washed samples. The initial and resulting material content after siphoning is also weighted and reported.

The detailed investigation of the gangue kaolin samples is done with these pretreatment steps, and the information gained by these pretreatments can be used in comparing the synthesis results.

4.3 Synthesis Procedure for Zeolite 4A

The main synthesis process starts with the high-degree heat treatment. This high-degree heat treatment is necessary for breaking the quartz structure for using the silicon in it and it is also necessary for the aluminum source to get involved in the system with the help of the sodium source.

After the high-temperature heating step is done, the synthesis continues with the aging step. In the aging step, materials are mixed in a high density polyethylene (HDPE) bottle first with the preferred amounts to obtain the wanted molar ratios of

SiO_2, Al_2O_3, Na_2O, and H_2O, and then a magnetic stirrer bar is placed in the bottle. Later, the mixture in the bottle is heated and mixed with a magnetic stirrer. When the time is over for the aging step, the magnetic stirrer bar is taken out of the bottle.

Next, the synthesis continues with the reaction step. In the reaction step, the mixture from the aging step is taken to the furnace for another heating for some time. In this step, crystallization occurs and produces Zeolite 4A.

After the reaction step, the samples are taken from the furnace and let sit until it cools down. This step is followed by centrifugation for washing with distilled water and drying in a preheated 80℃ oven overnight. The synthesis products are ready for XRD and SEM analysis after all the mentioned procedures above are finished.

4.3.1 Synthesis with Metakaolinization Products

In the metakaolinization method, the kaolin samples were first put into calcination with temperatures of 800 ℃, 850 ℃, 900 ℃, and 950 ℃. Different temperatures were applied to examine the effect of heat in the final products for the zeolite 4A synthesis. After the calcination of samples, the rest of the synthesis process is the same for all differently heated samples.

Firstly, the calcined clay samples were taken and ground with a hammer to obtain the powder form of the samples, having a grain size of less than 150 microns (ASTM mesh no 100). Then the samples were mixed with sodium aluminate ($NaAlO_2$) and aluminum hydroxide ($Al(OH)_3$) in the pre-calculated weights to make a solid mix. However, $NaAlO_2$ was not used in the first samples' synthesis because the content of the sample was appropriate for the Zeolite 4A without using it. Later, the solid mix is put into high-density polyethylene (HDPE) bottles and DI water is added before the next step of the synthesis. The mixture was created concerning the chemical formula of 2.44 SiO_2: 1 Al_2O_3: 3.14 Na_2O: 110 H_2O. The point at the gel was created, a magnetic stirrer bar is added to the HDPE bottle, then the aging step is applied next. In the aging step, a magnetic stirrer is used at 400 rpm and 60 ℃ of

heat is applied to the gel in the HDPE bottle for 4 hours and the magnetic stirrer bar is taken out from the mixture.

After the aging step, the synthesis continues with the reaction step. In this step, the mixture is taken in a furnace at 100 ℃ and waited for 4 hours, and the zeolite crystals are formed.

4.3.2 Synthesis with One-Pot Fusion Products

In the one-pot fusion method, two routes were followed and the difference between the methods is the sodium source used. With the first route, powder kaolin samples were first mixed with aluminum hydroxide ($Al(OH)_3$) and sodium hydroxide (NaOH) with precalculated weights. With the second route, the clay samples were first mixed with aluminum hydroxide ($Al(OH)_3$) and sodium carbonate (Na_2CO_3). After preparing the mixture, the rest of the synthesis is the same for both routes. The solid mixture is first heated at high temperatures which are 800, and 850 ℃ for both NaOH and Na_2CO_3 fusions, and additionally 900 ℃ for Na_2CO_3 fusion. Later, the heated product is ground with a hammer to obtain powder material. After that, DI water is added to the powder to obtain a molar ratio of 2.44 SiO_2: 1 Al_2O_3: 3.14 Na_2O: 110 H_2O.

4.4 Characterization

The characterization of the kaolin samples is important for perceiving the crystallinity of the material and determining the amount of the material needed for the synthesis concerning its chemical data. Moreover, characterization is also important for the synthesized zeolite 4A to see the results of the experiment if it gives positive outcomes. Kaolin samples were prepared for characterization. The samples were first ground in an agate mortar and the product was sieved to obtain small particle-sized material without pellets which is useful for synthesis and characterization. The kaolin sample powders were characterized by laser diffraction

based particle size analyzer, XRD and XRF, and zeolite products were characterized by XRD and SEM. Rigaku Ultima IV with Cu Kα radiation was used for XRD for obtaining crystallinity data, Rigaku ZSX Primus II was used for XRF to get chemical data, and Mastersizer 2000 was used for obtaining the particle size from the samples.

4.4.1 X-Ray Fluorescence (XRF)

X-ray fluorescence (XRF) spectrometer is a non-destructive instrument that is used for the chemical analysis of rocks, minerals, and liquid materials with the help of x-rays. It operates on the same wavelength-dispersive spectroscopic principles as an electron microprobe (EPMA) and depends on fundamental principles that are common to several other instruments like scanning electron microscopy (SEM) and X-ray diffraction (XRD) tools. The behavior of atoms, when they interact with radiation, allows x-ray fluorescence to be used to analyze major and trace elements in rocks and minerals ("X-Ray Fluorescence (XRF)," 2013). The raw kaolin samples were characterized with XRF for obtaining the chemical data in the Middle East Technical University Central Laboratory.

4.4.2 X-Ray Diffraction (XRD)

X-ray powder diffraction (XRD) is a quick analytical technique that can offer information on unit cell dimensions and is mostly used for the phase identification of crystalline materials. The studied material is finely powdered and homogenized, and the bulk composition is calculated on an average basis with X-ray diffraction. Constructive interference between monochromatic X-rays and a crystalline sample is the basis of X-ray diffraction (Dutrow, 1912). The kaolin samples and synthesized zeolite products in this study were investigated with XRD in the Middle East Technical University Central Laboratory.

4.4.3 Scanning Electron Microscopy (SEM)

Scanning electron microscopy (SEM) generates a variety of signals at the surface of solid specimens using a focused beam of high-energy electrons. The signals generated by electron-sample interactions provide information on the sample's exterior morphology (texture), chemical composition, crystalline structure, and orientation of the materials that make up the sample (*Scanning Electron Microscopy (SEM)*, 2017). The synthesized zeolite products were investigated with SEM in the Middle East Technical University Central Laboratory.

4.4.4 Laser Particle Size Analyzer

Laser diffraction-based particle size analyzers use the technique of laser diffraction to measure the size of particles. Particle size is calculated by measuring the angle of light scattered by the particles as they pass through a laser beam. There are multiple light detectors used in laser particle size analyzers, and with more light detectors the sensitivity of the analyzer improved (labcompare, 2019). The kaolin samples used in this study were investigated with a laser diffraction-based particle size analyzer in the Middle East Technical University Central Laboratory.

CHAPTER 5

RESULTS

The results of the characterization for gangue kaolin samples and zeolite synthesis products are shown in this chapter.

5.1 Raw Material Character

The particle size analysis of the samples is done by a laser diffraction-based particle size analyzer. The particle size analyzer measures the samples 3 times with a 16 second interval and gives an average value for the analysis.

The particle size analysis result of sample kaolin 1 is shown in Figure 5.1. For kaolin 1, 90% of the sample is smaller than 18.901 micrometers, 50% is smaller than 5.680 micrometers, and 10% is smaller than 1.511 micrometers. The specific surface area is calculated as 1.62 m^2/g for the sample.

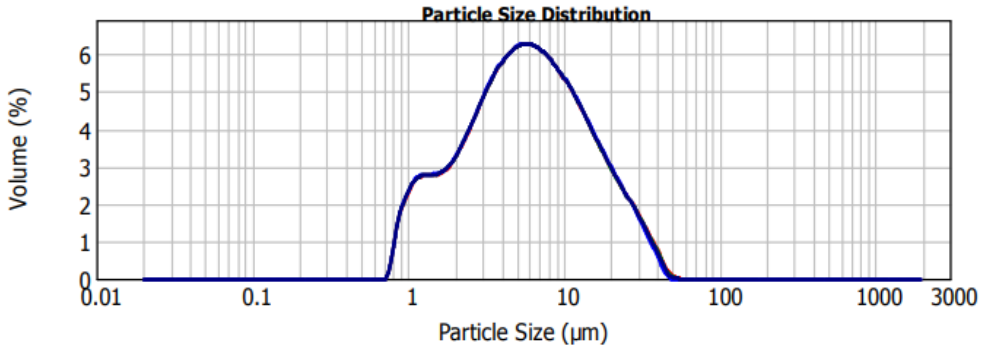

Figure 5.1. Particle size distribution of Kaolin 1. Dark blue line indicates the average measurement

The particle size analysis result of sample Kaolin 2 is shown in Figure 5.2. For kaolin 2, 90% of the sample is smaller than 9.069 micrometers, 50% is smaller than 3.703

micrometers, and 10% is smaller than 1.441 micrometers. The specific surface area is calculated as 2.13 m^2/g for the sample.

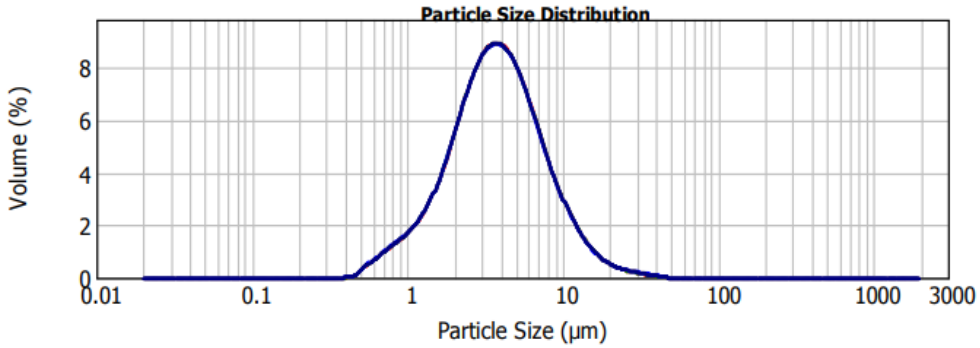

Figure 5.2. Particle size distribution of Kaolin 2. Dark blue line indicates the average measurement

The particle size analysis of sample Kaolin 3 is shown in Figure 5.3. For kaolin 3, 90% of the sample is smaller than 22.898 micrometers, 50% is smaller than 4.708 micrometers, and 10% is smaller than 1.218 micrometers. The specific surface area is calculated as 1.95 m^2/g for the sample.

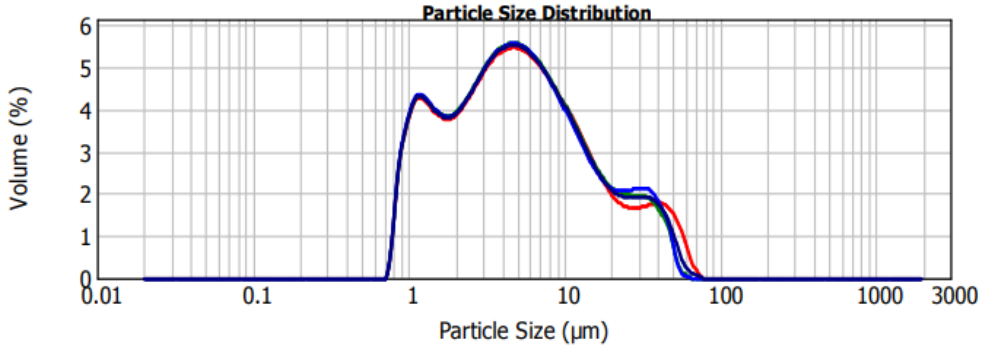

Figure 5.3. Particle size distribution of Kaolin 3. Dark blue line indicates the average measurement

The particle size analysis of sample Kaolin 4 is shown in Figure 5.4. For kaolin 4, 90% of the sample is smaller than 7.845 micrometers, 50% is smaller than 3.492 micrometers, and 10% is smaller than 1.377 micrometers. The specific surface area is calculated as 2.26 m^2/g for the sample.

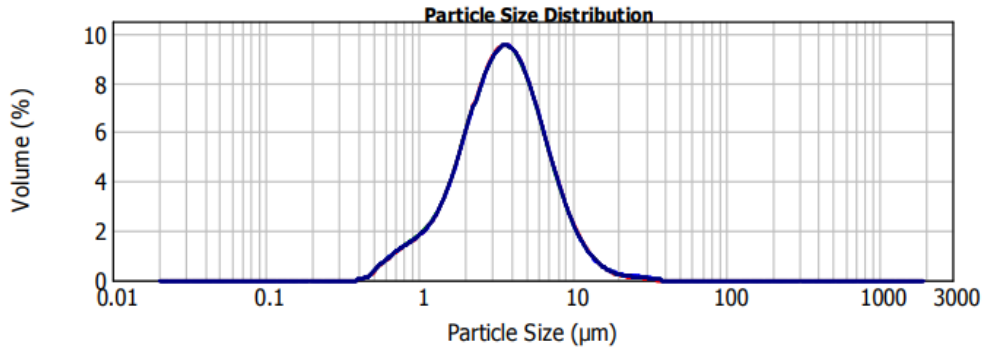

Figure 5.4. Particle size distribution of Kaolin 4. Dark blue line indicates the average measurement

The particle size distribution of all samples is given in Table 5.1.

Table 5.1. Particle size distribution of kaolin samples (wt: weight)

Particle Size (µm)	*Kaolin 1*	*Kaolin 2*	*Kaolin 3*	*Kaolin 4*
d_{10} (<%10 in wt.)	1.511	1.441	1.218	1.377
d_{50} (<%50 in wt.)	5.680	3.703	4.708	3.492
d_{90} (<%90 in wt.)	18.901	9.069	22.898	7.845

Table 5.1 shows that kaolin 3 has the largest particle size distribution with the smallest d_{10} value and the largest d_{90} value. Kaolin 4 has the smallest particle size range, and the smallest d_{50} and d_{90} values belong to kaolin 4. Kaolin 1 has the largest d_{10} and d_{50} values.

The mineral analysis of the samples was done by XRD, and the mineral group names were used for the XRD output. Although the minerals included in the samples were investigated according to the properties of kaolinite and montmorillonite, they were named by their group names as kaolin and smectite in this study.

Random raw and clay mineral washed XRD patterns of the first sample in Figure 5.5 shows that the minerals seen in the patterns are illite, kaolin, quartz, and smectite (Caroll, 1970).

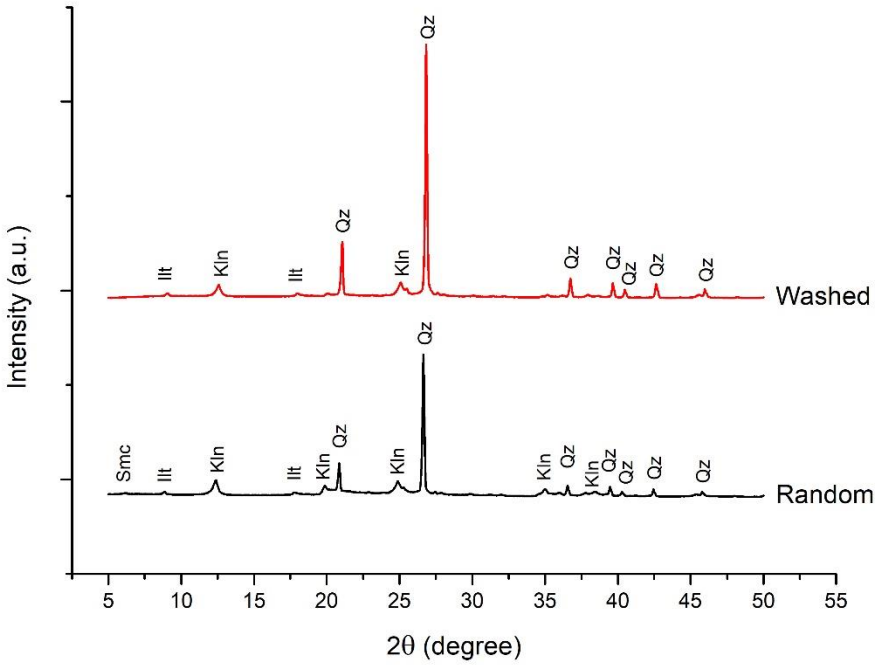

Figure 5.5. The powder X-ray diffractogram of the sample Kaolin 1, random raw and clay mineral washed samples. Kln: kaolin, Smc: smectite, Ilt: illite, Qz: Quartz

In the random raw sample, [001] peak of smectite is small but seen as 14.18 Å (6.23 2θ). [001] peak of illite is seen as 9.99 Å (8.38 2θ) and [002] is 4.99 Å (17.73 2θ) (*USGS OFR01-041: Illite Group Minerals*, n.d.). Kaolins [001] peak is seen as 7.15 Å (12.36 2θ), [002] as 3.58 Å (24.84 2θ), [020] as 4.47 Å (19.84 2θ), and [202] as 2.34 Å (38.3 2θ) (Biel et al., 2020; Geng et al., 2022; Sachan & Penumadu, 2007). Additionally, the 2.56 Å peak at 34.95 2θ is expected to be another peak of kaolin (Kovo et al., 2009). The [100] peak of quartz is seen as 4.25 Å (20.87 2θ), [101] as 3.34 Å (26.64 2θ), [110] as 2.45 Å (36.54 2θ), [102] as 2.28 Å (39.47 2θ), [200] as 2.12 Å (42.44 2θ), and [201] peak as 1.98 Å (45.78 2θ) (*Quartz R040031 - RRUFF Database: Raman, X-Ray, Infrared, and Chemistry*, n.d.). Therefore, the peak of 2.23 Å at 40.29 2θ is expected to be quartz, which gets sharper in the clay mineral washed sample (Wang et al., 2018).

In the clay mineral washed sample, [001] and [002] peaks of illite are still seen as 9.73 Å (9.07 2θ), and 4.93 Å (17.96 2θ) with decreased intensity. The [001] and [002] kaolin peaks are also seen with d spacing values of 7.04 Å (12.55 2θ), and 3.54 Å (25.07 2θ) with a decreased intensity. The [100] peak of quartz is seen as 4.21 Å (21.06 2θ), [101] as 3.31 Å (26.84 2θ), [110] as 2.44 Å (36.73 2θ), [102] as 2.27 Å (39.65 2θ), [200] as 2.11 Å (42.63 2θ), and [201] as 1.97 Å (45.97 2θ). And the peak of 2.22 Å at 40.48 2θ is expected to be quartz.

The mineral weight percentages of random raw and clay mineral washed samples of the sample Kaolin 1 were calculated with Relative Intensity Ratio (RIR) by XRD analysis. In the random raw sample, quartz is calculated as 48.2%, kaolin as 39%, illite as 3.9%, and smectite as 8.9%. In the washed sample, quartz is calculated as 65.2%, kaolin as 31.7%, and illite as 3.08%, while smectite couldn't be calculated.

The kaolin and illite peaks were expected to get lost in the clay mineral washed sample, but some of the peaks are still observable. Although they are not totally lost, the intensities of kaolin and illite are decreased when compared to the intensity of quartz. This means that in the flocculation stage of the samples, the clay particles flocculated with quartz particles smaller than 2 microns and fell together in the solution before getting washed. This results in an increased intensity of quartz peaks and a decreased intensity of clay minerals peaks when compared with the random raw sample. Moreover, the [003] peak of illite at 26.79 2θ is not seen in both random raw and clay mineral washed samples XRD results because of the dominance of quartz.

Figure 5.6 shows XRD patterns of the oriented slides of Kaolin 1, and it gives more detailed information about the clay minerals in that sample.

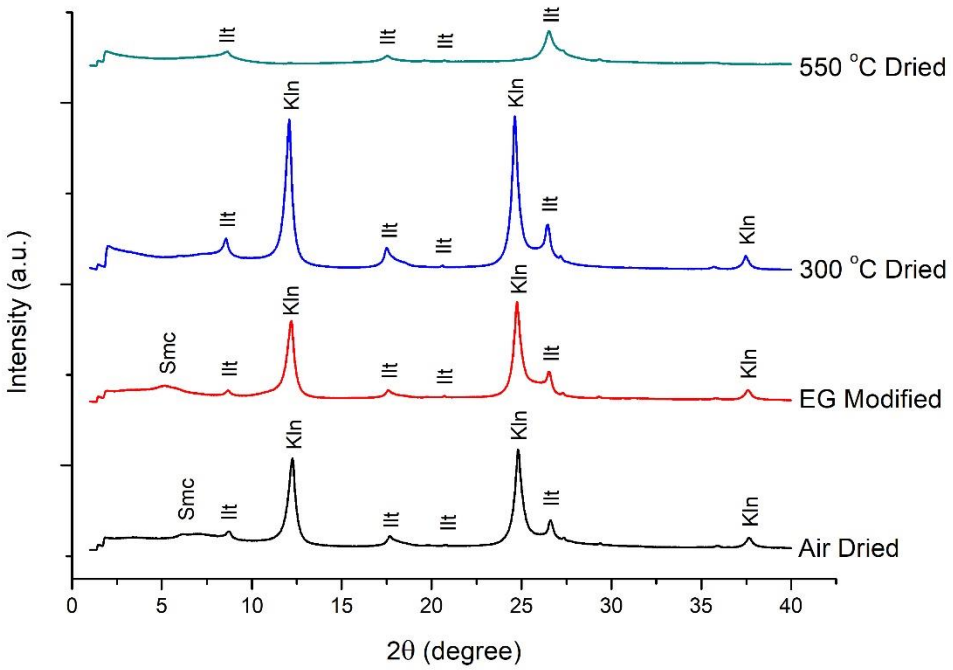

Figure 5.6. X-ray diffractogram of the oriented slides of the sample Kaolin 1. Kln: kaolin, Smc: smectite, Ilt: illite, Qz: quartz, EG: ethylene glycol

Firstly, smectite is seen in the air dried and ethylene glycol treated samples. The [001] peak of smectite is seen as 12.69 Å (6.96 2θ) in the air-dried sample and it changed to 17.16 Å (5.14 2θ) in the ethylene glycol treated sample due to swelling.

Illite is not affected by ethylene glycol treatment, and it doesn't get lost by increasing the temperature even at 550 ℃. In the air-dried sample, [001], [002], [003], and [111] peaks are seen as 10.1 Å (8.74 2θ), 5.01 Å (17.66 2θ), 3.34 Å (26.59 2θ), and 4.29 Å (20.68 2θ) respectively (X. Jin et al., 2021). In the ethylene glycol treated sample, [001], [002], [003], and [111] peaks are seen as 10.15 Å (8.69 2θ), 5.04 Å (17.57 2θ), 3.35 Å (26.58 2θ), and 4.28 Å (20.72 2θ). In the 300 ℃ dried sample, [001], [002], [003], and [111] peaks are seen as 10.27 Å (8.6 2θ), 5.07 Å (17.47 2θ), 3.36 Å (26.44 2θ), and 4.14 Å (21.5 2θ). In the 550 ℃ dried sample, [001], [002], [003], and [111] peaks are seen as 10.27 Å (8.6 2θ), 5.05 Å (17.53 2θ), 3.36 Å (26.49 2θ), and 4.28 Å (20.69 2θ).

Lastly, kaolin peaks are also seen. In the air dried sample, [001] peak of kaolin is seen as 7.21 Å (12.25 2θ), [002] as 3.59 Å (24.76 2θ), and [003] as 2.38 Å (37.65 2θ) (Sachan & Penumadu, 2007). In the ethylene glycol treated sample, [001] peak is seen as 7.25 Å (12.18 2θ), [002] as 3.6 Å (24.71 2θ), and [003] as 2.39 Å (37.55 2θ). In the 550 ℃ treated sample, there is no kaolin peak as expected.

The mineral weight percentages of air-dried (AD) samples of Kaolin 1 are calculated with the RIR method by XRD. In the air-dried sample, kaolin is calculated as 71.6%, illite as 24.9%, and smectite as 3.5%.

The reason for not having smectite peaks in the random raw and clay mineral washed samples might be due to poor crystallization of the mineral which cannot be seen while the other minerals dominate the structure. After the washing of the sample Kaolin 1, quartz is eliminated from the taken liquid and the peak of smectite became visible.

The [003] peak of illite at around 26.5 2θ is not seen in the random and washed samples, but it is visible in the treated samples XRD results. The [101] peak of quartz at around 26.6 2θ covers the [003] illite peak in the random and washed samples, that's why illite is not seen in the random raw and clay mineral washed samples but observable in the treated samples.

Continuing with the Kaolin 2 random raw and clay mineral washed XRD results, the same peaks of kaolin, illite, and quartz are seen, and [001] peak of smectite is more obviously seen as a little wave at the random raw sample 14.44 Å (6.11 2θ) (Ait-Akbour et al., 2015) (Figure 5.7).

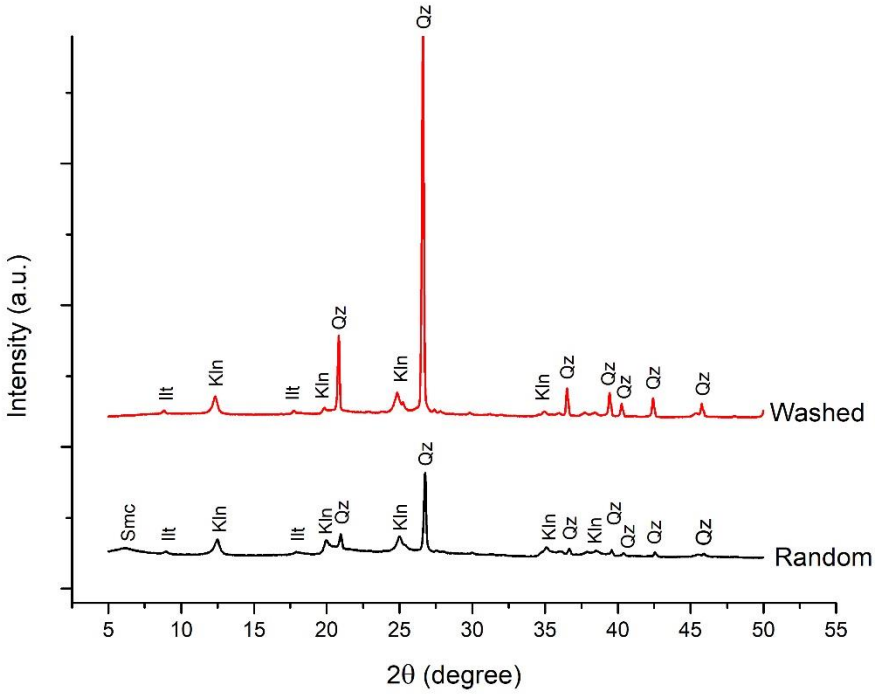

Figure 5.7. The powder X-ray diffractogram of the sample Kaolin 2, random raw and clay mineral washed samples. Kln: kaolin, Smc: smectite, Ilt: illite, Qz: quartz

In the random raw sample, [001] and [002] peaks of illite are seen as 9.86 Å (8.96 2θ) and 4.93 Å (17.97 2θ). Kaolins [001] peak is seen as 7.08 Å (12.47 2θ), [002] as 3.55 Å (25.0 2θ), [020] as 4.44 Å (19.94 2θ), [202] as 2.33 Å (38.49 2θ), and 2.57 Å (34.85 2θ) also refers to kaolin. The [100] peak of quartz is seen as 4.22 Å (20.98 2θ), [101] as 3.32 Å (26.75 2θ), [110] as 2.45 Å (36.63 2θ), [102] as 2.28 Å (39.45 2θ), [200] as 2.12 Å (42.55 2θ), [201] as 1.97 Å (45.89 2θ), and 2.23 Å (40.36 2θ) is also a quartz peak.

In the clay mineral washed sample, [001] and [002] peaks of illite are seen as 10.01 Å (8.82 2θ), and 5.0 Å (17.71 2θ). Kaolins [001] peak is seen as 7.17 Å (12.33 2θ), [002] as 3.57 Å (24.85 2θ), [020] as 4.47 Å (19.81 2θ), and 2.56 Å at 34.95 2θ is also a kaolin peak. The [100] peak of quartz is seen as 4.25 Å (20.83 2θ), [101] as 3.34 Å (26.61 2θ), [110] as 2.45 Å (36.51 2θ), [102] as 2.28 Å (39.43 2θ), [200] as 2.12

Å (42.41 2θ), [201] as 1.98 Å (45.76 2θ), and 2.23 Å at 40.25 2θ is also a quartz peak.

The quartz weight percentage is calculated as 30.3%, kaolin as 36.4%, illite as 4.8%, and smectite as 28.6% in the Kaolin 2 random raw sample by the RIR method. In the clay mineral washed sample, quartz is calculated as 65.7%, kaolin as 32.1%, and illite as 2.13%, and smectite couldn't be calculated.

The intensity of the quartz peaks increased remarkably after the washing of the sample as expected. The quartz and kaolin peaks are seen together over 35.0 2θ mainly in the random raw sample (Wang et al., 2021). As seen from the figure, the clay minerals peaks get smaller while the quartz peaks are intensified a lot by washing the sample.

The oriented slides XRD patterns of Kaolin 2 (Figure 5.8) show that the small wave at the raw materials XRD refers to smectite. Smectite swells with the application of ethylene glycol and changes its position when compared to the air-dried sample. At air dried samples of smectite, the [001] peak is seen as 14.95 Å (5.91 2θ), and at the ethylene glycol treated sample that peak changes its position to the left and seen as 17.45 Å (5.06 2θ) (Borralleras et al., 2019; Caroll, 1970).

Illite's [001], [002], [003], and [111] peaks are seen in all the samples. In the air-dried sample, they are seen as 10.26 Å (8.6 2θ), 5.04 Å (17.57 2θ), 3.36 Å (26.44 2θ), and 4.29 Å (20.64 2θ). In the ethylene glycol sample, they are seen as 10.18 Å (8.67 2θ), 5.04 Å (17.57 2θ), 3.35 Å (26.54 2θ), and 4.28 Å (20.69 2θ). In the 300 ℃ dried sample, they are seen as 10.19 Å (8.66 2θ), 5.04 Å (17.56 2θ), 3.36 Å (26.49 2θ), and 4.29 Å (20.67 2θ). Lastly, in the 550 ℃ dried sample, they are seen as 10.21 Å (8.64 2θ), 5.06 Å (17.5 2θ), 3.36 Å (26.45 2θ), and 4.29 Å (20.67 2θ)

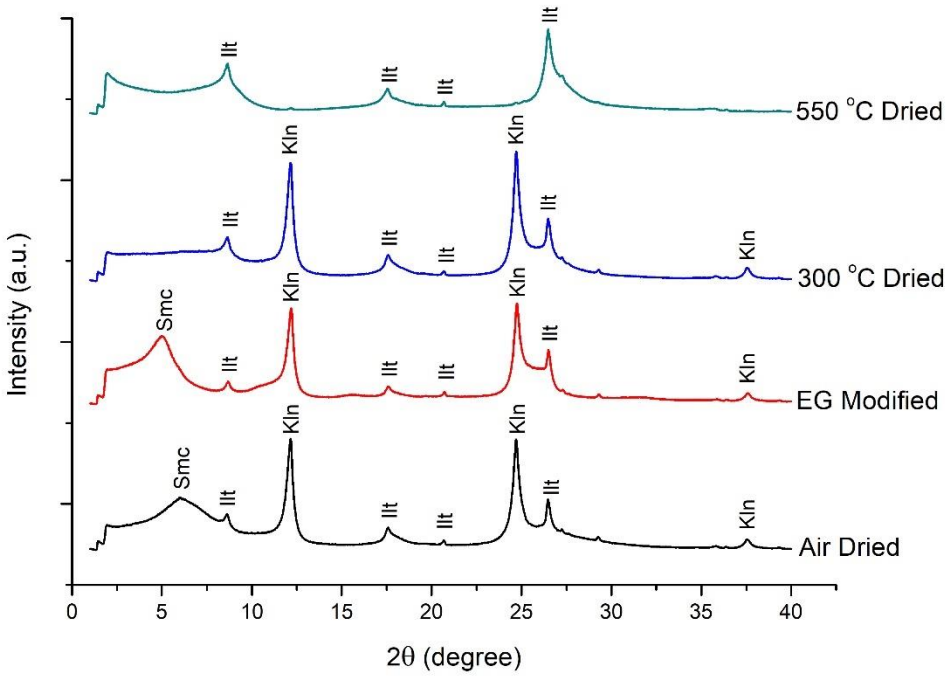

Figure 5.8. X-ray diffractogram of the oriented slides of the sample Kaolin 2. Kln: kaolin, Smc: smectite, Ilt: illite, Qz: quartz, EG: ethylene glycol

The kaolin peaks are also observable in the treated samples. In the air-dried sample, [001] peak of kaolin is seen as 7.26 Å (12.16 2θ), [002] as 3.6 Å (24.67 2θ), and [003] as 2.39 Å (37.53 2θ). In the ethylene glycol treated sample, [001] is seen as 7.25 Å (12.19 2θ), [002] as 3.59 Å (24.71 2θ), and [003] as 2.39 Å (37.55 2θ). In the 300 ℃ dried sample, [001] is seen as 7.26 Å (12.16 2θ), [002] as 3.6 Å (24.64 2θ), and [003] as 2.39 Å (37.57 2θ). Lastly in the 550 ℃ dried sample, kaolin peaks are lost.

In the air-dried sample of Kaolin 2, kaolin is calculated as 45%, illite as 37.2%, and smectite as 17.8% by the RIR method.

The random raw and clay mineral washed XRD results of Kaolin 3 are shown in the Figure 5.9. The smectite [001] peak is so small in the random raw sample with the basal spacing value of 14.35 Å (6.16 2θ), although it is not seen well in the figure.

In the random raw sample, illite's [001] peak is not seen clearly but found as 10.04 Å (8.8 2θ) by the XRD, and [002] as 4.94 Å (17.92 2θ), but [003] peak is not seen because of the quartz [101] peak. Kaolin's [001] peak is seen as 7.19 Å (12.28 2θ), [002] as 3.58 Å (24.82 2θ), [020] as 4.48 Å (19.79 2θ), [202] as 2.35 Å (38.26 2θ), and 2.56 Å (34.9 2θ) is also a kaolin peak. The [100] peak of quartz is seen as 4.25 Å (20.86 2θ), [101] as 3.34 Å (26.62 2θ), [110] as 2.45 Å (36.54 2θ), [102] as 2.28 Å (39.45 2θ), [200] as 2.12 Å (42.44 2θ), [201] as 1.98 Å (45.77 2θ), and 2.23 Å (40.27 2θ) is also a quartz peak.

In the clay mineral washed sample, [001] and [002] peaks of illite are seen as 9.88 Å (8.94 2θ), and 4.97 Å (17.82 2θ). Kaolin's [001] peak is seen as 7.1 Å (12.45 2θ), [002] as 3.55 Å (25.0 2θ), and [020] as 4.46 Å (19.86 2θ). The [100] peak of quartz is seen as 4.23 Å (20.94 2θ), [101] as 3.34 Å (26.64 2θ), [110] as 2.45 Å (36.61 2θ), [102] as 2.27 Å (39.53 2θ), [200] as 2.12 Å (42.51 2θ), [201] as 1.97 Å (45.86 2θ), and 2.23 Å at 40.36 2θ is also a quartz peak.

The quartz weight percentage is calculated as 51.3%, kaolin as 32.4%, illite as 2.2%, and smectite as 14.0% in the Kaolin 3 random raw sample by the RIR method. In the clay mineral washed sample, quartz is calculated as 75.1%, kaolin as 23%, and illite as 1.91%, and smectite couldn't be calculated.

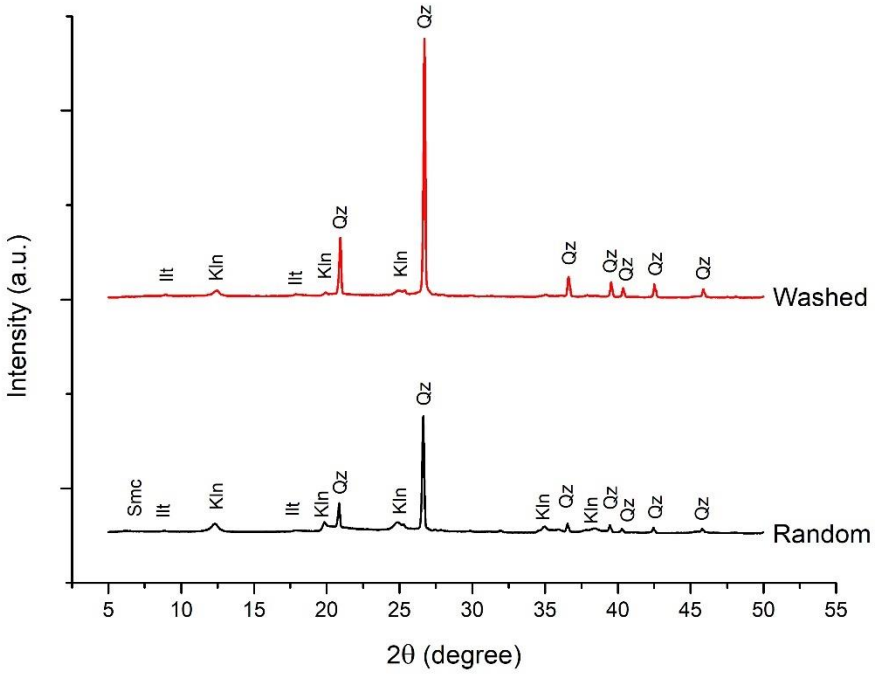

Figure 5.9. The powder X-ray diffractogram of the sample Kaolin 3, random raw and clay mineral washed samples. Kln: kaolin, Smc: smectite, Ilt: illite, Qz: Quartz

The random raw and clay mineral washed samples of Kaolin 3 do not show a big difference with the first and the second samples. The kaolin and quartz peaks are distinct (Caroll, 1970; Li et al., 2019) in the random raw sample results unlike illite, and in the clay mineral washed sample only quartz is distinct (Figure 5.9). The intensities of kaolin peaks decreased at the clay mineral washed sample while quartz peaks intensified as expected.

In the oriented slides XRD patterns of Kaolin 3, smectite peaks are seen clearer. The wavy peak of 13.93 Å (6.34 2θ) at air dried sample is smectite [001] which swelled with ethylene glycol treatment and slide a little bit to left at the EG Modified graph with a basal spacing of 16.86 Å (5.24 2θ) (Figure 5.10) (Borralleras et al., 2019; Caroll, 1970).

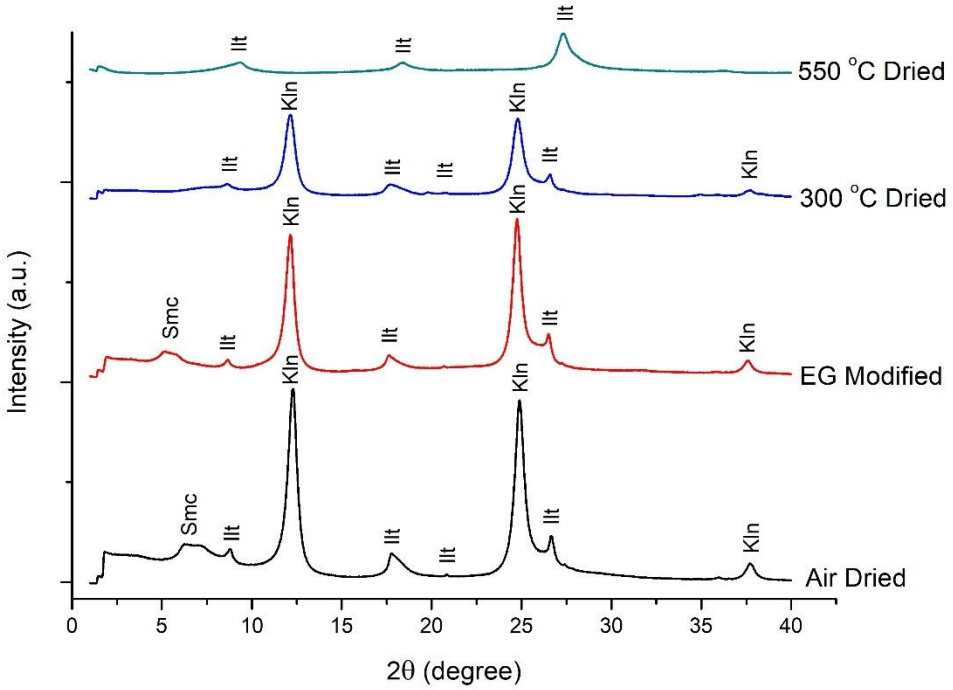

Figure 5.10. X-ray diffractogram of the oriented slides of the sample Kaolin 3. Kln: kaolin, Smc: smectite, Ilt: illite, Qz: quartz, EG: ethylene glycol

Illite's [001], [002], and [003] peaks are seen in all the samples. In the air-dried sample, they are seen as 10.08 Å (8.76 2θ), 5.0 Å (17.26 2θ), and 3.33 Å (26.66 2θ). In the ethylene glycol sample, they are seen as 10.17 Å (8.68 2θ), 5.0 Å (17.71 2θ), and 3.35 Å (26.56 2θ). In the 300 ℃ dried sample, they are seen as 10.19 Å (8.66 2θ), 5.02 Å (17.63 2θ), and 3.34 Å (26.61 2θ). Lastly, the small peaks which don't get lost at 550 ℃ treatment refer to illite peaks (Németh et al., 2016), they are seen as 9.31 Å (9.49 2θ), 4.8 Å (18.44 2θ), and 3.26 Å (27.28 2θ).

The [001] kaolin peak in the air-dried sample is seen as 7.20 Å (12.27 2θ), [002] as 3.57 Å (24.87 2θ), and [003] as 2.38 Å (37.69 2θ). In the ethylene glycol treated sample, [001] is seen as 7.29 Å (12.12 2θ), [002] as 3.59 Å (24.74 2θ), and [003] as 2.39 Å (37.58 2θ). In the 300 ℃ dried sample, [001] is seen as 7.29 Å (12.12 2θ), [002] as 3.59 Å (24.76 2θ), and [003] as 2.38 Å (37.63 2θ). Lastly, in the 550 ℃ dried sample, kaolin peaks are lost.

In the air-dried sample of Kaolin 3, kaolin is calculated as 83.1%, illite as 16.5%, and smectite as 0.4% by the RIR method.

The random raw and clay mineral washed XRD results of Kaolin 4 are shown in Figure 5.11. The smectite [001] peak is seen clearly in the random raw sample with the basal spacing value of 13.86 Å (6.37 2θ), and in the clay mineral washed sample as 13.84 Å (6.38 2θ).

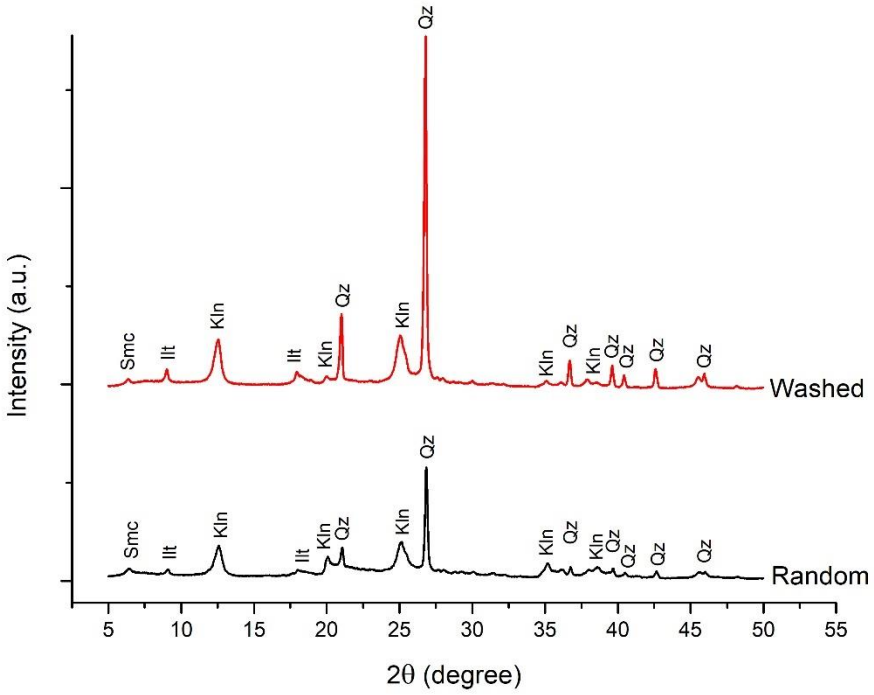

Figure 5.11. The powder X-ray diffractogram of the sample Kaolin 4, random raw and clay mineral washed samples. Kln: kaolin, Smc: smectite, Ilt: illite, Qz: Quartz

In the random raw sample, illite's [001] peak is seen as 9.72 Å (9.08 2θ), and [002] as 4.83 Å (18.32 2θ), but the [003] peak is not seen because of the quartz [101] peak like in the other samples. Kaolin's [001] peak is seen as 7.02 Å (12.58 2θ), [002] as 3.54 Å (25.1 2θ), [020] as 4.41 Å (20.11 2θ), [202] as 2.32 Å (38.61 2θ), and 2.54 Å at 35.19 2θ is also a kaolin peak. The [100] peak of quartz is seen as 4.22 Å (21.02 2θ), [101] as 3.31 Å (26.83 2θ), [110] as 2.44 Å (36.75 2θ), [102] as 2.26 Å (39.68

2θ), [200] as 2.11 Å (42.67 2θ), [201] as 1.98 Å (45.58 2θ), and 2.23 Å at 40.44 2θ is also a quartz peak.

In the clay mineral washed sample, [001] and [002] peaks of illite are seen as 9.78 Å (9.02 2θ), and 4.94 Å (17.92 2θ). Kaolin's [001] peak is seen as 7.05 Å (12.54 2θ), [002] as 3.55 Å (25.04 2θ), and [020] as 4.45 Å (19.9 2θ). The [100] peak of quartz is seen as 4.22 Å (21.01 2θ), [101] as 3.32 Å (26.79 2θ), [110] as 2.44 Å (36.67 2θ), [102] as 2.27 Å (39.6 2θ), [200] as 2.12 Å (42.58 2θ), [201] as 1.99 Å (45.49 2θ).

The quartz weight percentage is calculated as 26.1%, kaolin as 61.3%, illite as 2.5%, and smectite as 10.1% in the Kaolin 4 random raw sample by the RIR method. In the clay mineral washed sample, quartz is calculated as 51.7%, kaolin as 32.2%, and illite as 10.1%, and smectite as 6%.

In the oriented slides XRD patterns of Kaolin 4, smectite peaks are seen distorted. The wavy peak of 14.68 Å (6.02 2θ) at air dried sample is a smectite [001] peak which swelled with ethylene glycol treatment and slide a little bit to left at the EG Modified graph with a basal spacing of 17.34 Å (5.09 2θ) (Figure 5.12) (Borralleras et al., 2019; Caroll, 1970).

Illite's [001], [002], [003], and [111] peaks are seen in all the samples. In the air-dried sample, they are seen as 10.23 Å (8.63 2θ), 5.05 Å (17.53 2θ), 3.36 Å (26.47 2θ), and 4.29 Å (20.67 2θ). In the ethylene glycol sample, they are seen as 10.15 Å (8.7 2θ), 5.04 Å (17.57 2θ), 3.35 Å (26.52 2θ), and 4.28 Å (20.73 2θ). In the 300 ℃ dried sample, they are seen as 10.01 Å (8.82 2θ), 5.01 Å (17.68 2θ), 3.34 Å (26.65 2θ), and 4.26 Å (20.82 2θ). Lastly, at 550 ℃ treatment, the small peaks are expected to be illite peaks (Németh et al., 2016), they are seen as 10.2 Å (8.65 2θ), 5.04 Å (17.56 2θ), 3.36 Å (26.47 2θ), and 4.29 Å (20.67 2θ).

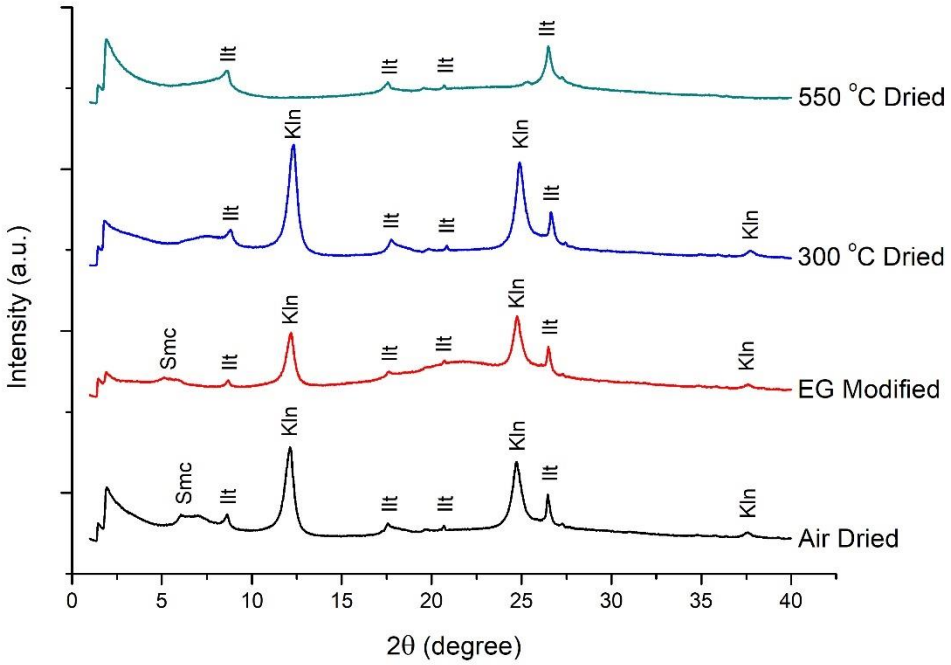

Figure 5.12. X-ray diffractogram of the oriented slides of the sample Kaolin 4. Kln: kaolin, Smc: smectite, Ilt: illite, Qz: quartz, EG: ethylene glycol

The [001] kaolin peak in the air-dried sample is seen as 7.29 Å (12.11 2θ), [002] as 3.6 Å (24.69 2θ), and [003] as 2.39 Å (37.57 2θ). In the ethylene glycol treated sample, [001] is seen as 7.26 Å (12.16 2θ), [002] as 3.59 Å (24.73 2θ), and [003] as 2.39 Å (37.57 2θ). In the 300 ℃ dried sample, [001] is seen as 7.19 Å (12.3 2θ), [002] as 3.57 Å (24.87 2θ), and [003] as 2.38 Å (37.71 2θ). And in the 550 ℃ dried sample, kaolin peaks are lost.

In the air-dried sample of Kaolin 4, kaolin is calculated as 67.7%, illite as 15.4%, and smectite as 16.9% by the RIR method.

The last sample, which is kaolin 4, shows more specific peaks of illite and smectite in the random raw and clay mineral washed XRD results (Figure 5.11). The small peaks at 6.18 and 9.72 2θ refer to smectite (Bajda et al., 2011) and illite respectively (Marsh et al., 2018). The kaolin and quartz peaks are similar to the other samples

results, and clay minerals peak intensity decreased by washing the sample numerous times while quartz peak intensity increased as expected.

In the oriented slide samples, behaviors of smectite and illite are seen clearly. Smectite swells and shifts its position with the application of ethylene glycol and shifts again closer to the illite peak by heating at 300 ℃, which is wavy (Figure 5.12) (Bajda et al., 2011; Caroll, 1970). Illite peaks are seen at 8.63 and 17.53 degrees which don't get lost by heating or change with ethylene glycol. Kaolin peaks get lost by heating with 550 ℃ (Caroll, 1970), and as a non-clay mineral, quartz didn't get affected by any of the treatments.

The SEM and energy dispersive spectroscopy (EDS) images of samples are taken. Due to small particle sizes, not all the minerals are identical, however the minerals included in the samples can be revealed with the help of EDS and XRD results of the samples.

The SEM and the EDS images of kaolin 1 are given in Figure 5.13 and Figure 5.14. Kaolin and smectite are found commonly in all the images in Figure 5.13. Silicon and aluminum mostly belong to the kaolin mineral, while magnesium and calcium come from smectite. Potassium content comes from the illite mineral in the sample. Additionally, there is a high iron oxide content in the sample (Figure 5.13 (B)). The platy form of kaolin mineral is seen in Figure 5.14 (B) and (C). Figure 5.14 (A) shows mostly kaolin minerals with platy and irregular form. Lastly, the small titanium content (Figure 5.13 (B), Figure 5.14 (B)) might come from smectite or ilmenite in the sample.

Figure 5.15 and Figure 5.16 show the SEM and EDS images of sample kaolin 2. High sulfur and iron content indicate that pyrite is present in the sample (Figure 5.15 (A, B, and C)). The magnesium and calcium content comes from smectite mineral (Figure 5.15 (D), Figure 5.16 (A)). Small amounts of potassium come from the illite mineral (Figure 5.15 (D), Figure 5.16 (A)), and small amounts of titanium (Figure 5.15 (D)) come from smectite in the sample. The platy morphology of the minerals

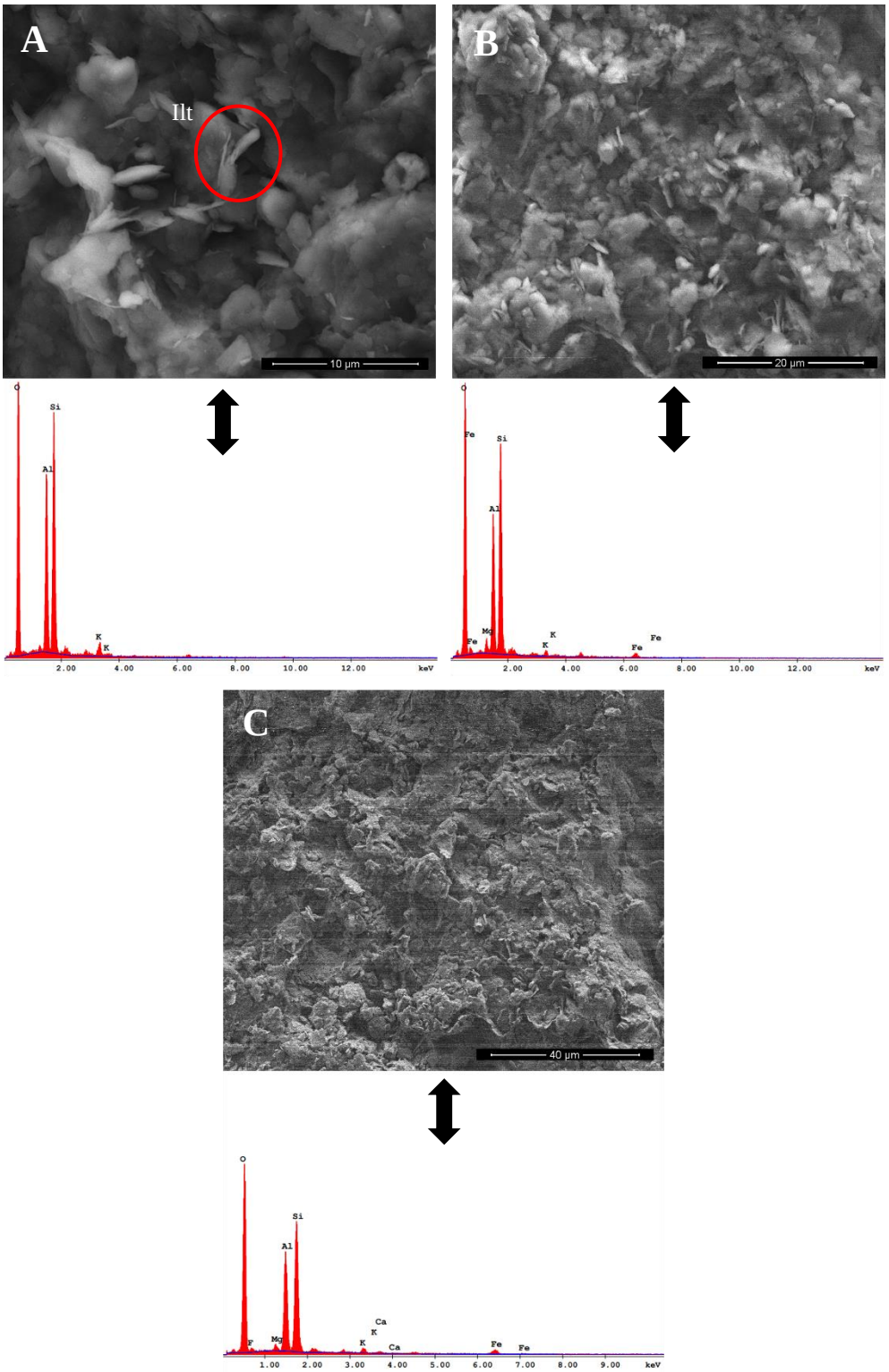

Figure 5.13. SEM and EDS images of kaolin 1. A: kaolin, illite, B: kaolin, illite, smectite, C: kaolin, smectite. Ilt: ilite

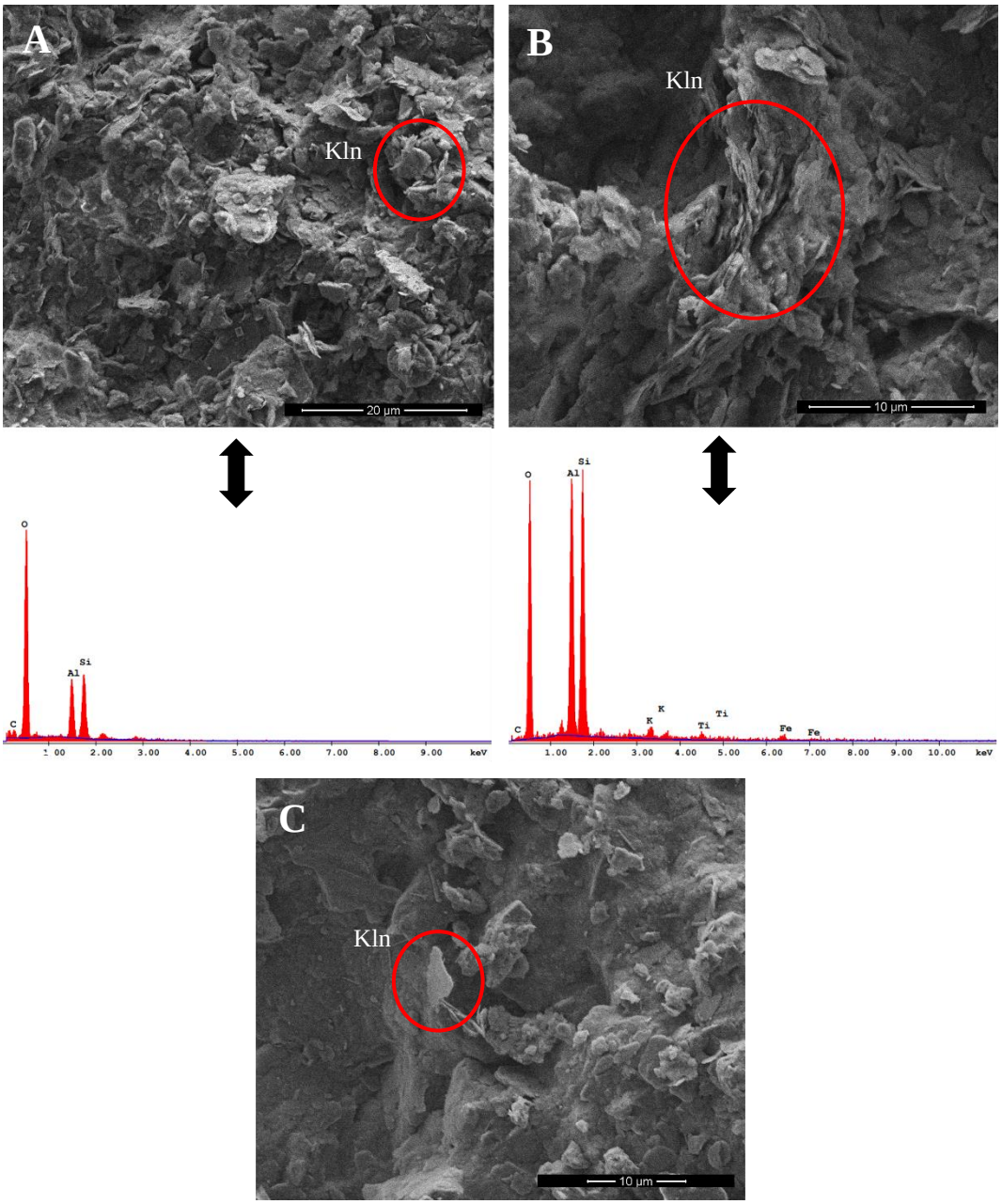

Figure 5.14. SEM and EDS images of kaolin 1. A: kaolin, B: kaolin, illite, C: platy morphology of kaolin. Kln: kaolin

is seen in Figure 5.16 (C), and low magnification SEM image of the sample shows irregular particle sizes in Figure 5.16 (B). In the Figure 5.15 (A) and (B), the higher magnification image (B) has higher silicon and aluminum, which means that pyrite should be at lower left part of the lower magnification image (A). However,

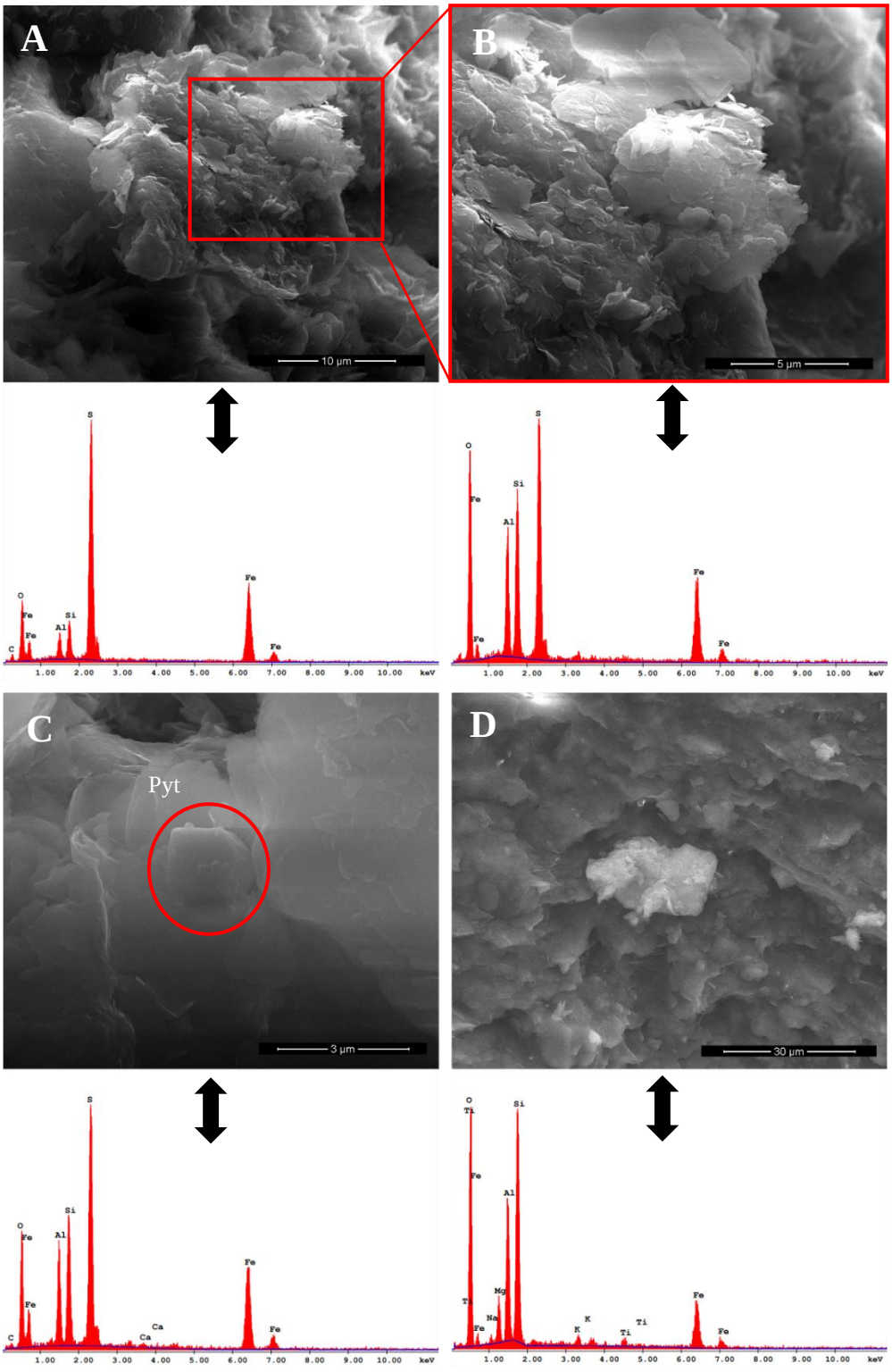

Figure 5.15. SEM and EDS images of kaolin 2. A: pyrite, kaolin, B: pyrite, kaolin, C: pyrite, kaolin, smectite, D: kaolin, smectite, illite. Pyt: pyrite

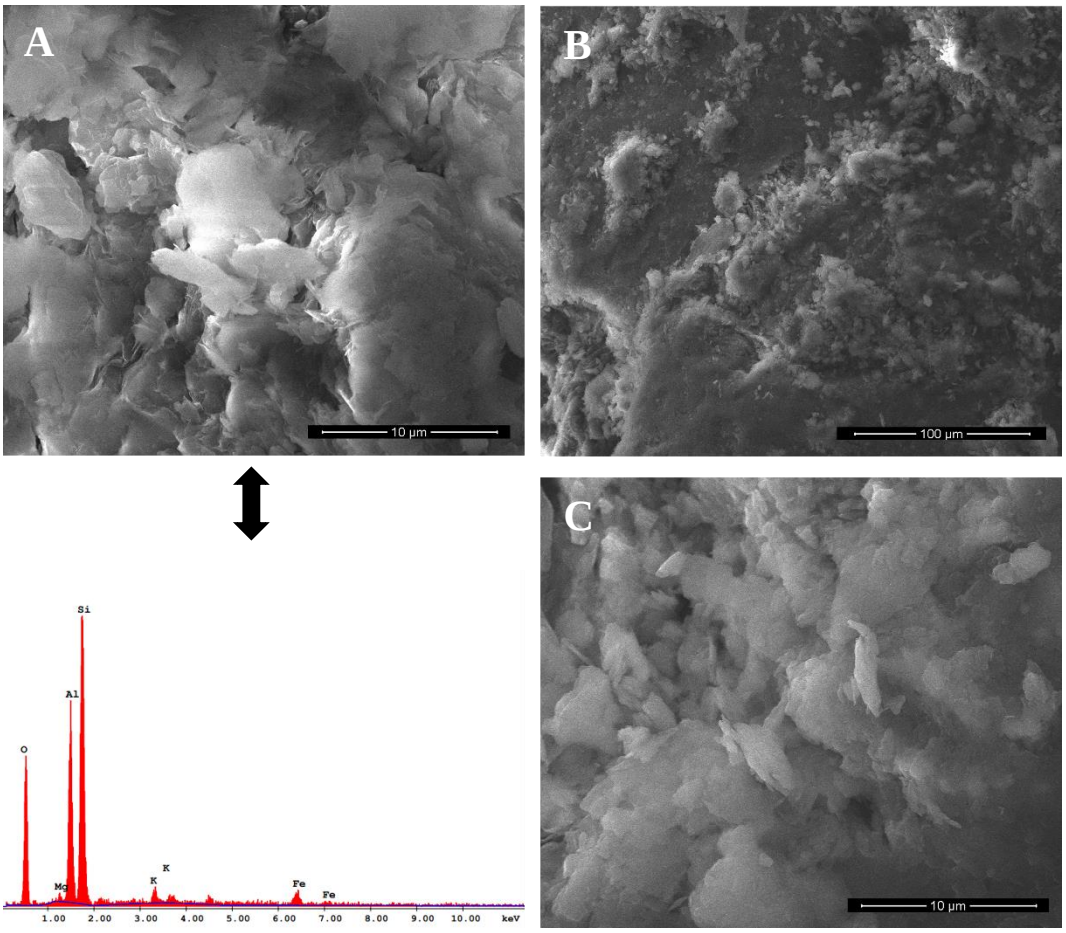

Figure 5.16. SEM and EDS images of kaolin 2. A: kaolin, smectite, illite, B: low magnification image of kaolin 2, C: platy morphology of minerals.

It is not identical due to the clay minerals covering the top of the sample, that's why the iron and sulfur content comes from the background.

Figure 5.17 shows SEM and EDS images of sample kaolin 3. The EDS images indicate that pyrite is present in the sample, due to the presence of iron and sulfur content. (Figure 5.17 (A) and (B)). However, the small iron content and high calcium and sulfur content in Figure 5.17 (C) indicates that gypsum is also present in the sample. Silicon and aluminum belong to the clay minerals of kaolin and smectite, while calcium (Figure 5.17) and magnesium (Figure 5.17 (C)) come from the smectite mineral. Potassium content seen in Figure 5.17 (B), and (C) come from illite mineral. The fine-grained particle distribution of kaolin 3 (Figure 5.17,

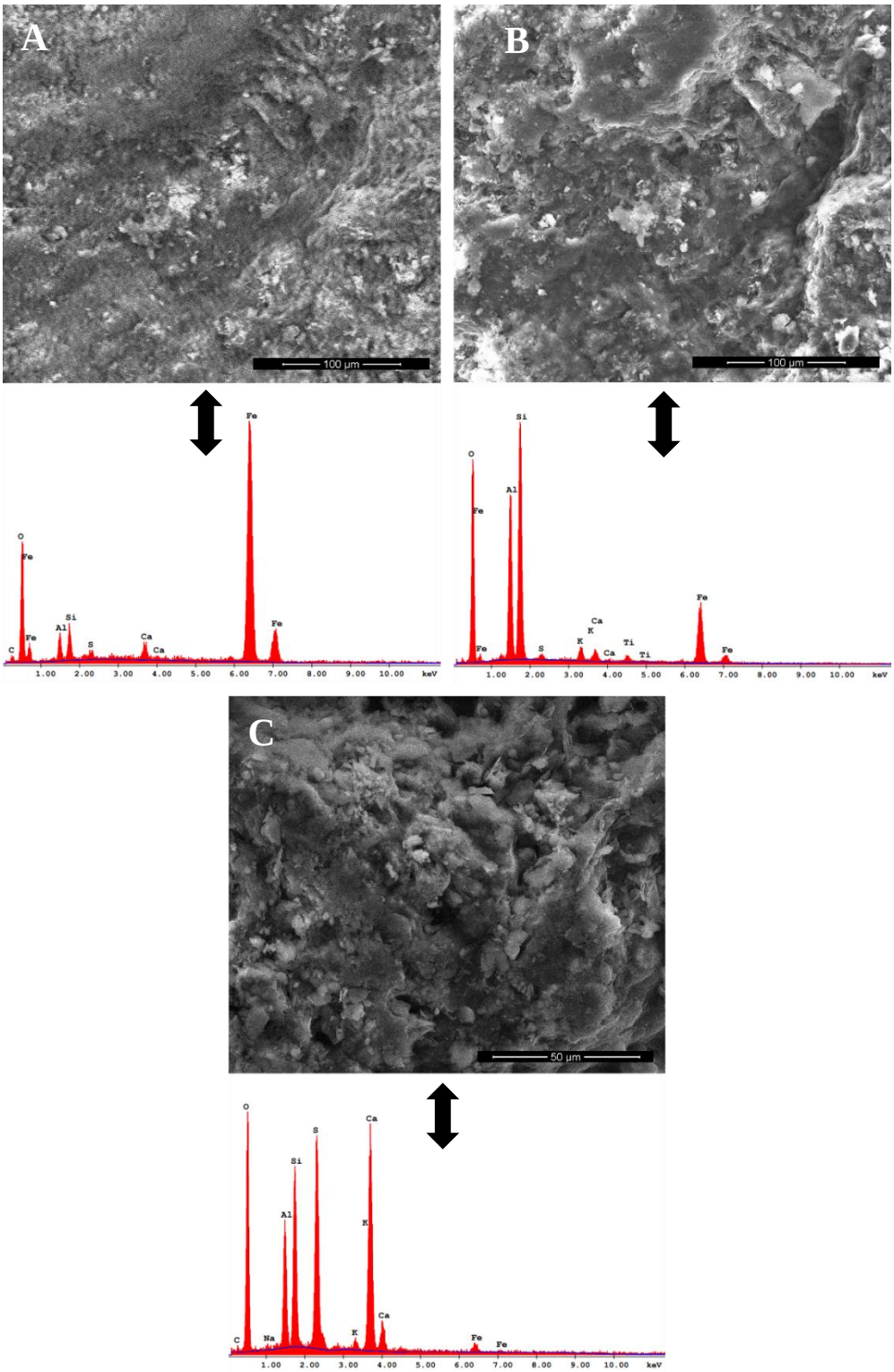

Figure 5.17. SEM and EDS images of kaolin 3. A: pyrite, kaolin, smectite, B: pyrite, kaolin, smectite, illite, C: pyrite, kaolin, smectite, illite

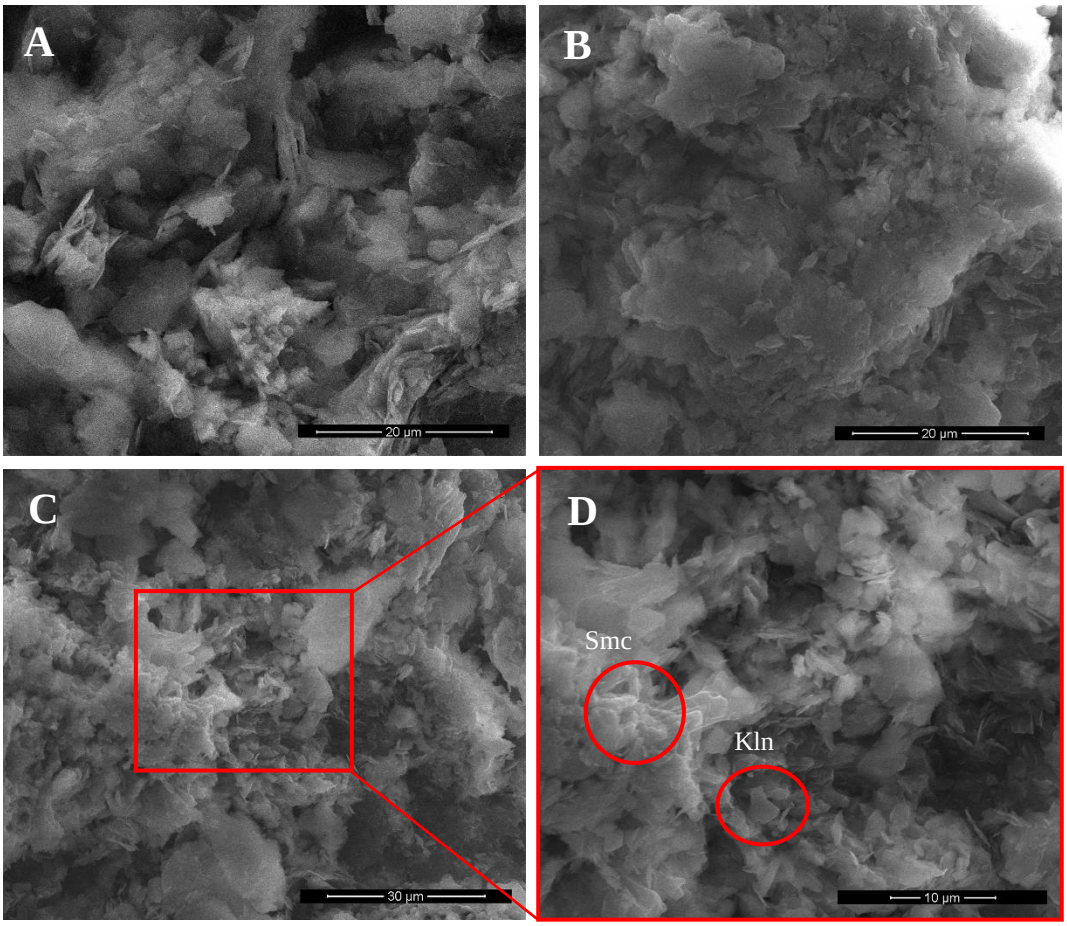

Figure 5.18. Irregular particle size distribution of kaolin 3, SEM image. Kln: kaolin, Smc: semectite

Figure 5.18) indicates that the formation of the sample is authigenic, and the crystallization is incomplete.

The SEM and EDS images of the sample kaolin 4 are shown in Figure 5.19, and Figure 5.20. The silicon and aluminum content seen in EDS images of Figure 5.19, and Figure 5.20 belong to kaolin, smectite, and illite. The high sulfur and iron content in Figure 5.19 (A) indicates that pyrite is present in the sample, and the high sulphur and calcium content seen in Figure 5.19 (B, C) indicates that gypsum is also present which means that sulfur comes from both pyrite and gypsum. However, low iron content and the absence of sulfur Figure 5.19Figure 5.20 indicates that iron content also stays as iron-oxide instead of being included in

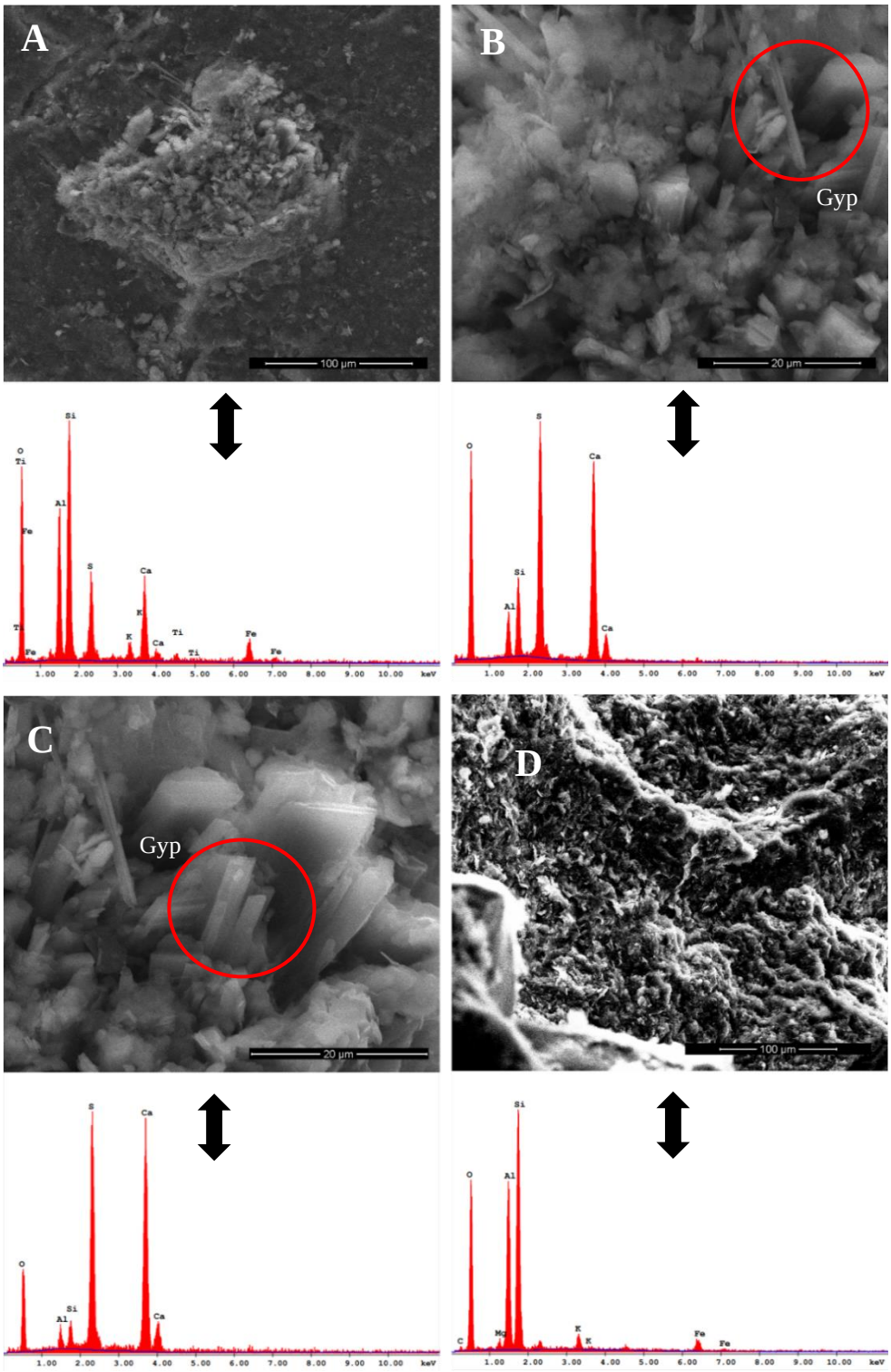

Figure 5.19. SEM and EDS images of kaolin 4. A: pyrite, kaolin, smectite, gypsum B: kaolin, gypsum, C: kaolin, smectite gypsum, D: kaolin, smectite, illite. Gyp: gypsum

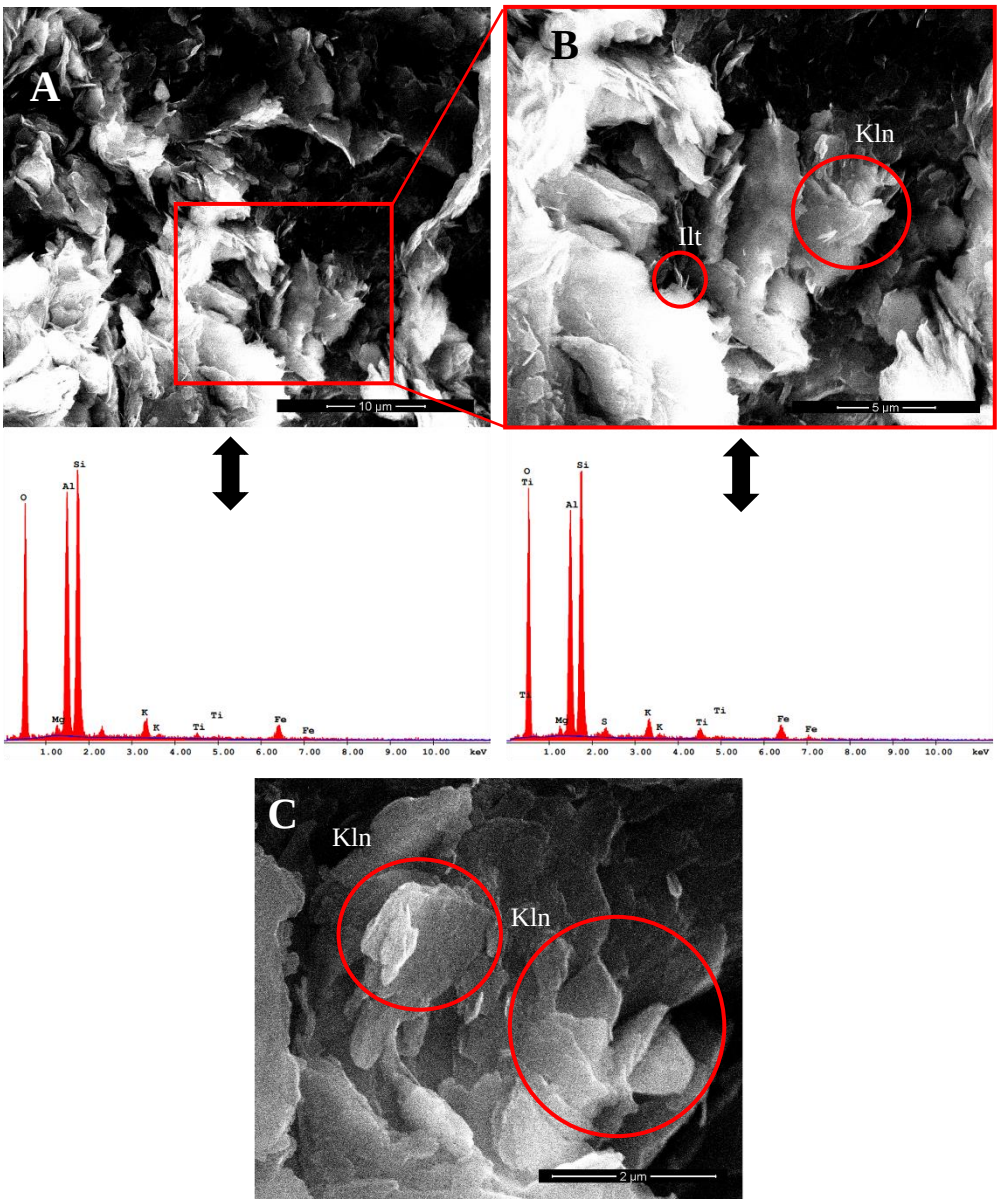

Figure 5.20. SEM and EDS images of kaolin 4. A: kaolin, smectite, illite, B: kaolin, smectite, illite, C: kaolin, illite. Kln: kaolin, Ilt: illite

pyrite and gypsum. The potassium content of the sample (Figure 5.19 (D), Figure 5.20 (B, C)) belongs to the illite mineral.

The high titanium content seen in Figure 5.19 (A), and Figure 5.20 (B) might indicate that the mineral ilmenite is also present in the sample. The platy morphology of the minerals in kaolin 4 is shown in Figure 5.20 (C).

The kaolin samples ingredients are obtained by X-Ray fluorescence to calculate the amounts needed for each kaolin sample for the synthesis of zeolite 4A, and the results are shown in Table 5.2.

Table 5.2. X-Ray Fluorescence results of kaolin samples (oxide compositions weight% of the samples)

Wt%	Kaolin 1	Kaolin 2	Kaolin 3	Kaolin 4
SiO_2	62.26	56.25	58.47	56.02
Al_2O_3	28.97	29.27	31.58	32.46
Na_2O	0.13	0.12	0.16	0.14
K_2O	2.16	1.80	2.00	2.37
Fe_2O_3	2.50	4.39	4.40	4.31
TiO_2	1.88	1.44	1.67	1.57
CaO	0.53	1.28	0.47	0.24
MgO	0.81	1.08	0.68	0.87
SO_3	0.59	4.22	0.27	1.63
Total	99.83	99.85	99.70	99.61
Si/Al ratio	1.82	1.63	1.57	1.46

As seen in Table 5.2, the value of silicon-aluminum ratios of the kaolin samples are close to 1 which is an advantage for zeolite 4A synthesis. The ideal kaolin has a chemical ratio of 46.54% SiO_2, 39.5% Al_2O_3, and 13.96% H_2O (Gougazeh, 2018), but it is not possible to find such kaolin in nature. The possible impurities in kaolin are usually quartz, feldspar, muscovite, biotite, titanium oxides, and iron oxides (Ramaswamy & Raghavan, 2011). According to Table 5.2, there are iron impurities in each kaolin sample. For industrial use, iron content is wanted to be less than 1% (Gougazeh, 2018; Zegeye et al., 2013). The iron content in these kaolin samples is enough for making it gangue kaolin, and there is also quartz impurity in all the samples which will be mentioned in the following XRD results of the samples. Additionally, there is also titanium (TiO_2) and potassium (K_2O) impurities less than iron impurity. The iron and sulfur content in the samples come from pyrite (Çelik et al., 2017).

The clay and non-clay amounts of kaolin samples were calculated after the siphoning process, and the calculated amounts are shown in Table 5.3. The highest clay content is found in the sample kaolin 2, followed by kaolin 4, kaolin 3, and lastly kaolin 1. The samples with higher clay content are expected to give better results for zeolite crystallization.

Table 5.3. Weight amount of clay and non-clay content of kaolin samples

Weight in 10 grams	Kaolin 1	Kaolin 2	Kaolin 3	Kaolin 4
Clay	5.763	8.267	6.59	7.892
Non-Clay	4.237	1.733	3.41	2.108

According to Table 5.3, the samples kaolin 2 and 4 have a high clay content, which may result in giving the best results for zeolite crystallization. The sample kaolin 3 is coming after the second and fourth samples in clay content. Kaolin 1 has the lowest clay content and the highest Si/Al ratio which means that the silicon of the sample might be included in the quartz.

5.2 Results of Zeolite Synthesis

Results for the zeolite syntheses with different methods are shown in this section.

5.2.1 Results of Zeolite Synthesis with Metakaolinization Method

The first route is taking only the kaolin samples into the furnace to heat them for the rest of the synthesis process. This step is called metakaolinization. With this method, the kaolin samples were added to the other laboratory chemicals in high-density polyethylene (HDPE) bottles after the heat was applied, then DI water is added to the solid mixture for the rest of the synthesis. Different levels of temperature were

applied for the metakaolinization method for examining the effect of heat on the synthesis results.

The results of the experiments with the metakaolinization method are discussed with XRD and SEM analysis. To begin with the first sample, kaolin 1, XRD results are shown in Figure 5.21. In this figure, products of the same synthesis process with different calcination temperatures are shown.

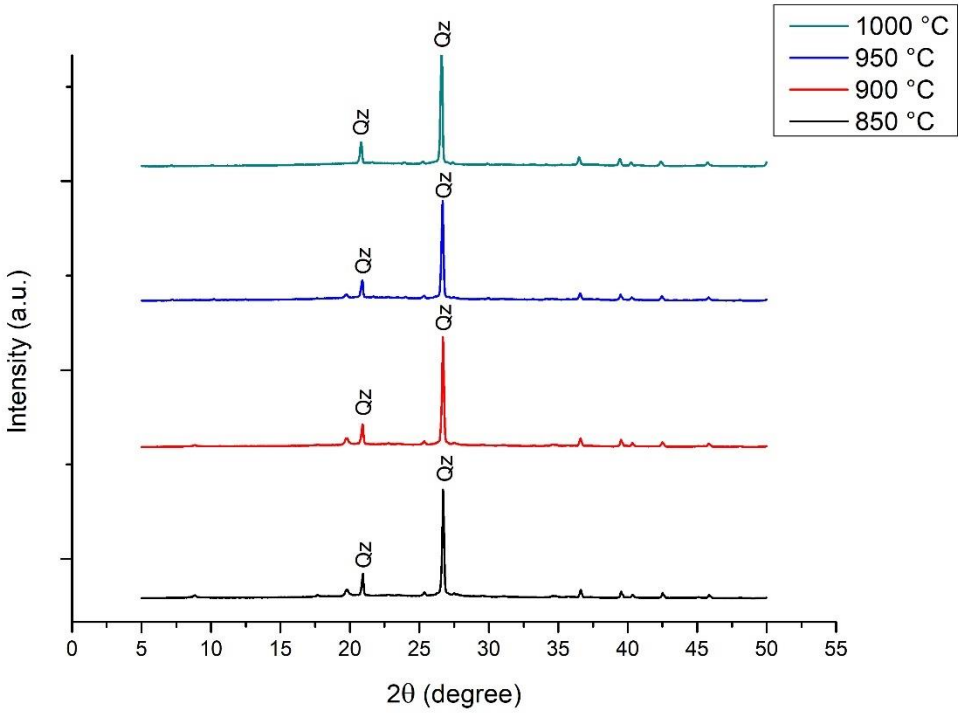

Figure 5.21. XRD patterns of the zeolite synthesis with the sample Kaolin 1 by using metakaolinization method at calcination temperatures of 850 ℃, 900 ℃, 950 ℃, and 1000 ℃. Qz: quartz

In Figure 5.21, XRD results show that there is no crystallization occurs with kaolin 1 metakaolinization method even at high temperatures, and structure of quartz didn't get disturbed with increasing temperature. The [100] and [101] peaks of quartz are seen in all the synthesis results.

The SEM images of the same products in Figure 5.22 support the idea that there is no cubic crystals of zeolite 4A occurred. At the 950 ℃ calcination synthesis product, it looks like there are some small crystals that occurred somehow, but the XRD result of that synthesis can't show it if the percentage of the synthesized crystals is lower than 5%. Figure 5.21 shows that the synthesis product of 950 ℃ calcination has the same patterns as the other uncrystallized products.

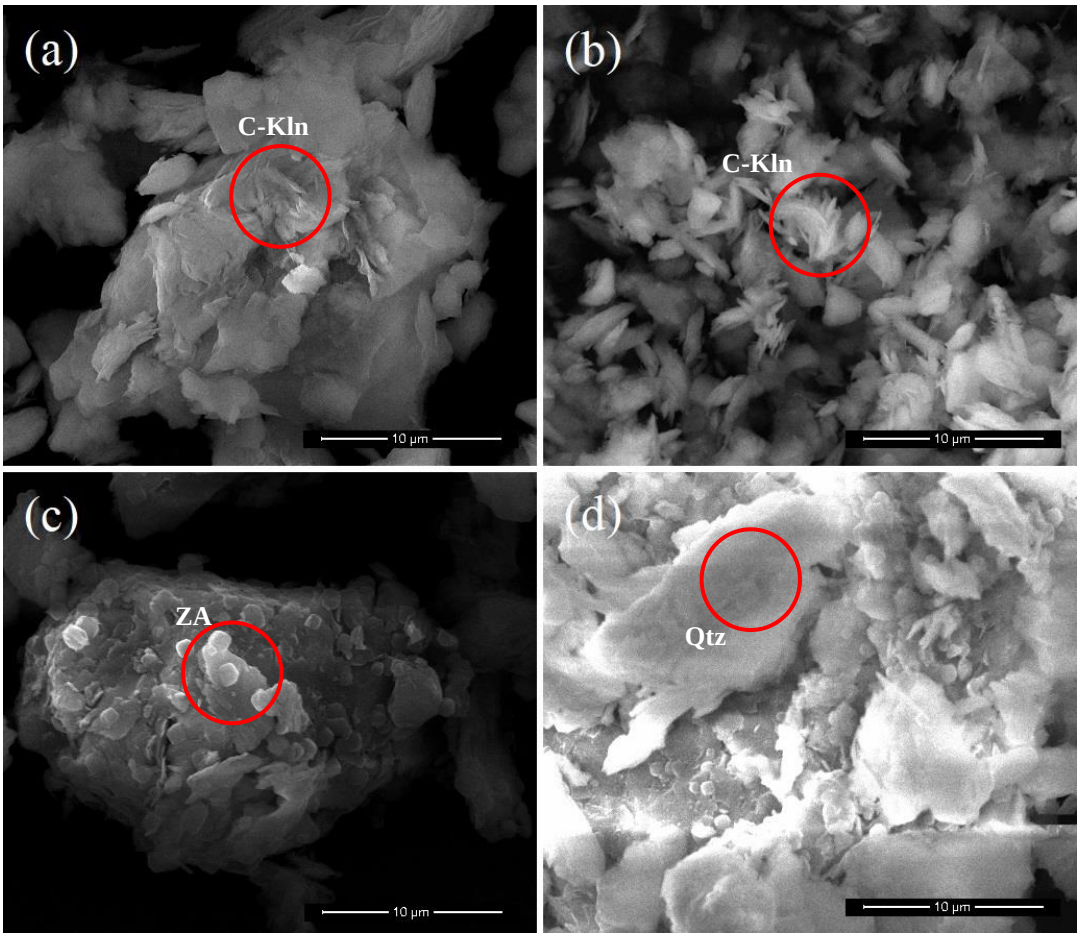

Figure 5.22. SEM images of the zeolite synthesis products from Kaolin 1 with metakaolinization method at calcination temperatures of (a) 850 ℃, (b) 900 ℃, (c) 950 ℃, (d) 1000 ℃. C-Kln: calcined kaolin, Qtz: quartz, ZA: zeolite 4A

The XRD results of synthesis products with the metakaolinization method using Kaolin 2 are shown in Figure 5.23. The [100] and [101] peaks of quartz are seen in

all products. The [200], [220], [222] and [420] peaks of zeolite 4A are seen as 12.23 Å (7.23 2θ), 8.67 Å (10.19 2θ), 7.08 Å (12.48 2θ), 5.50 Å (16.12 2θ) in the 900 ℃ synthesis product, 12.29 Å (7.18 2θ), 8.7 Å (10.15 2θ), 7.10 Å (12.45 2θ), 5.50 Å (16.10 2θ) in the 950 ℃ synthesis product, and 11.89 Å (7.43 2θ), 8.50 Å (10.4 2θ), 6.96 Å (12.70 2θ), and 5.42 Å (16.33 2θ) in the 1000 ℃ synthesis product respectively.

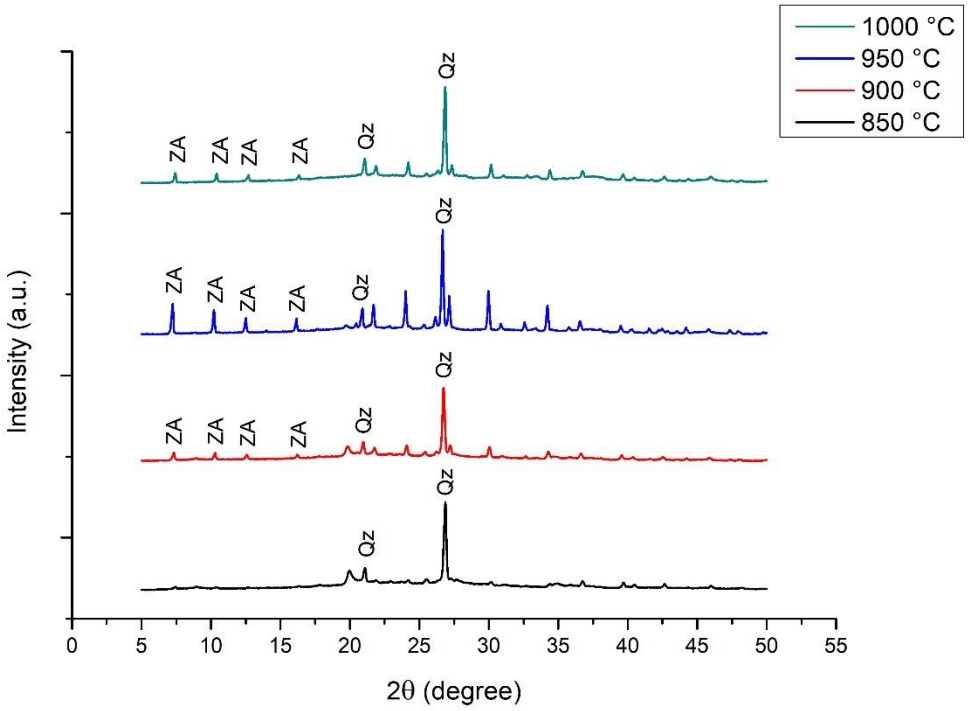

Figure 5.23. XRD patterns of the zeolite synthesis with the sample Kaolin 2 by using metakaolinization method at calcination temperatures of 850 ℃, 900 ℃, 950 ℃, and 1000 ℃. Qz: quartz, ZA: zeolite 4A

Synthesis products with the metakaolinization method using kaolin 2 XRD results in Figure 5.23 show that crystallization occurred best at the calcination temperature of 950 ℃ compared to other calcination temperature synthesis products. The other synthesis products do not show sufficient crystallization, while the product of 850 ℃ calcination temperature shows no evidence for crystallization occurred.

The SEM images of the same products show some unexpected results except for the 850 ℃ calcination temperature synthesis product when their XRD patterns are considered, because XRD results do not show some strong evidence for the zeolite 4A crystals occurred in the other products.

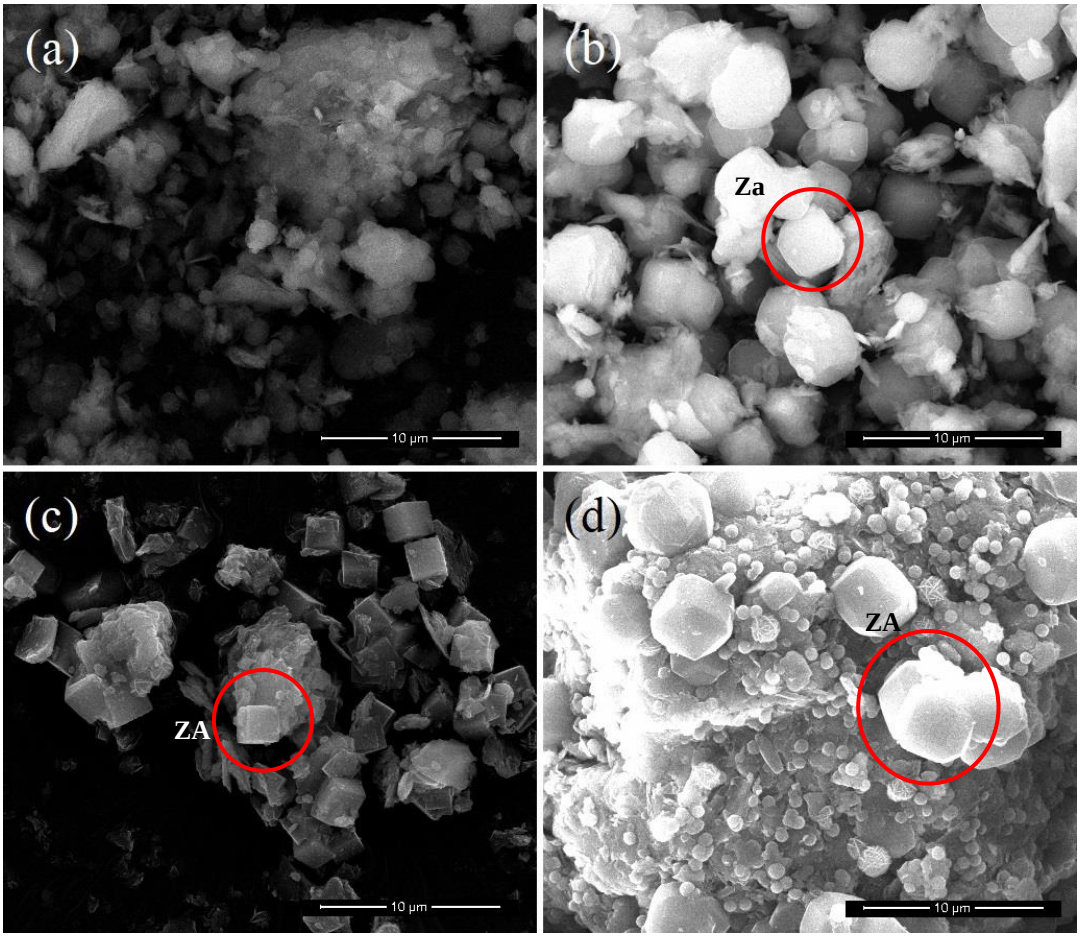

Figure 5.24. SEM images of the zeolite synthesis products from Kaolin 2 with metakaolinization method at calcination temperatures of (a) 850 ℃, (b) 900 ℃, (c) 950 ℃, (d) 1000 ℃. ZA: zeolite 4A

As seen in Figure 5.24, zeolite crystals didn't occur only in synthesis with 850 ℃. The other products show cubic zeolite 4A crystals. Figure 5.23 shows that the best crystallization occurred at synthesis with 950 ℃ calcination temperature, and in the

SEM images in Figure 5.24, the 950 ℃ synthesis product crystals show the sharpest crystal edges.

XRD results in Figure 5.25 show that crystallization occurred in both temperatures of 850 and 900 ℃ by using kaolin 3, but the structure of quartz is not disturbed which is seen at 20.85 and 26.63 2θ in both results. This indicates that, although the quartz didn't get disturbed and the silicon content of it couldn't properly get into the system, the zeolite crystals occurred. That means if the quartz was broken and the silicon content in it could be used properly, better crystallization would occur.

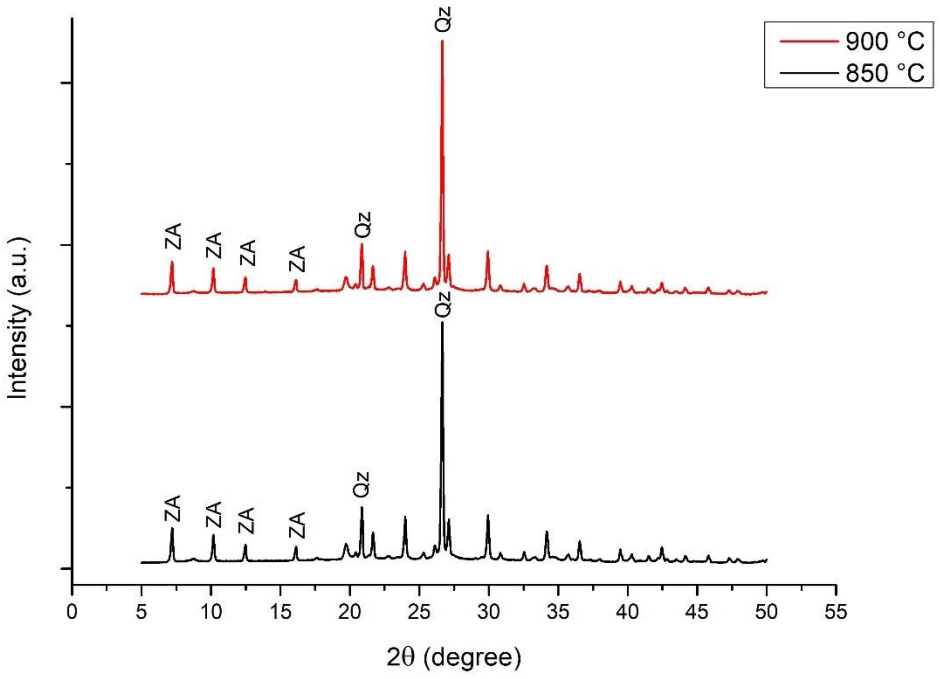

Figure 5.25. XRD patterns of the zeolite synthesis with the sample Kaolin 3 by using metakaolinization method at calcination temperatures of 850 ℃, 900 ℃. Qz, quartz, ZA: zeolite 4A

The zeolite 4A crystals [200], [220], [222], and [420] peaks are seen as 12.26 Å (7.20 2θ), 8.70 Å (10.17 2θ), 7.09 Å (12.48 2θ), and 5.50 (16.10 2θ) at 850 ℃, and 12.28

Å (7.19 2θ), 8.70 Å (10.16 2θ), 7.10 Å (12.45 2θ), and 5.51 Å (16.08 2θ) at 950 ℃ synthesis XRD results respectively.

As seen from the SEM images of synthesis products by metakaolinization method using kaolin 3 from Figure 5.26, cubic zeolite crystals occurred, and there are no major differences between the two different calcination temperatures products in both their sizes and roundness. This is an expected result when considering the XRD results of the products.

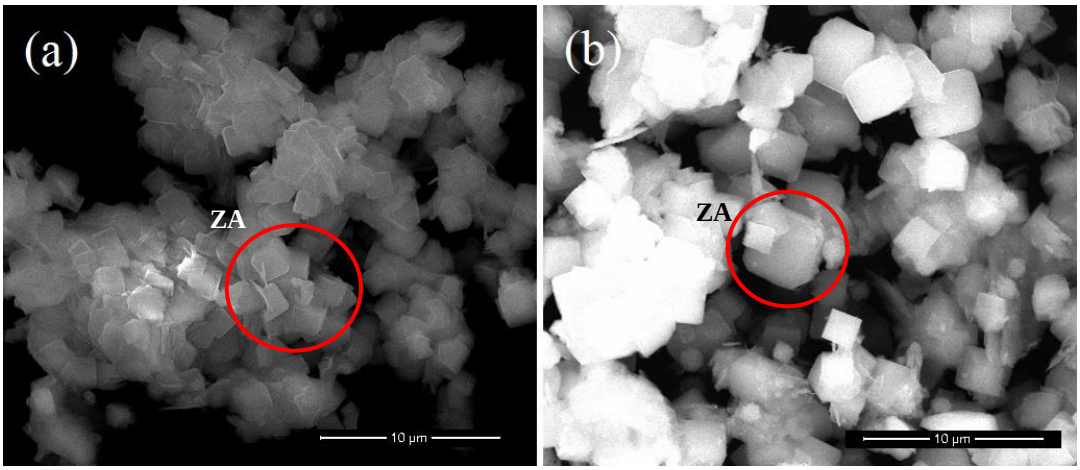

Figure 5.26. SEM images of the zeolite synthesis products from Kaolin 3 with metakaolinization method at calcination temperatures of (a) 850 ℃, (b) 900 ℃. ZA: zeolite 4A

The reason for not trying other calcination temperatures for the synthesis is because there are no major differences between the products, and the crystallization occurred in both syntheses unlike in the first two samples of kaolin.

The XRD results of the synthesis products by metakaolinization method using kaolin 4 in figure Figure 5.27 shows that crystallization occurred in both temperatures of 850 and 900 ℃, which doesn't show some difference from each other. Moreover, kaolin sample 4 gives the best results for crystallinity compared to other kaolin samples synthesis products with the metakaolinization method. The [101] peak of quartz is still present at 26.63 2θ in both products, but zeolite 4A is clearly observable in both.

The [200], [220], [222], and [420] peaks of zeolite 4A are seen as 12.29 Å (7.19 2θ), 8.68 Å (10.18 2θ), 7.10 Å (12.46 2θ), and 5.50 (16.11 2θ) at 850 ℃, and 12.30 Å (7.18 2θ), 8.70 Å (10.16 2θ), 7.10 Å (12.45 2θ), and 5.50 Å (16.09 2θ) at 950 ℃ syntheses XRD results respectively which are almost same with each other.

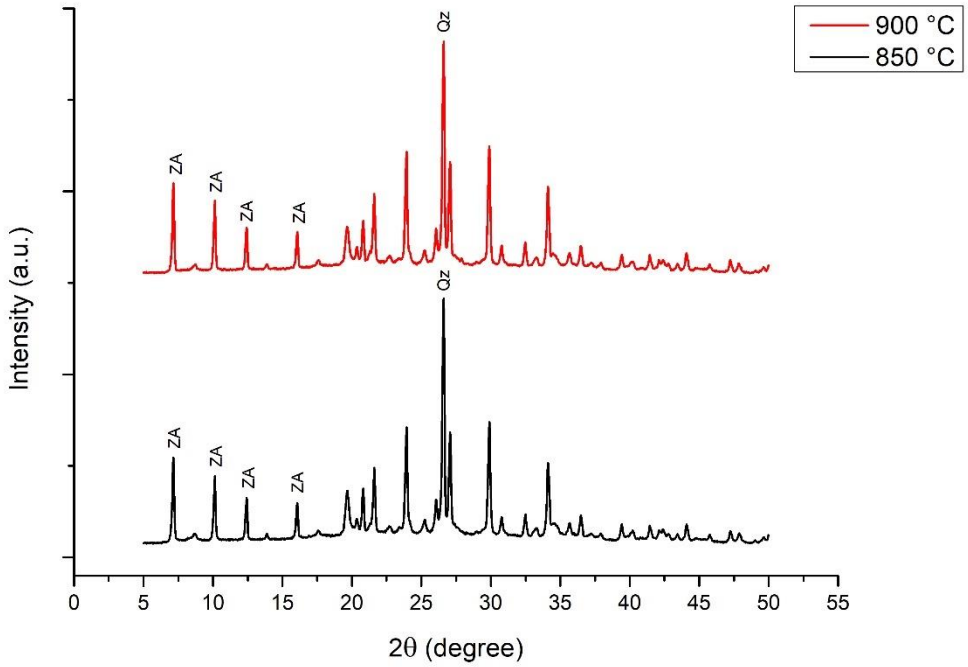

Figure 5.27. XRD patterns of the zeolite synthesis with the sample Kaolin 4 by using metakaolinization method at calcination temperatures of 850 ℃, 900 ℃. Qz: quartz, ZA: zeolite 4A

The SEM images of the synthesis products done by kaolin 4 in Figure 5.28 show that the cubic crystals of zeolite 4A were formed, and there is no big difference between the products of different calcination temperatures, which is supported by the XRD results too. The best results are taken by the kaolin 4 when compared to others by both XRD and SEM images.

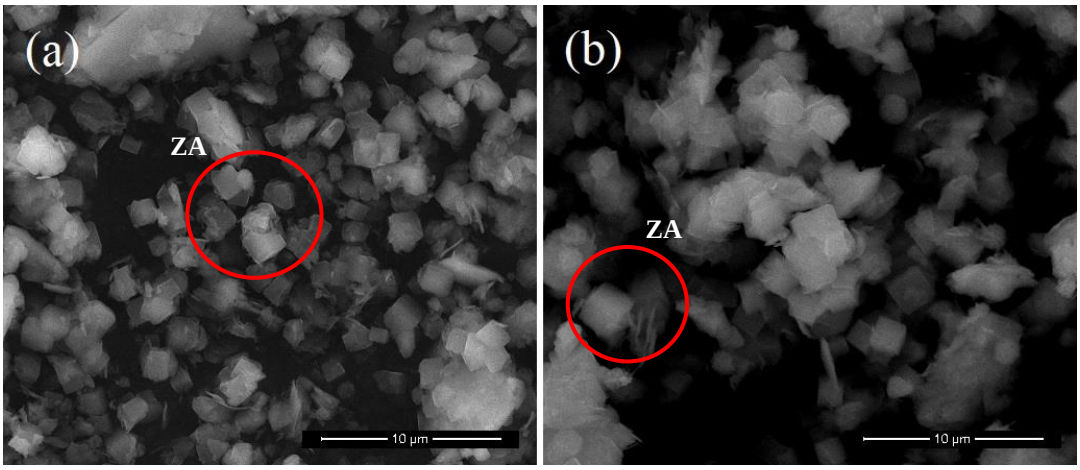

Figure 5.28. SEM images of the zeolite synthesis products from Kaolin 4 with metakaolinization method at calcination temperatures of (a) 850 °C, (b) 900 °C. ZA: zeolite 4A

5.2.2 Results of Zeolite Synthesis with One-Pot Fusion Method

The second route is to mix the kaolin samples with other necessary laboratory chemicals before being taken into the furnace for heat treatment, and this step is called fusion. In the fusion method, only DI water is added to the mixture in HDPE bottles after the heat treatment for the rest of the process. Different levels of temperature were also applied for the fusion route to see the effect of heat with this method. The advantage of the fusion method is it creates an alkali medium if there is any OH source used in it, which makes the aluminum source get in the system during heat treatment.

There are two different sodium sources used in synthesis with the One-Pot fusion method, which are sodium hydroxide (NaOH) and sodium carbonate (Na_2CO_3). The synthesis procedure and the aluminum source are the same for both sodium sources, and the results are shown in the following sections.

5.2.2.1 Results of Zeolite Synthesis with One-Pot Fusion Method by Using NaOH

In literature, NaOH is used regularly in synthesizing zeolite 4A with kaolin (Otieno et al., 2019; P. Wang et al., 2020), because NaOH is an effective reagent for the aluminum to get in the system in producing zeolite, otherwise, crystallization might not occur properly as it is seen in the metakaolinization method.

As it is seen from Figure 5.29, XRD results of products of zeolite synthesis done by one pot fusion method using NaOH with sample kaolin 1, the crystallization occurred well in both fusion temperatures. The results show that two types of zeolite crystals, which are zeolite 13X and zeolite 4A, were formed in the syntheses.

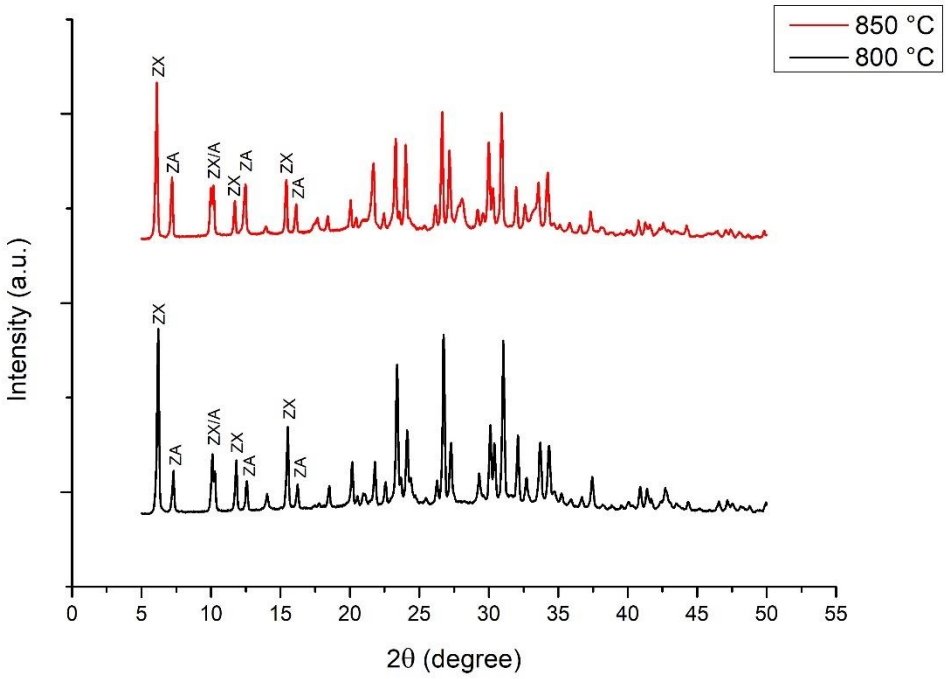

Figure 5.29. XRD patterns of the zeolite synthesis with the sample Kaolin 1 by one-pot Fusion method using NaOH at fusion temperatures of 800 ℃, and 850 ℃. ZA: zeolite 4A, ZX: zeolite 13X

The [111], [311], and [331] peaks of zeolite 13X are seen as 14.20 Å (6.22 2θ), 7.47 Å (11.83 2θ), and 5.70 Å (15.53 2θ) at 800 ℃, and 14.45 Å (6.11 2θ), 7.55 Å (11.71 2θ), and 5.75 Å (15.40 2θ) at 850 ℃ respectively.

The [200], [222], and [420] peaks of zeolite 4A are seen as 12.1 Å (7.29 2θ), 7.03 Å (12.57 2θ), and 5.50 Å (16.10 2θ) at 800 ℃, and 12.29 Å (7.18 2θ), 7.10 Å (12.47 2θ), and 5.50 Å (16.10 2θ) 850 ℃ synthesis XRD results respectively.

The [220] peaks of both zeolite 13X and 4A overlap each other in both results which are seen at 10.13 2θ.

There is a small difference between these two syntheses. The characteristic [111] peak of zeolite 13X and [200] peak of zeolite 4A changed in intensity (Purna Chandra Rao et al., 2006). The intensity of zeolite 4A increased with increasing fusion temperature as it is seen, but zeolite 13X is still the main product in these two syntheses.

The SEM images of the synthesis of the one-pot fusion method by using NaOH show that cubic crystals of zeolite 4a and zeolite 13X with different morphologies were formed well together as expected from XRD results. Zeolite 13X's crystal shape has more corners than zeolite 4A's crystal, and they have the same crystal size as seen in Figure 5.30.

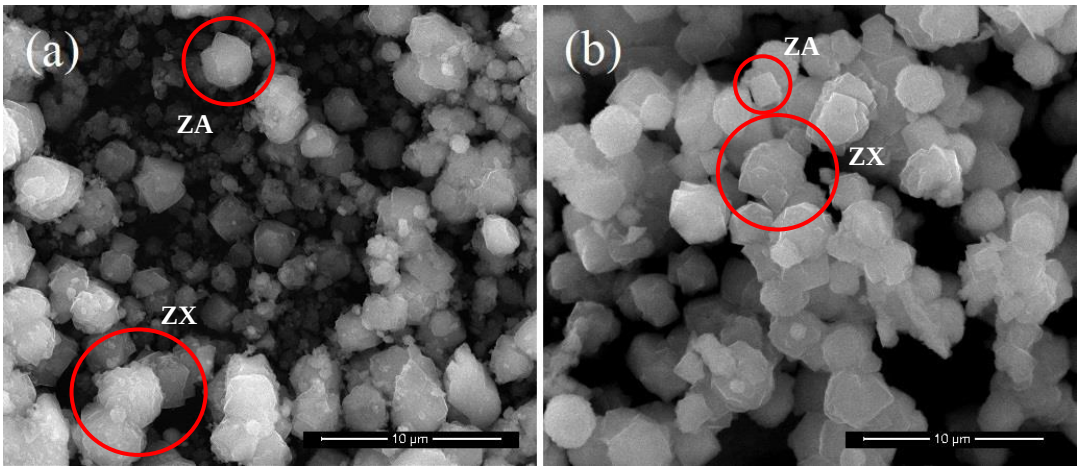

Figure 5.30. SEM images of the zeolite synthesis products from Kaolin 1 with one-pot fusion method using NaOH at calcination temperatures of (a) 800 ℃, (b) 850 ℃. ZA: zeolite 4A, ZX: zeolite 13X

The XRD results of synthesis products done by NaOH one-pot fusion method using kaolin 2 in Figure 5.31 shows that crystallization occurred in both fusion temperatures of 800 and 850 ℃.

The [111], [311], and [331] peaks of zeolite 13X are seen as 14.18 Å (6.22 2θ), 7.47 Å (11.83 2θ), and 5.70 Å (15.54 2θ) at 800 ℃ respectively, but can't be seen clearly at 850 ℃ synthesis result.

The [200], [222], and [420] peaks of zeolite 4A are seen as 12.09 Å (7.31 2θ), 7.02 Å (12.59 2θ), and 5.45 Å (16.24 2θ) at 800 ℃, and 12.25 Å (7.21 2θ), 7.10 Å (12.47 2θ), and 5.50 Å (16.11 2θ) 850 ℃ synthesis XRD results respectively. Additionally, the [220] peak is also seen as 8.68 Å (10.18 2θ) 850 ℃ synthesis.

The [220] peaks of both zeolite 13X and 4A overlap each other in the 800 ℃ synthesis result which is seen at 10.19 2θ.

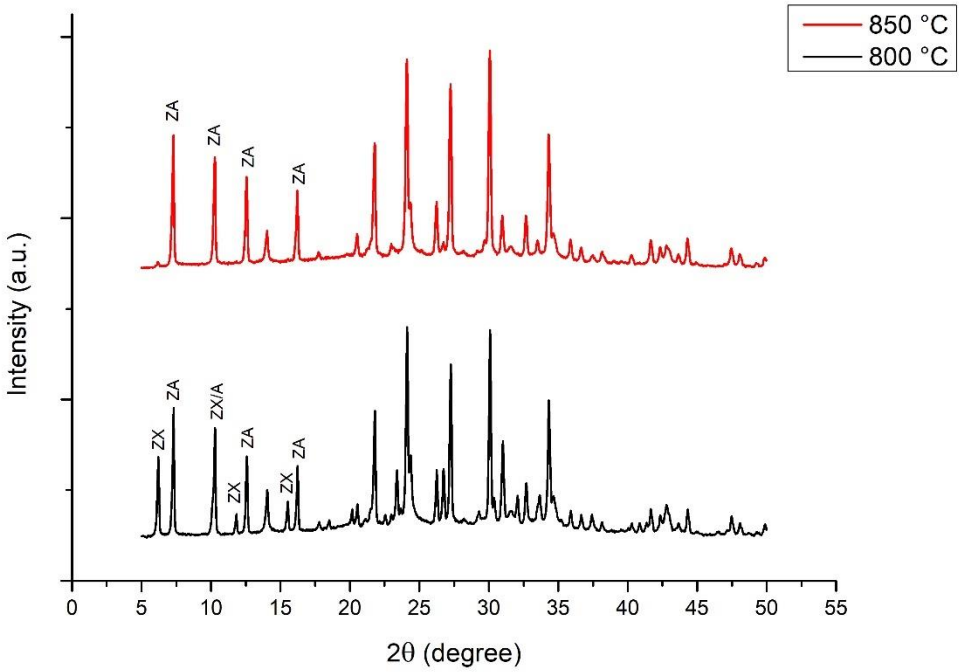

Figure 5.31. XRD patterns of the zeolite synthesis with the sample Kaolin 2 by one-pot fusion method using NaOH at fusion temperatures of 800 ℃, and 850 ℃. ZA: zeolite 4A, ZX: zelite 13X

The main peaks for zeolite 13X and zeolite 4A are seen at the 800 ℃ fusion product (Sowunmi et al., 2018). With the increasing fusion temperature, zeolite 13X peaks intensity decreased much and the main product becomes zeolite 4A (Ugal et al., 2010) at synthesis with 850 ℃ fusion temperature according to XRD results. But there might still be a little amount of zeolite 13X at 850 ℃ synthesis product.

The SEM images of the products do not show some big differences from each other. Zeolite 13X and zeolite 4A crystals are seen in both images in Figure 5.32. The cubic crystals in both images are zeolite 4A crystals while the others with more corners refer to zeolite 13X crystals.

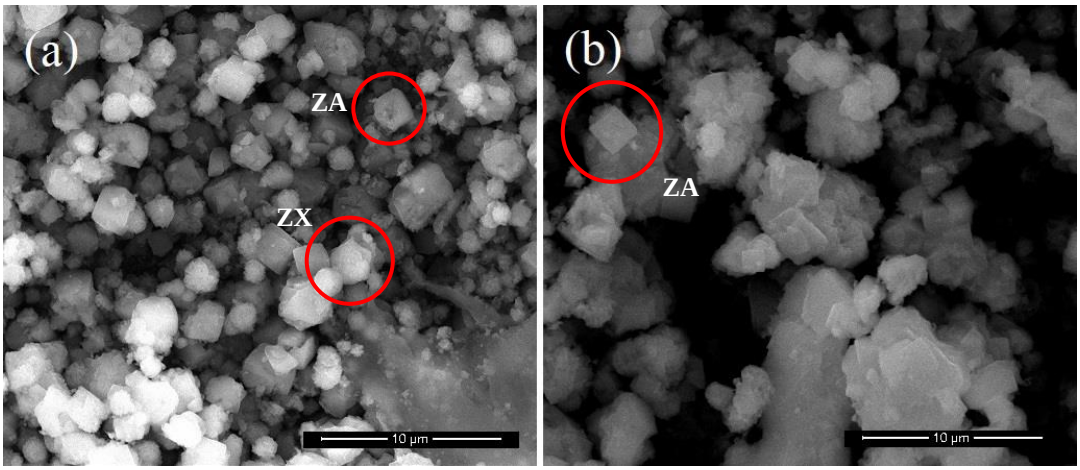

Figure 5.32. SEM images of the zeolite synthesis products from Kaolin 2 with one-pot fusion method using NaOH at calcination temperatures of (a) 800 ℃, (b) 850 ℃. ZA: zeolite 4A, ZX: zeolite 13X

The amount of zeolite 4A crystals increased at 850 ℃ synthesis product relative to 13X crystals as expected from XRD results. Although the XRD result of the 850 ℃ fusion synthesis product shows good crystallinity, there are some uncrystallized products seen in its SEM image. However, crystallization occurred obviously in both products considering XRD results.

The XRD images of synthesis products of NaOH one-pot fusion method with kaolin 3 in Figure 5.33 shows some different patterns in different temperatures of 800 and 850 ℃ fusion temperatures when compared to other synthesis products using other kaolin samples.

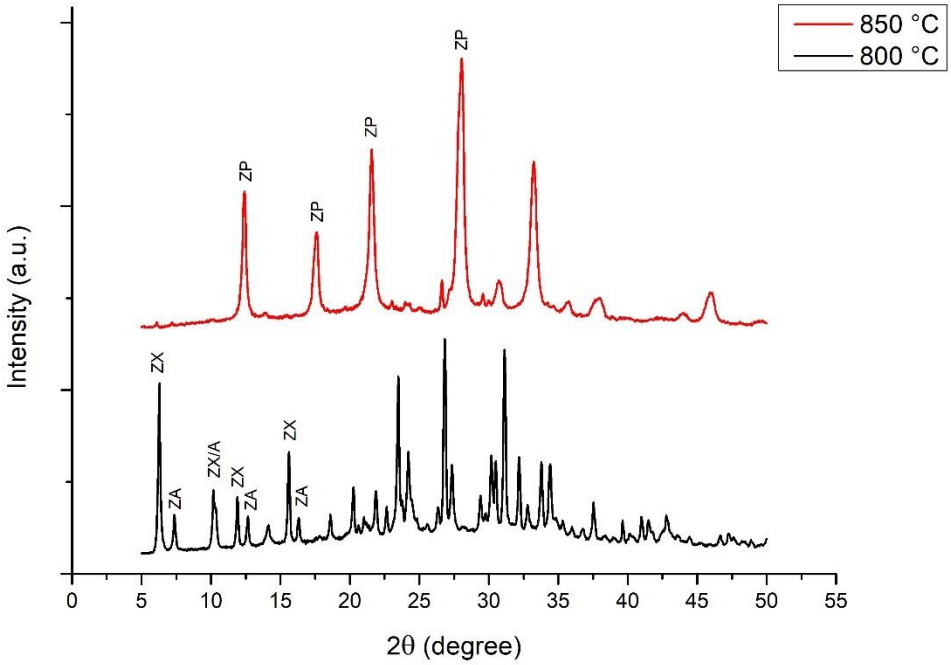

Figure 5.33. XRD patterns of the zeolite synthesis with the sample Kaolin 3 by one-pot fusion method using NaOH at fusion temperatures of 800 ℃, and 850 ℃. ZA: zeolite 4A, ZP: zeolite P, ZX: zeolite 13X

The crystallization obviously occurred in both fusion temperatures. At 800 ℃ fusion product, the main peaks of zeolite 13X and zeolite 4A are seen as the first two peaks respectively, which means that both are formed with the synthesis. But the 850 ℃ fusion product shows totally different patterns.

The [111], [311], and [331] peaks of zeolite 13X are seen as 14.02 Å (6.30 2θ), 7.42 Å (11.91 2θ), and 5.67 Å (15.61 2θ) at 800 ℃ respectively, but can't be seen clearly at 850 ℃ synthesis result.

The [200], [222], and [420] peaks of zeolite 4A are seen as 12.01 Å (7.35 2θ), 6.99 Å (12.65 2θ), and 5.43 Å (16.30 2θ) at 800 ℃ synthesis result while it's not present at 850 ℃ synthesis result.

The [220] peaks of both zeolite 13X and 4A overlap each other in the 800 ℃ synthesis result which is seen at 10.25 2θ.

The 850 ℃ fusion product created another zeolite type named zeolite P. As seen from Figure 5.33, the bottom of the peaks at 850 ℃ are wider than the 800 ℃ synthesis XRD pattern. Zeolite P has wider peaks when compared to zeolite 4A and zeolite 13X, which is the main way for distinguishing zeolite P, especially from 4A and 13X (Azizi et al., 2013; Eiad-Ua et al., 2018).

The [101], [200], [112], and [301] peaks of zeolite P are seen as 7.13 Å (12.41 2θ), 5.03 Å (17.62 2θ), 4.12 Å (21.55 2θ), and 3.18 Å (28.06 2θ) at 850 ℃ synthesis result while it's not present at 800 ℃ synthesis.

The SEM images (Figure 5.34) of the synthesis products show that the main type of zeolite that occurred at 800 ℃ fusion is zeolite 13X instead of zeolite 4A, which is expected considering the XRD results. The morphology of zeolite 13X is more spherical compared to zeolite 4A, however it still has edges. Although zeolite 4A crystals are not seen easily in Figure 5.34 a, the XRD results show zeolite 4A patterns, which means that zeolite 4A is a competing product in this synthesis.

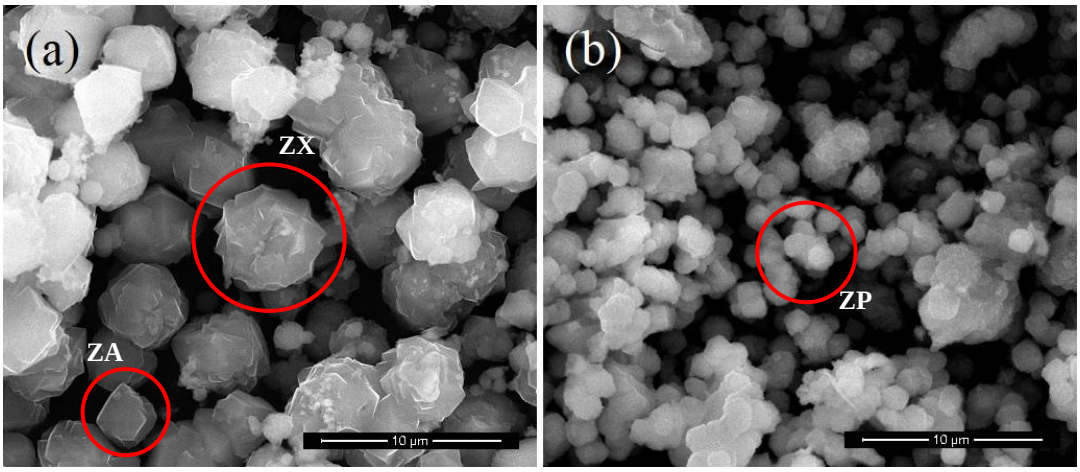

Figure 5.34. SEM images of the zeolite synthesis products from Kaolin 3 with one-pot fusion method using NaOH at calcination temperatures of (a) 800 ℃, (b) 850 ℃. ZA: zeolite 4A, ZP: zeolite P, ZX: zeolite 13X

To continue with the 850 ℃ fusion synthesis product, the zeolite crystals are seen much more rounded than the crystals that occurred at the lower fusion temperature. This rounded shape of crystals supports the idea that zeolite P is formed with this synthesis, which is also seen in the XRD result of the synthesis.

XRD results of the NaOH one-pot fusion method using kaolin 4 show in Figure 5.35 that crystallization occurred well in both fusion temperatures of 800 and 850 ℃.

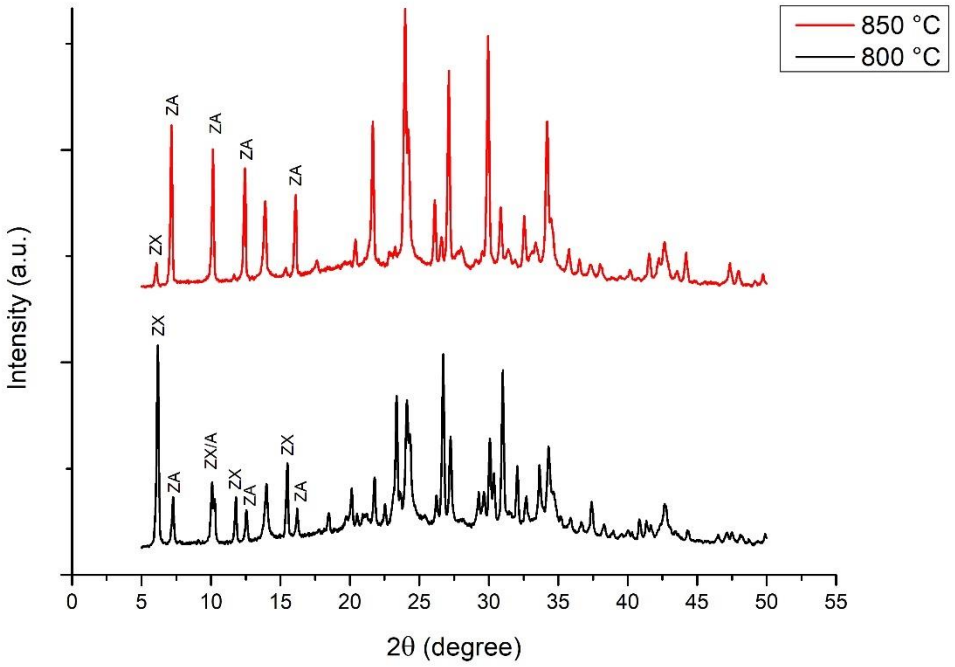

Figure 5.35. XRD patterns of the zeolite synthesis with the sample Kaolin 4 by one-pot fusion method using NaOH at fusion temperatures of 800 ℃, and 850 ℃. ZA: zeolite 4A, ZX: zeolite 13X

The difference between these two syntheses is the main types of zeolites formed. Zeolite 13X is the main product at 800 ℃ fusion synthesis, while at 850 ℃ synthesis zeolite 4A is the main product. Zeolite 13X has the main characteristic [111] peak at 6.20 2θ which is seen at 800 ℃ fusion synthesis products first peak, while zeolite

4A has the main peak just near that, which has an increased intensity at 850 ℃ fusion synthesis product (Purna Chandra Rao et al., 2006; Sowunmi et al., 2018).

The [111], [311], and [331] peaks of zeolite 13X are seen as 14.26 Å (6.20 2θ), 7.49 Å (11.80 2θ), and 5.71 Å (15.50 2θ) at 800 ℃ respectively, but only [111] peak is observable at 850 ℃ synthesis result which is seen as 14.48 Å (6.10 2θ).

The [200], [222], and [420] peaks of zeolite 4A are seen as 12.14 Å (7.28 2θ), 7.05 Å (12.55 2θ), and 5.47 Å (16.20 2θ) at 800 ℃, and 12.26 Å (7.20 2θ), 7.09 Å (12.48 2θ), and 5.49 Å (16.12 2θ) 850 ℃ synthesis XRD results respectively. Additionally, the [220] peak is also seen as 8.66 Å (10.20 2θ) 850 ℃ synthesis.

The [220] peaks of both zeolite 13X and 4A overlap each other in the 800 ℃ synthesis result which is seen at 10.17 2θ.

The SEM images also show that crystallization occurred with both temperatures using kaolin 4 in Figure 5.36. The main phase of the crystallization is zeolite 13X at 800 ℃ fusion synthesis product. And at the 850 ℃ fusion synthesis, zeolite 4A crystals are the main products as expected from the XRD results. At the 850 ℃ synthesis, the cubic crystals percentage is higher, while at the 800 ℃ the crystals are seen more as rounded.

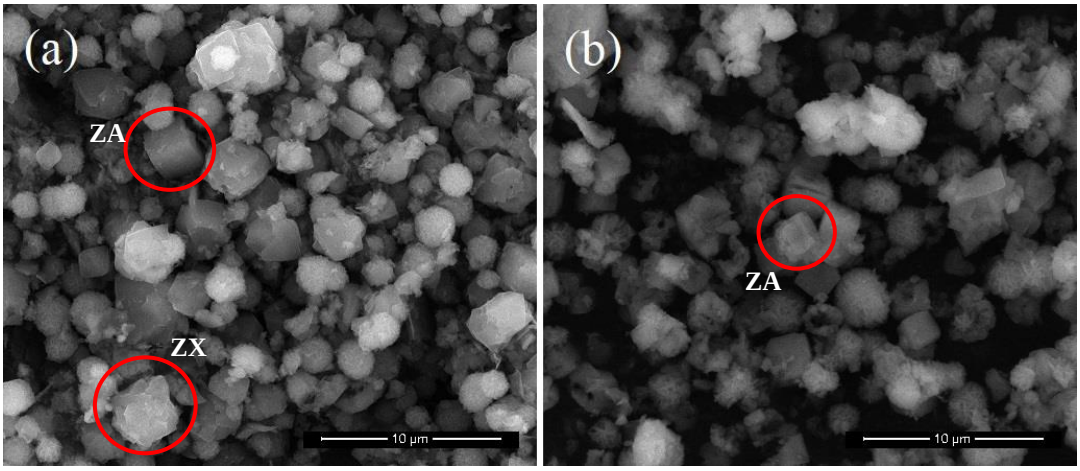

Figure 5.36. SEM images of the zeolite synthesis products from Kaolin 4 with one-pot fusion method using NaOH at fusion temperatures of (a) 800 ℃, (b) 850 ℃. ZA: zeolite 4A, ZX: zeolite 13X

The reason for doing synthesis with NaOH with only two different fusion temperatures is because seeing the zeolite crystals occurred in the first attempts, which is an expected result because in the literature it is commonly seen.

5.2.2.2 Results of Zeolite Synthesis with One-Pot Fusion Method by Using Na_2CO_3

In this method, Na_2CO_3 is used as a sodium source instead of NaOH. Zeolite synthesis with one pot-fusion method using Na_2CO_3 is done before in literature with commercial kaolin (Kirdeciler & Akata, 2020), but here, gangue kaolin samples were used with Na_2CO_3 to obtain zeolite 4A. The procedure of the synthesis is the same as the one-pot fusion method using NaOH, but Na_2CO_3 is used as a sodium source instead of NaOH.

The XRD results of the synthesis done by one-pot fusion with Na_2CO_3 using kaolin 1 show that crystallization started to occur at 850 ℃, and zeolite 13X is more dominant than zeolite 4A (Figure 5.37). At 900 ℃ synthesis, the intensity of zeolite 13X increased a little more. The main crystals that occurred at both 850 and 900 ℃ fusion temperature syntheses are zeolite 13X, but zeolite 4A is also formed. The synthesis with a fusion temperature of 800 ℃ didn't form zeolite crystals as seen in Figure 5.37. The melting point for sodium carbonate is 851 ℃ (Wang et al., 2016), which is the reason for crystallization does not occur at 800 ℃ fusion temperature synthesis.

The [111], [311], and [331] peaks of zeolite 13X are seen as 14.36 Å (6.14 2θ), 7.53 Å (11.74 2θ), and 5.74 Å (15.43 2θ) at 850 ℃, and 14.15 Å (6.24 2θ), 7.46 Å (11.84 2θ), and 5.69 Å (15.55 2θ) at 900 ℃ respectively. Additionally, [220] peak of zeolite 13X is seen as 8.75 Å (10.10 2θ) at 900 ℃ synthesis result.

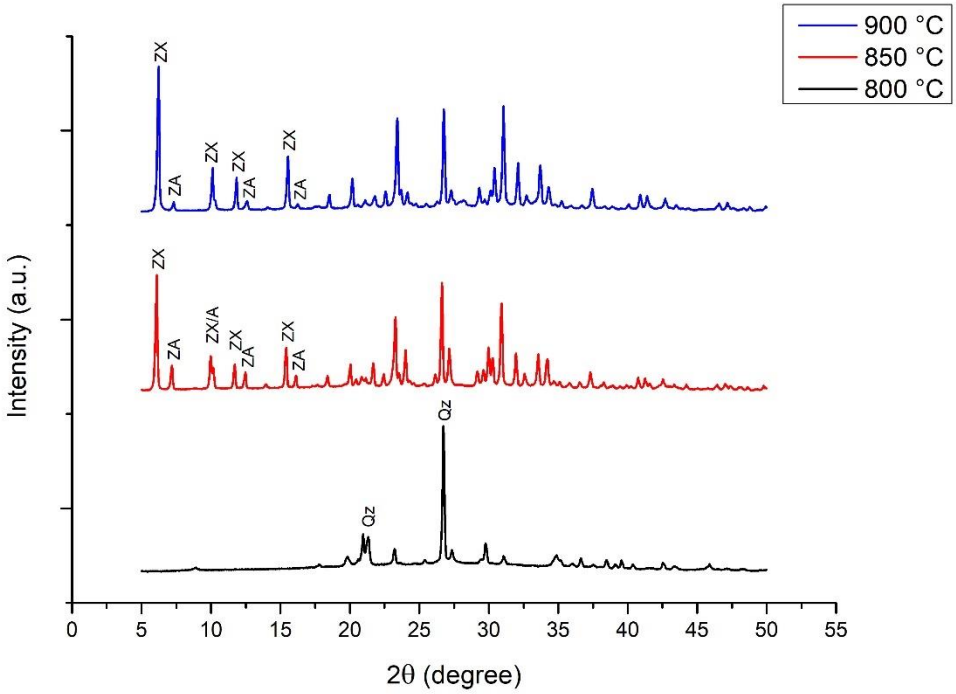

Figure 5.37. XRD patterns of the zeolite synthesis with the sample Kaolin 1 by one-pot fusion method using Na_2CO_3 at fusion temperatures of 800 ℃, 850 ℃, and 900 ℃. Qz: quartz, ZA: zeolite 4A, ZP: zeolite P, ZX: zeolite 13X

The [200], [222], and [420] peaks of zeolite 4A are seen as 12.25 Å (7.21 2θ), 7.08 Å (12.50 2θ), and 5.48 Å (16.17 2θ) at 850 ℃, and 12.06 Å (7.32 2θ), 7.02 Å (12.6 2θ), and 5.45 Å (16.25 2θ) 900 ℃ synthesis XRD results, respectively.

The [220] peaks of both zeolite 13X and 4A overlap each other in the 850 ℃ synthesis result which is seen at 10.13 2θ.

The SEM images of the syntheses show that crystallization didn't occur at 800 ℃ as expected from the XRD results, and at higher degrees, zeolite 13X occurred as the main type of zeolite while zeolite 4A is barely seen in the Figure 5.38 b and c.

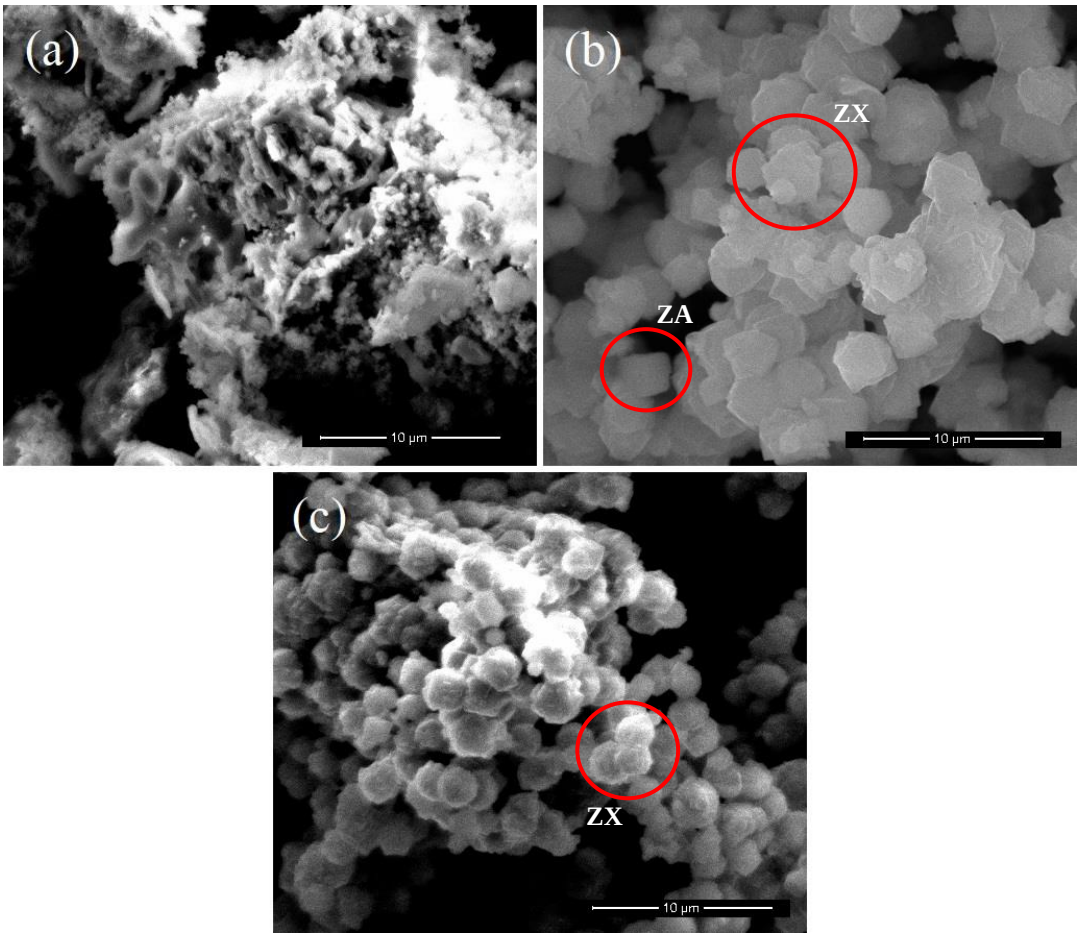

Figure 5.38. SEM images of the zeolite synthesis products from Kaolin 1 with one-pot fusion method using Na_2CO_3 at fusion temperatures of (a) 800 ℃, (b) 850 ℃, (c) 900 ℃. ZA: zeolite 4A, ZX: zeolite 13X

XRD results of synthesis products with kaolin 2 show that zeolite crystals started to form at 850 ℃ (Figure 5.39). At 850 ℃ fusion temperature synthesis, zeolite 4A formed mainly, while at 900 ℃ zeolite 13X is also formed with zeolite 4A.

The [111], [311], and [331] peaks of zeolite 13X are seen as 14.22 Å (6.21 2θ), 7.48 Å (11.82 2θ), and 5.71 Å (15.50 2θ) at 900 ℃, and not observable at 850 ℃ result.

The [200], [222], and [420] peaks of zeolite 4A are seen as 12.19 Å (7.24 2θ), 7.06 Å (12.52 2θ), and 5.47 Å (16.19 2θ) at 850 ℃, and 12.11 Å (7.29 2θ), 7.04 Å (12.56 2θ), and 5.46 Å (16.21 2θ) 900 ℃ synthesis XRD results respectively. Additionally,

the [220] peak of zeolite 4A is seen as 8.64 Å (10.23 2θ) in the 850 ℃ synthesis result.

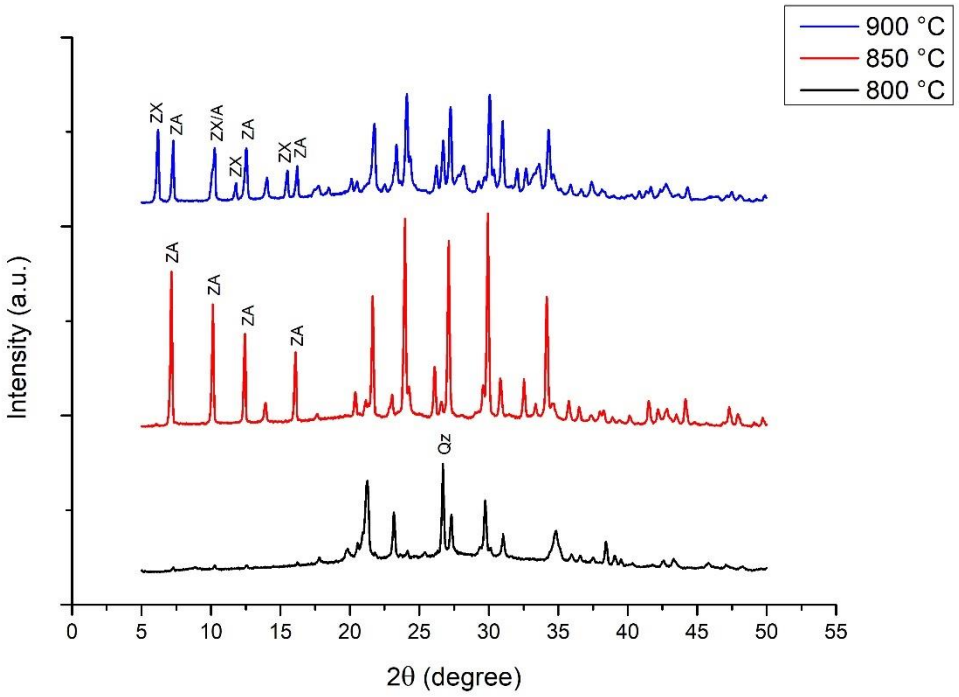

Figure 5.39. XRD patterns of the zeolite synthesis with the sample Kaolin 2 by one-pot fusion method using Na_2CO_3 at fusion temperatures of 800 ℃, 850 ℃, and 900 ℃. Qz: quartz, ZA: zeolite 4A, ZX: zeolite 13X

The [220] peaks of both zeolite 13X and 4A overlap each other in the 900 ℃ synthesis result which is seen at 10.18 2θ.

The SEM images show that at 850 ℃ fusion temperature synthesis, mostly zeolite 4A formed but there are 13X crystals too (Figure 5.40). The zeolite 13X peaks are not apparent in the XRD result in figure 5.27, but the SEM image shows that it formed, which means it must be less than 5%, making it a competing phase. At 900 ℃ synthesis, zeolite 4A and 13X formed together with close amounts as expected from XRD results. The 800 ℃ fusion temperature synthesis didn't form crystallization as expected.

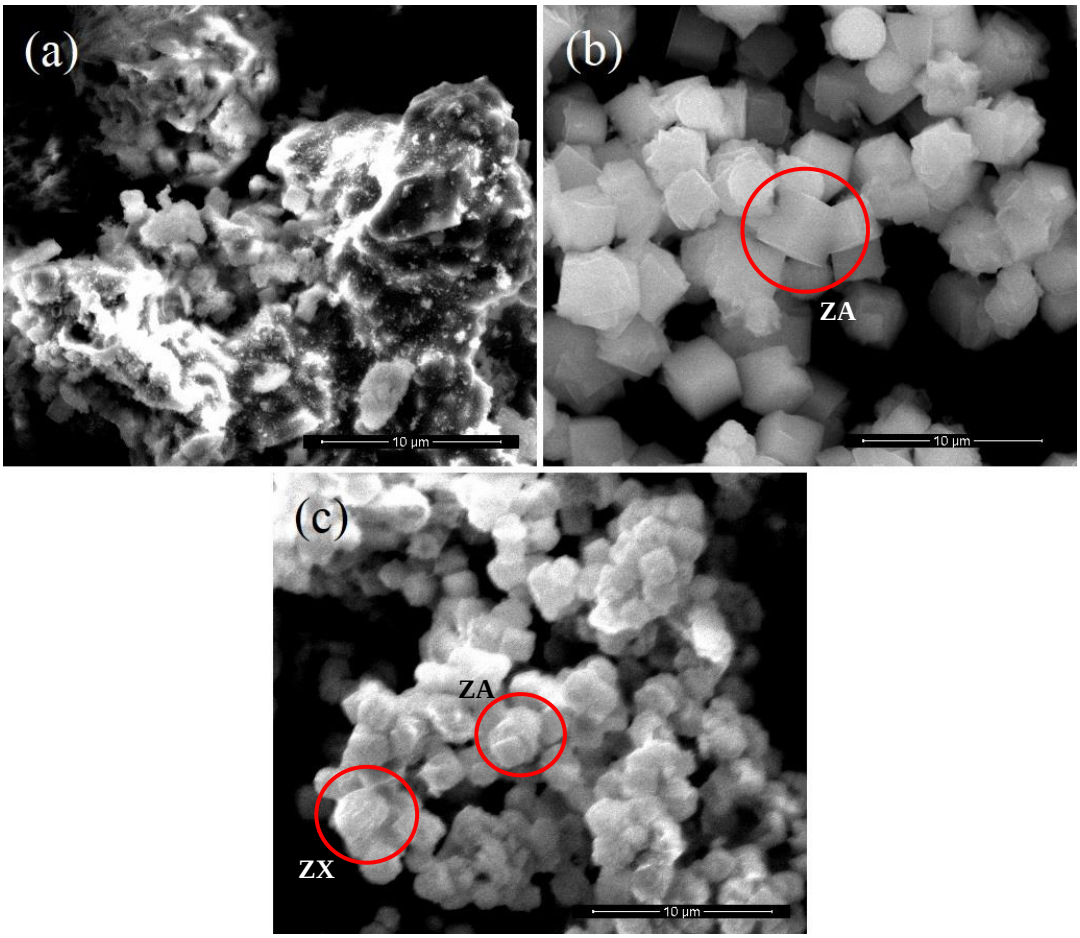

Figure 5.40. SEM images of the zeolite synthesis products from Kaolin 2 with one-pot fusion method using Na_2CO_3 at fusion temperatures of (a) 800 ℃, (b) 850 ℃, (c) 900 ℃. ZA: zeolite 4A, ZX: zeolite 13X

XRD results of the syntheses with kaolin 3 show that crystallization again started to occur at 850 ℃ fusion temperature as expected (Figure 5.41). However, the main phases are unexpectedly zeolite P for both 850 and 900 ℃ fusion temperature syntheses products including zeolite 13X and 4A with a little amount as competing phases.

The [111] peak of zeolite 13X is seen as 14.34 Å (6.16 2θ) 850 ℃, and 14.33 Å (6.16 2θ) at 900 ℃ results.

The [200] peak of zeolite 4A is seen as 12.35 Å (7.15 2θ) at 850 ℃, and 12.19 Å (7.25 2θ) at 900 ℃ synthesis results.

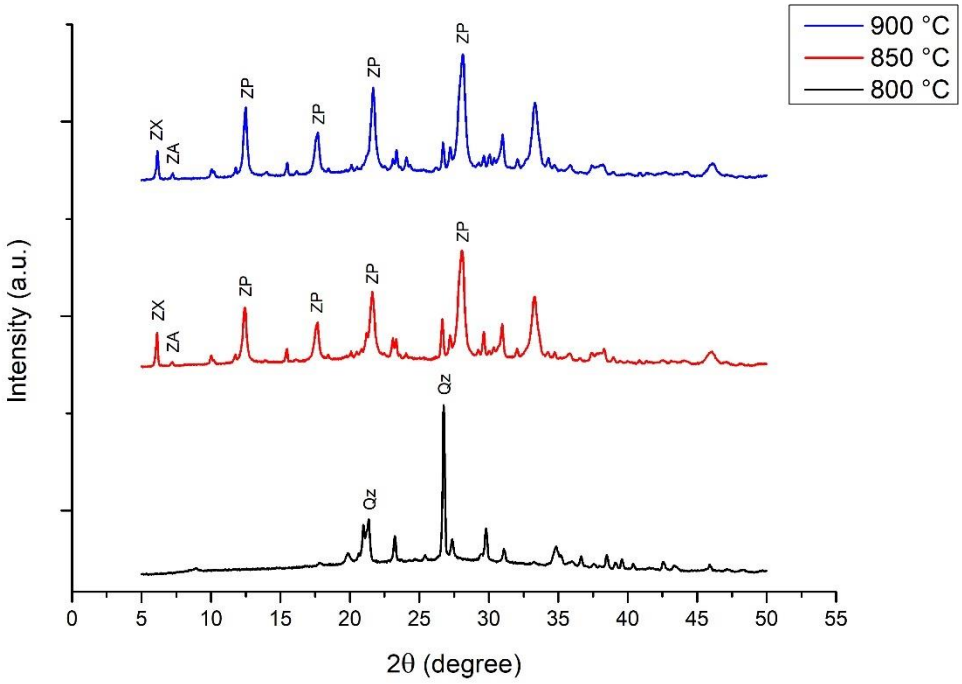

Figure 5.41. XRD patterns of the zeolite synthesis with the sample Kaolin 3 by one-pot fusion method using Na_2CO_3 at fusion temperatures of 800 ℃, 850 ℃, and 900 ℃. Qz: quartz, ZA: zeolite 4A, ZP: zeolite P, ZX: zeolite 13X

The [101], [200], [112] and [301] peaks of zeolite P are seen as 7.10 Å (12.46 2θ), 5.01 Å (17.69 2θ), 4.10 Å (21.64 2θ), and 3.18 Å (28.06 2θ) at 850 ℃, and 7.08 Å (12.48 2θ), 5.01 Å (17.67 2θ), 4.10 Å (21.67 2θ), and 3.18 Å (28.06 2θ) at 900 ℃ synthesis results.

The SEM images of the syntheses using the sample kaolin 3 show that zeolite P is formed in the fusion temperatures of 850 and 900 ℃ (Figure 5.42). From the XRD results, zeolite 13X and zeolite 4A are also seen in a minor amount but only zeolite 13X is seen as a competing phase in the SEM images in Figure 5.42 b.

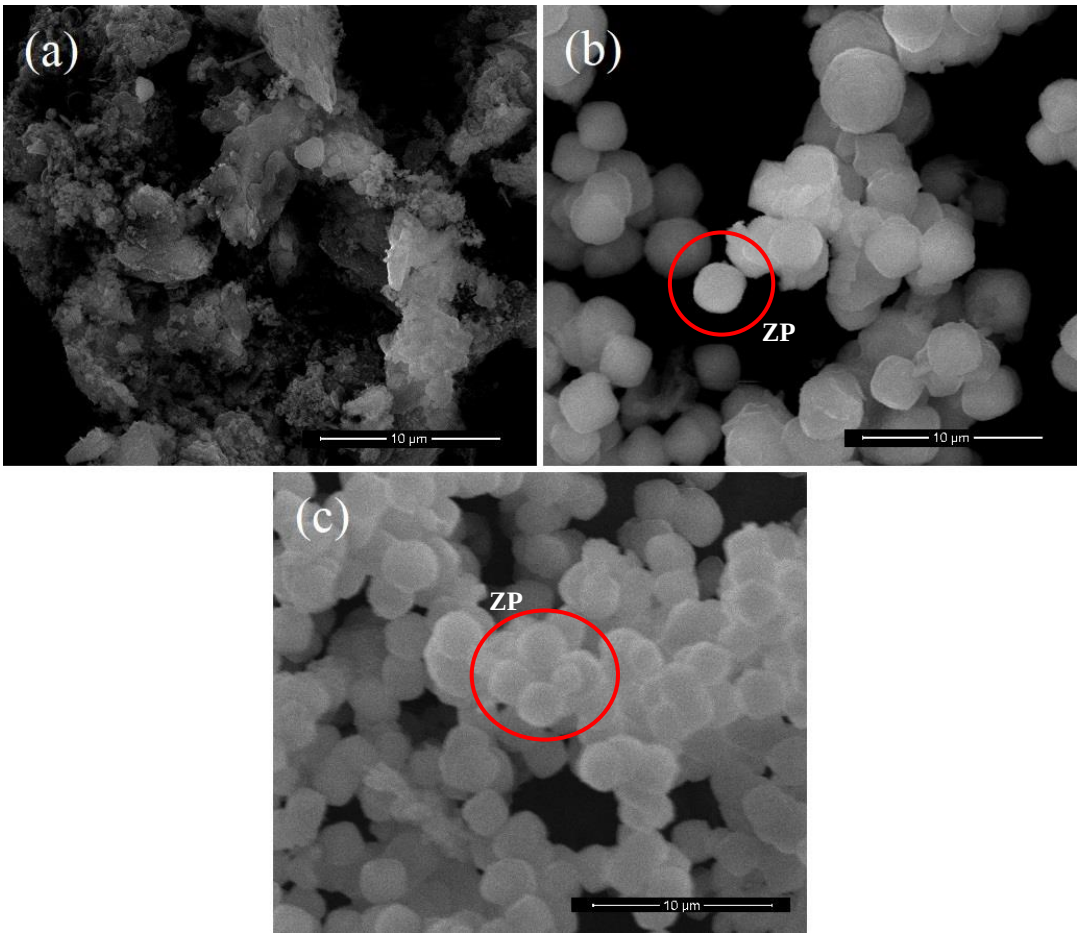

Figure 5.42. SEM images of the zeolite synthesis products from Kaolin 3 with one-pot fusion method using Na_2CO_3 at fusion temperatures of (a) 800 ℃, (b) 850 ℃, (c) 900 ℃. ZP: zeolit P

XRD results of syntheses using kaolin 4 with Na_2CO_3 fusion show that zeolite 4A and 13X are formed together at the fusion temperatures of 850 and 900 ℃ (Figure 5.43). The main phase of crystallization is zeolite 4A at the 850 ℃ fusion temperature synthesis, while zeolite 13X is the main phase at 900 ℃ fusion temperature. 800 ℃ fusion temperature synthesis does not look like crystallization occurred, but the peaks are a little more intense when compared to other kaolin samples' synthesis results in Figure 5.37, Figure 5.39, and Figure 5.41.

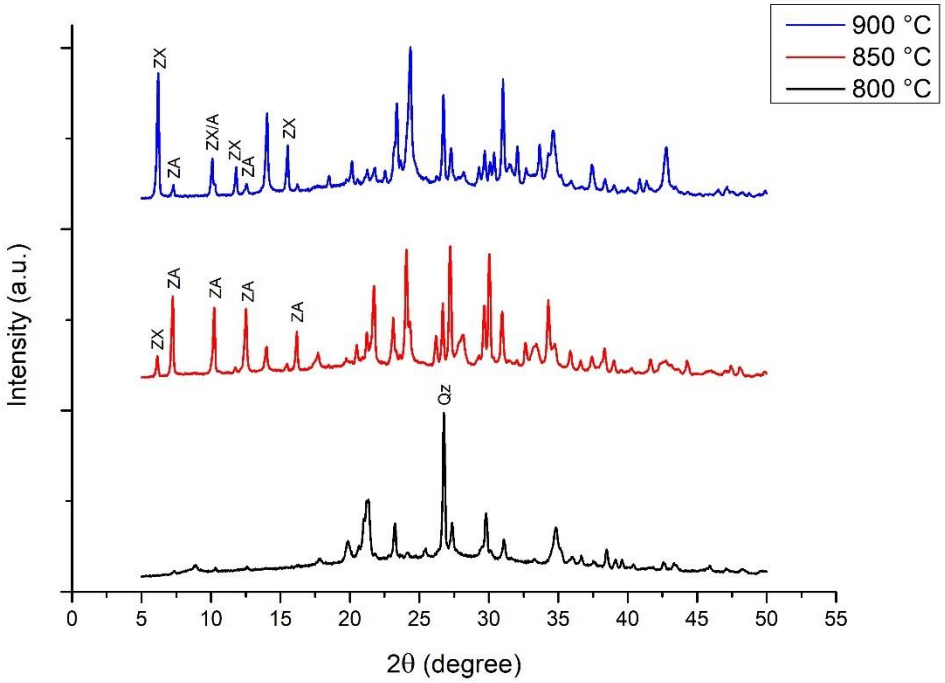

Figure 5.43. XRD patterns of the zeolite synthesis with the sample Kaolin 4 by one-pot fusion method using Na_2CO_3 at fusion temperatures of 800 ℃, 850 ℃, and 900 ℃. Qz: quartz, ZA: zeolite 4A, ZX: zeolite 13X

At 850 ℃ synthesis, only the [111] peak of zeolite 13X is apparent and seen as 14.42 Å (6.12 2θ). At 900 ℃, [111], [311], and [331] peaks of zeolite 13X are seen as 14.20 Å (6.22 2θ), 7.48 Å (11.82 2θ), and 5.71 Å (15.52 2θ) respectively.

The [200], [222], and [420] peaks of zeolite 4A are seen as 12.25 Å (7.21 2θ), 7.08 Å (12.49 2θ), and 5.49 Å (16.14 2θ) at 850 ℃, and 12.11 Å (7.29 2θ), 7.05 Å (12.54 2θ), and 5.45 Å (16.24 2θ) at 900 ℃ synthesis XRD results respectively. Additionally, [220] peak of zeolite 4A is also seen at 850 ℃ synthesis result as 8.66 Å (10.20 2θ).

At the 900 ℃ synthesis result, the [220] peaks of both zeolite 13X and 4A overlap each other at 10.18 2θ.

As seen from SEM images (Figure 5.44) of one-pot fusion synthesis using Na_2CO_3 with kaolin sample 4, there is some crystallization occurred at the synthesis with fusion temperature of 800 ℃, although the XRD result of that synthesis in Figure 5.43 does not show some obvious crystallization. The cubic crystals of zeolite 4A are seen as the main phase at 850 ℃ fusion synthesis product with zeolite 13X as the competing phase while at the 900 ℃ fusion synthesis product the main phase is zeolite 13X and the zeolite 4A crystals are the competing phase.

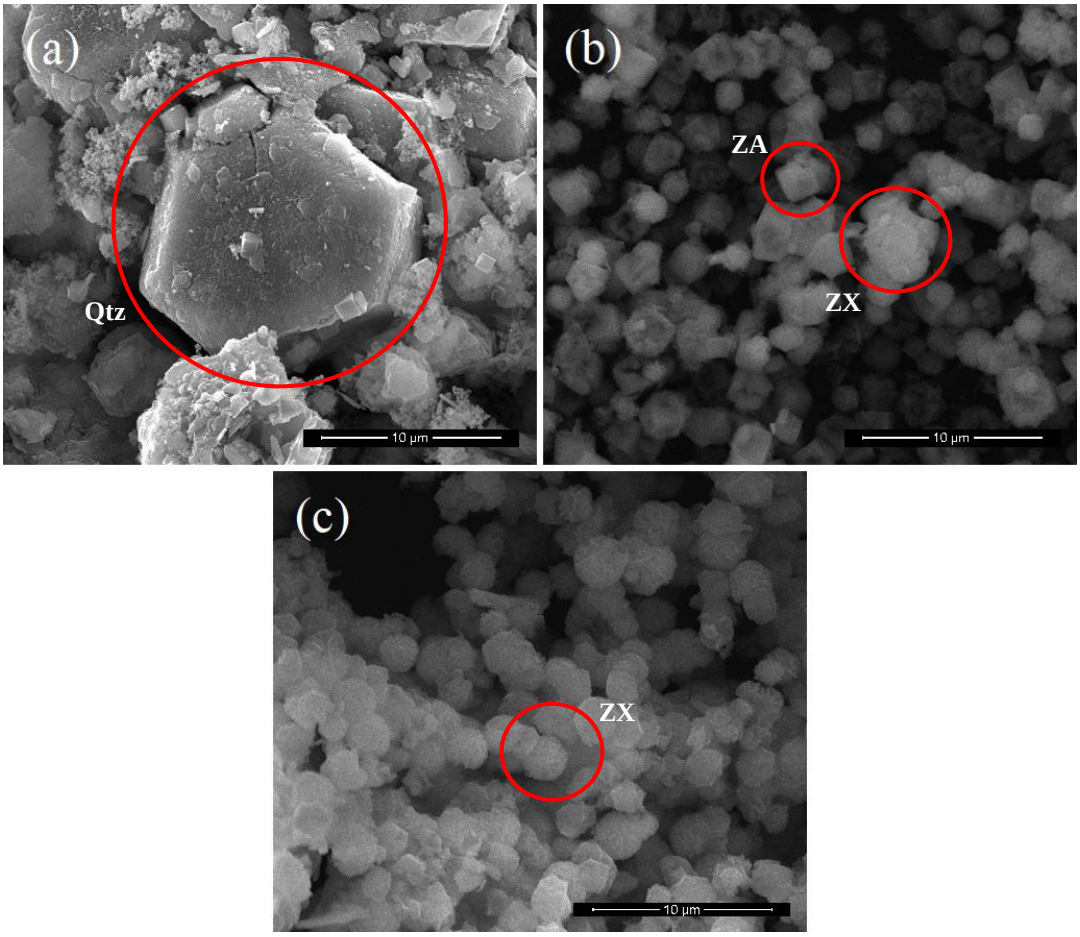

Figure 5.44. SEM images of the zeolite synthesis products from Kaolin 4 with one-pot fusion method using Na_2CO_3 at fusion temperatures of (a) 800 ℃, (b) 850 ℃, (c) 900 ℃. ZA: zeolite 4A, ZX: zeolite 13X, Qtz: quartz

In the synthesis results done by one-pot fusion using Na_2CO_3, sample kaolin 2 gave better crystallization for zeolite 4A. Smectite content might be the reason for better zeolite 4A crystallization because kaolin 2 has the highest smectite content.

CHAPTER 6

DISCUSSIONS

Use of only laboratory chemicals produces pure zeolite crystals, however zeolite crystals formed by using gangue kaolin as a raw material can also be in industrially favorable purities. Several studies showed that zeolite crystals produced by using cheap raw materials like kaolin can be used in industrial applications (Ayele, Pérez-Pariente, Chebude, & Diaz, 2016; Costa et al., 1988). Using almost pure kaolin in producing zeolite crystals can yield substantial profit (Costa et al., 1988), and zeolite is demanded in hundreds or thousands of tons in market. Therefore, use of gangue kaolin rather than pure kaolin as a raw material leads to a higher decrease in cost of zeolite production.

The syntheses' results indicated that the chemical ingredients of the samples, activation temperature, and activation methods play a role in the final products.

When the results of all syntheses are examined, it is seen that Zeolite 4A is the most abundant zeolite type. Zeolite 13X is also present in major quantities, and in some results, it is the second main phase in the final products. In addition, zeolite P has also been produced as another product of the synthesis.

Specifically for syntheses with Na_2CO_3 fusion, there is no crystallization occurred with the fusion temperature of 800 ℃, since the melting point of Na_2CO_3 is 850 ℃ (Wang et al., 2016), it could not react with the main silica and alumina sources in the reaction mixture. The structure of Na_2CO_3 is preserved and the sodium didn’t get in the system, which results in no crystallization occurring as shown in Table 6.1.

Zeolite 4A, zeolite 13X, and zeolite P were produced in the syntheses of this study (Table 6.1), and formation conditions were investigated.

Table 6.1. Experimental design, main and competing phases of the experiments, 4A: zeolite 4A, 13X: zeolite 13X, P: zeolite P, x: no crystallization

	Activation	Metakaolinization		NaOH Fusion		Na_2CO_3 Fusion	
Sample	Temperature	Main	Competing	Main	Competing	Main	Competing
K1	800			13X	4A	x	x
	850	x	x	13X	4A	13X	4A
	900	x	x			13X	4A
	950	x	x				
	1000	x	x				
K2	800			4A	13X	x	x
	850	x	x	4A	x	4A	13X
	900	4A	x			13X	4A
	950	4A	x				
	1000	4A	x				
K3	800			13X	4A	x	x
	850	4A	x	P	x	P	13X-4A
	900	4A	x			P	13X-4A
	950						
	1000						
K4	800			13X	4A	x	x
	850	4A	x	4A	13X	4A	13X
	900	4A	x			13X	4A
	950						
	1000						

6.1 Production of Zeolite 4A

In the metakaolinization method, zeolite 4A is formed as the main crystal type without zeolite 13X as a final product. Only sample kaolin 1 didn't produce any crystallization with the metakaolinization method, while sample kaolin 2 also didn't give zeolite crystals in the synthesis with 850 ℃ calcination temperature. Sample kaolin 1 has the highest Si/Al ratio when compared to other samples, and it also has a high quartz content shown by XRD results. Additionally, sodium aluminate ($NaAlO_2$) was not added as a reagent for the sample kaolin 1. The high quartz content which increases the Si/Al content of the raw material, and not using sodium

aluminate ($NaAlO_2$) can be the reasons for the syntheses didn't produce zeolite crystals. The synthesis with sample kaolin 2 with the calcination temperature of 850 ℃ also didn't produce crystals while it did at higher temperatures. Sample kaolin 2 has the second highest Si/Al ratio, and the XRD result of 850 ℃ synthesis with the metakaolinization method also shows that quartz is still present as the main type of mineral. The other kaolin samples produced zeolite 4A with the metakaolinization method although quartz still exists in the final product. The highest zeolite crystallization with the metakaolinization method is obtained with kaolin 4 and followed with the samples kaolin 3 and kaolin 2 respectively, while kaolin 1 didn't produce zeolite crystals as mentioned. This result coincides with the Si/Al ratios and, because the Si/Al ratio values of the samples from highest to lowest are as follows, respectively, kaolin 1, kaolin 2, kaolin 3, and kaolin 4. These results indicate that Si/Al ratio is the most important parameter for the zeolite synthesis with the metakaolinization method (Gandhi et al., 2021; He et al., 2021; Kirdeciler & Akata, 2020), as it is reported in the literature. The non-clay content of sample kaolin 1 is the highest among all samples as it was shown in Table 5.3, which results in the least successful syntheses.

In the NaOH fusion method, zeolite 4A is obtained as the main type of zeolite at the syntheses with kaolin 2 and kaolin 4. Kaolin 2 produced zeolite 4A with both fusion temperatures of 800, and 850 ℃, while kaolin 4 produced it at 850 ℃. The difference between kaolin 2 from other samples is its higher CaO and MgO content, which is expected to come from the smectite in the raw materials' original content. Additionally, the SO_3 content of kaolin 2 is the highest in all samples. Smectite content and the volatility of SO_3 might be reasons for zeolite 4A to occur. The reason why kaolin 4 can form zeolite 4A may be due to having the lowest Si/Al ratio in all samples which is the closest to the theoretical zeolite 4A crystal SiO_2/Al_2O_3 ratio (Melo et al., 2012).

In the Na_2CO_3 fusion method, zeolite 4A is obtained as the main zeolite type again in the syntheses using samples kaolin 2 and 4. Smectite content and the volatility of

SO_3 of kaolin 2, and the low Si/Al ratio of kaolin 4 are the expected reasons for the formation of zeolite 4A with these samples same as the NaOH fusion results.

Additionally, zeolite 4A is also formed as a competing type in several results. In both NaOH and Na_2CO_3 syntheses by using kaolin 1, zeolite 4A is formed with zeolite 13X in smaller amounts. Since the quartz content remains the same after metakaolinization, there was no zeolite formation observed with the metakaoliniation method, while the fusion of the same kaolin source resulted in soluble aluminosilicates, which later on can be transformed into zeolites. Furthermore, the solubility of these aluminosilicates increases the final Si/Al ratio of the product, which results in more favorable products of zeolite 13X that have a higher Si/Al ratio. With the sample kaolin 2, 900 ℃ Na_2CO_3 fusion synthesis, zeolite 4A formed as a competing type. Increasing fusion temperature is expected to be the reason for zeolite 4A to become a competing type because it is the main type with a fusion temperature of 850 ℃. Sample kaolin 3 has the highest iron and titanium (Fe_2O_3+TiO_2) content (Table 5.2) and produced zeolite 4A as a competing type in both NaOH and Na_2CO_3 syntheses. Lastly, kaolin 4's behavior is changed in NaOH and Na_2CO_3 syntheses for making zeolite 4A a competing type. In NaOH syntheses, zeolite 4A is formed as a competing type at lower fusion temperature, while it becomes a competing type at higher fusion temperature in Na_2CO_3 fusion syntheses. This might be again due to the increase in soluble silica content after the fusion of the main sources.

6.2 Production of Zeolite 13X

The syntheses in this study were arranged to produce zeolite 4A, and zeolite 13X was not the type of zeolite attempted to produce, but it was formed as the main crystal type in some of the syntheses.

In the metakaolinization method, zeolite 13X was not produced in any syntheses. The reason for that might be the silicon content of the quartz, which is not contributed

to the system by syntheses, because zeolite 13X is a type of zeolite having higher silicon content than zeolite 4A.

In NaOH fusion syntheses, zeolite 13X is formed as the main crystal type in kaolin 1, and lower fusion temperature syntheses with kaolin 3 and 4. Kaolin 1 has the highest Si/Al ratio, which might be the reason for producing zeolite 13X as the main type. In 800 ℃ syntheses of kaolin 3 and 4, it is also produced as the main type. For the samples kaolin 3 and 4, fusion temperature is more effective in the formation of zeolite 13X as the final product.

In Na_2CO_3 fusion syntheses, zeolite 13X is again produced as the main type with the sample kaolin 1, and the high Si/Al ratio of the source is expected to be the reason for this. In contrast to the NaOH fusion syntheses, the samples kaolin 2 and 4 produced zeolite 13X as the main type in higher fusion temperatures due to the higher reactivity of the sodium carbonate in elevated temperatures.

Zeolite 13X is also produced as a competing type of crystal in a few syntheses with NaOH and Na_2CO_3. Sample kaolin 2 produced it as a competing type in lower fusion temperatures of both NaOH and Na_2CO_3 fusion syntheses. Kaolin 3 produced it as a competing type only in Na_2CO_3 fusion syntheses. Lastly, kaolin 4 produced it as a competing type in higher fusion temperature in NaOH synthesis, while it is produced as a competing type in lower fusion temperature in Na_2CO_3 synthesis. These results might be due to the reactivity increase in elevated temperatures of the used sodium hydroxide and sodium carbonate as fusion agents.

6.3 Production of Zeolite P

Zeolite P is an impurity for this study, and it is formed as a main type of crystallization. It is produced only with the sample kaolin 3, in the NaOH and Na_2CO_3 fusion syntheses. In the NaOH fusion, it formed at the fusion temperature of 850 ℃ and it is the only type of zeolite produced. In the Na_2CO_3 fusion syntheses, it is produced as the main type at the fusion temperatures of 850, and 900 ℃, while

zeolite 13X and 4A are produced as competing types. Zeolite P has a similar Si/Al content with zeolite 4A, and it is the main competing phase in literature itself (Y. Liu et al., 2019).

The most distinct difference of kaolin 3 from the other samples is the highest amount of heavy metal content. Additionally, it has the smallest d_{10} value (Table 5.1), and the largest particle size distribution. The high heavy metal content and particle size properties of kaolin 3 may be the reasons to be the only one sample that produces zeolite P. Besides that, it has the lowest SO_3 content, which may also affect the results.

6.4 Production of a Zeolite 4A- Zeolite 13X Mixture

Zeolite 4A and 13X can be formed together in some of the NaOH and Na_2CO_3 fusion syntheses as reported in the literature by several studies (El-Naggar et al., 2008; Hu et al., 2017; Kostinko, 1982).

Kaolin 1 produced zeolite 13X as the main type and zeolite 4A as competing in both NaOH and Na_2CO_3 fusion syntheses, and as mentioned before, the high Si/Al ratio of the sample is expected to be the reason for this.

In NaOH fusion syntheses, kaolin 2 produced zeolite 4A as the main type and 13X as competing with 800 ℃ fusion temperature and produced only zeolite 4A in the 850 ℃ synthesis. Kaolin 3 and 4 produced zeolite 13X as the main type at 800 ℃ NaOH fusion temperature results while zeolite 4A is competing. And at the 850 ℃ fusion, zeolite 13X is eliminated at both samples' kaolin 2 and 3, while kaolin 3 produced only zeolite P at 850 ℃ fusion synthesis. Kaolin 4 produced zeolite 13X as the main type and zeolite 4A as competing at 800 ℃ synthesis, while it is the reverse for 850 ℃ fusion synthesis. These results indicate that activation temperature and Si/Al ratio of kaolin samples are the most important factors for the final zeolite products to be formed. Kaolin 1 has the highest Si/Al ratio among all sources and

produced zeolite 13X as the main type, but the other kaolin samples produced zeolite 13X at lower activation temperatures.

In Na_2CO_3 fusion syntheses, the activation temperature affected the results for samples kaolin 2 and 4. Zeolite 4A is formed as the main type and 13X as competing in the lower activation temperatures, while zeolite 13X becomes the main type in higher activation temperatures. This might be due to the higher melting temperature of the sodium carbonate than sodium hydroxide (Ahmadi & Seyedina, 2019; G. Wang et al., 2016), which affects the formation of soluble aluminosilicate formation directly. Sample kaolin 1 produced zeolite 13X as the main type and 4A as competing in 850 and 900 ℃ fusion temperature synthesis, and sample kaolin 3 produced both zeolite 4A and 13X as competing types in both activation temperatures, while producing zeolite P as the main crystal type. These results indicate that the content of the kaolin samples is also an important factor in the types of crystals occurring.

CHAPTER 7

CONCLUSIONS

In this study, synthetic zeolites were successfully synthesized using gangue kaolin samples that are formed during the Late Oligocene located in the Thrace region of Turkey within the coal beds by 3 different methods. By doing that, the potential of an economically valueless raw material in producing a value-added industrial material was investigated, and positive results were taken.

The gel formulations were optimized to synthesize zeolite 4A, but some impurities were also observed such as zeolite 13X and zeolite P. Although zeolite 4A was formed in most of the syntheses, zeolite 13X and zeolite P were also formed as the main types in several synthesis results. The gangue kaolins properties and the synthesis conditions were investigated in the different synthesis methods for making interpretations of the synthesis results.

The gangue kaolins properties played a big role in the types of crystals occurring. The Si/Al ratio, quartz content, smectite content, the total amount of heavy metal content, the SO_3 content, particle size properties, and the amount of clay in the whole rock for each sample have been investigated. The smectite content of the samples is specially investigated and it is thought to be one of the most important properties for having better zeolite crystallization with the one-pot fusion method by using Na_2CO_3 syntheses.

The synthesis conditions were kept constant in all experiments while raw material activation methods were optimized. In the metakaolinization method, four different calcination temperatures were applied for the first two samples, and two different calcination temperatures were applied to the third and fourth samples. In the one-pot fusion method by using NaOH, two different fusion temperatures were applied for

all samples. Lastly, in the one-pot fusion method by using Na_2CO_3, three different fusion temperatures were applied to all samples.

Three different synthesis methods are applied in this study, and the results of each method are investigated. For the metakaolinization method, the Si/Al ratio and the use of $NaAlO_2$ are the probable reasons for the zeolite formation. For the one-pot fusion methods done by NaOH and Na_2CO_3, the chemical content of the gangue kaolins, and the variable high-temperature heating are the probable reasons. Briefly, the gangue kaolins properties and the synthesis conditions are shown to be the reasons for having different zeolite types (zeolite 4A, zeolite 13X, zeolite P) as the synthesis products.

For obtaining better zeolite crystallization, higher calcination and fusion temperatures can be tried in all methods. By doing that, the structure of quartz could be destroyed and the silicon of quartz can be used more efficiently. Other than the high-temperature treatment, the other synthesis conditions can also be investigated such as decreasing or increasing the reaction temperature or heat treatment in the aging step. Moreover, changing the aging and reaction time of the synthesis can also be investigated. Additionally, the clay-rich parts of the samples, after the siphoning, can be obtained and used as a raw material instead of whole rock samples.

Finally, Na_2CO_3 is used with gangue kaolin samples in zeolite synthesis in this study. In the literature, Na_2CO_3 is used with high quality kaolin samples to produce zeolite crystals, but in this study, it was shown that it can be done with low quality kaolin too. The potential of gangue kaolin in producing an economically valuable zeolite crystal is proven, which means that the kaolins that are considered worthless materials can be brought back into the economy, for instance in the production process of warm mix asphalt (WMA) additives, and desiccants in insulating windows, instead of losing it.

REFERENCES

Abukhadra, M. R., Ibrahim, S. M., Yakout, S. M., El-Zaidy, M. E., & Abdeltawab, A. A. (2019). Synthesis of Na+ trapped bentonite/zeolite-P composite as a novel catalyst for effective production of biodiesel from palm oil; Effect of ultrasonic irradiation and mechanism. *Energy Conversion and Management*, *196*(June), 739–750. https://doi.org/10.1016/j.enconman.2019.06.027

Adamis, Z., Williams, R. B., International Labour Organisation., United Nations Environment Programme., World Health Organization., Inter-Organization Programme for the Sound Management of Chemicals., & International Program on Chemical Safety. (2005). *Bentonite, kaolin, and selected clay minerals*. World Health Organization.

Ahmadi, M., & Seyedina, S. H. (2019). Investigation of NaOH Properties, Production and Sale Mark in the World. *Journal of Multidisciplinary Engineering Science and Technology*, *6*(10), 10809–10813.

Ahmed, A. H. (2014). Zeolite-encapsulated transition metal chelates: Synthesis and characterization. *Reviews in Inorganic Chemistry*, *34*(3), 153–175. https://doi.org/10.1515/revic-2013-0013

Ait-Akbour, R., Boustingorry, P., Leroux, F., Leising, F., & Taviot-Guého, C. (2015). Adsorption of PolyCarboxylate Poly(ethylene glycol) (PCP) esters on Montmorillonite (Mmt): Effect of exchangeable cations (Na+, Mg2+ and Ca2+) and PCP molecular structure. *Journal of Colloid and Interface Science*, *437*, 227–234. https://doi.org/10.1016/j.jcis.2014.09.027

Akın, S. Ş., Kirdeciler, S. K., Kazanç, F., & Akata, B. (2021). Critical analysis of zeolite 4A synthesis through one-pot fusion hydrothermal treatment approach for class F fly ash. *Microporous and Mesoporous Materials*, *325*(July). https://doi.org/10.1016/j.micromeso.2021.111338

Armbruster, T., & Gunter, M. E. (2001). Crystal structures of natural zeolites. *Reviews in Mineralogy and Geochemistry*, *45*, 1–67. https://doi.org/10.2138/rmg.2001.45.1

Atalay, Z. (2002). Stratigraphy facies and depositional environments of the lignite bearing formations (Danişmen and Ağaçlı Formations) in the Thrace region. *Bull. Fac. Eng. Cumhuriyet Univ. A Earth Sci.*, *19*, 61–80.

Ayele, L., Pérez-Pariente, J., Chebude, Y., & Diaz, I. (2016). Synthesis of zeolite a using kaolin from Ethiopia and its application in detergents. *New Journal of Chemistry*, *40*(4), 3440–3446. https://doi.org/10.1039/c5nj03097h

Ayele, L., Pérez-Pariente, J., Chebude, Y., & Díaz, I. (2015). Synthesis of zeolite A from Ethiopian kaolin. *Microporous and Mesoporous Materials*, *215*, 29–36.

https://doi.org/10.1016/j.micromeso.2015.05.022

Ayele, L., Pérez-Pariente, J., Chebude, Y., & Díaz, I. (2016). Conventional versus alkali fusion synthesis of zeolite A from low grade kaolin. *Applied Clay Science*, *132–133*, 485–490. https://doi.org/10.1016/j.clay.2016.07.019

Azizi, S. N., Alavi Daghigh, A., & Abrishamkar, M. (2013). Phase transformation of zeolite P to y and analcime zeolites due to changing the time and temperature. *Journal of Spectroscopy*, *1*(1). https://doi.org/10.1155/2013/428216

Bajda, T., Marchlewski, T., & Manecki, M. (2011). Pyromorphite formation from montmorillonite adsorbed lead. *Mineralogia*, *42*(2–3), 75–91. https://doi.org/10.2478/v10002-011-0008-5

Bhattacharyya, S., & Behera, P. S. (2017). Synthesis and characterization of nano-sized α-alumina powder from kaolin by acid leaching process. *Applied Clay Science*, *146*(January), 286–290. https://doi.org/10.1016/j.clay.2017.06.017

Biel, O., Ro, P., Florek, P., Mozgawa, W., & Kr, M. (2020). *Alkaline Activation of Kaolin Group Minerals*.

Bloodworth, A. J., Highley, D. E., & Mitchell, C. J. (1993). *Industrial Minerals Laboratory Manual:Kaolin BGS TechnicalReport WG/93/1*. 2014.

Borralleras, P., Segura, I., Aranda, M. A. G., & Aguado, A. (2019). Influence of experimental procedure on d-spacing measurement by XRD of montmorillonite clay pastes containing PCE-based superplasticizer. *Cement and Concrete Research*, *116*(October 2018), 266–272. https://doi.org/10.1016/j.cemconres.2018.11.015

Brown, G. T., Osinga, T. J., Parkington, M. J., & Steel, A. T. (1989). ALUMINOSILICATES AND DETERGENT COMPOSITIONS. In *European Patent Application*. https://patentimages.storage.googleapis.com/9a/8f/dd/76c8af3fba4453/EP0384070A2.pdf

Bu, X., Evans, G., Xie, G., Peng, Y., Zhang, Z., Ni, C., & Ge, L. (2017). Removal of fine quartz from coal-series kaolin by flotation. *Applied Clay Science*, *143*(November 2016), 437–444. https://doi.org/10.1016/j.clay.2017.04.020

Cardoso, A. M., Horn, M. B., Ferret, L. S., Azevedo, C. M. N., & Pires, M. (2015). Integrated synthesis of zeolites 4A and Na-P1 using coal fly ash for application in the formulation of detergents and swine wastewater treatment. *Journal of Hazardous Materials*, *287*, 69–77. https://doi.org/10.1016/j.jhazmat.2015.01.042

Caro, J., Noack, M., Kölsch, P., & Schäfer, R. (2000). Zeolite membranes - state of their development and perspective. *Microporous and Mesoporous Materials*, *38*(1), 3–24. https://doi.org/10.1016/S1387-1811(99)00295-4

Caroll, D. (1970). *Clay Minerals : A Guide to Their X-ray Identification*. The Geological Society of America, INC.

Cavenati, S., Grande, C. A., & Rodrigues, A. E. (2004). Adsorption Equilibrium of Methane, Carbon Dioxide, and Nitrogen on Zeolite 13X at High Pressures. *Journal of Chemical & Engineering Data*, *49*(4), 1095–1101. https://doi.org/10.1021/je0498917

Čejka, J., van Bekkum, H., Corma, A., & Schüth, F. (2007). *Introduction to Zeolite Science and Practice* (3rd ed.). Elsevier.

Çelik, Y., Karayiğit, A. İ., Querol, X., Oskay, R. G., Mastalerz, M., & Kayseri Özer, M. S. (2017). Coal characteristics, palynology, and palaeoenvironmental interpretation of the Yeniköy coal of Late Oligocene age in the Thrace Basin (NW Turkey). *International Journal of Coal Geology*, *181*(May), 103–123. https://doi.org/10.1016/j.coal.2017.08.015

Cheng, S., Du, T., Long, Y., Liu, L., & Li, G. (2020). Value added utilization of ferronickel slags as raw materials of 4A zeolite for CO2 reduction. *Adsorption*, *26*, 1113–1126. https://doi.org/10.1007/s10450-020-00246-z

Choi, H. J., & Hong, S. B. (2021). Effect of framework Si/Al ratio on the mechanism of CO2 adsorption on the small-pore zeolite gismondine. *Chemical Engineering Journal*, *November*, 133800. https://doi.org/10.1016/j.cej.2021.133800

Colella, C., & Wise, W. S. (2014). The IZA Handbook of Natural Zeolites: A tool of knowledge on the most important family of porous minerals. *Microporous and Mesoporous Materials*, *189*, 4–10. https://doi.org/10.1016/j.micromeso.2013.08.028

Collins, F., Rozhkovskaya, A., Outram, J. G., & Millar, G. J. (2020). A critical review of waste resources, synthesis, and applications for Zeolite LTA. *Microporous and Mesoporous Materials*, *291*(March 2019), 109667. https://doi.org/10.1016/j.micromeso.2019.109667

Costa, E., de Lucas, A., Uguina, M. A., & Carlos Ruíz, J. (1988). Synthesis of 4A Zeolite from Calcined Kaolins for Use in Detergents. *Industrial and Engineering Chemistry Research*, *27*(7), 1291–1296. https://doi.org/10.1021/ie00079a033

Demir, D., Bilim, F., Aydemir, A., & Ates, A. (2012). Modelling of Thrace Basin, NW Turkey using gravity and magnetic anomalies with control of seismic and borehole data. *Journal of Petroleum Science and Engineering*, *86–87*, 44–53. https://doi.org/10.1016/j.petrol.2012.03.013

Dill, H. G., Kus, J., Dohrmann, R., & Tsoy, Y. (2008). Supergene and hypogene alteration in the dual-use kaolin-bearing coal deposit Angren, SE Uzbekistan. *International Journal of Coal Geology*, *75*(4), 225–240.

https://doi.org/10.1016/j.coal.2008.07.003

Dutrow, B. L. (1912). *X-ray Powder Diffraction (XRD)* (pp. 1–4).

Dyer, A. (2006). 1. Classification 1.1. *Zeolites*, *December*, 1–5.

Ediger, V. S., Berk, I., & Kösebalaban, A. (2014). Lignite resources of Turkey: Geology, reserves, and exploration history. *International Journal of Coal Geology*, *132*, 13–22. https://doi.org/10.1016/j.coal.2014.06.008

Eiad-Ua, A., Amnaphiang, P., Asawaworarit, P., Houngkamhang, N., Chollacoop, N., & Fuji, M. (2018). Zeolite P from kaolin via hydrothermal method. *AIP Conference Proceedings*, *2010*(September 2018). https://doi.org/10.1063/1.5053197

El-Naggar, M. R., El-Kamash, A. M., El-Dessouky, M. I., & Ghonaim, A. K. (2008). Two-step method for preparation of NaA-X zeolite blend from fly ash for removal of cesium ions. *Journal of Hazardous Materials*, *154*(1–3), 963–972. https://doi.org/10.1016/j.jhazmat.2007.10.115

El-Sabbagh, S. H., Ahmed, N. M., & Ward, A. A. (2012). Effect of kaolin-metal oxides core-shell pigments on the properties of styrene-butadiene rubber composites. *Materials and Design*, *40*, 343–355. https://doi.org/10.1016/j.matdes.2012.04.004

Erarslan, C., & Örgün, Y. (2017). Mineralogical and geochemical characterization of the Saray and Pınarhisar coals, Northwest Thrace Basin, Turkey. *International Journal of Coal Geology*, *173*, 9–25. https://doi.org/10.1016/j.coal.2017.01.015

Erarslan, C., Örgün, Y., & Bozkurtoğlu, E. (2014). Geochemistry of trace elements in the Keşan coal and its effect on the physicochemical features of ground- and surface waters in the coal fields, Edirne, Thrace Region, Turkey. *International Journal of Coal Geology*, *133*, 1–12. https://doi.org/10.1016/j.coal.2014.09.003

Farideh, B., & Mansoor, A. (2015). Conventional hydrothermal synthesis of nanoporous molecular sieve 13X for selective adsorption of trace amount of hydrogen sulfide from mixture with propane. *Journal of Natural Gas Science and Engineering*. https://doi.org/10.1016/j.jngse.2015.08.019

Gajic, I. M. S., Stojiljkovic, S. T., & Savic, I. M. (2014). *Industrial application of clays and clay minerals Complimentary Contributor Copy*. *January*.

Gandhi, D., Bandyopadhyay, R., & Soni, B. (2021). Zeolite Y from kaolin clay of Kachchh, India: Synthesis, characterization and catalytic application. *Journal of the Indian Chemical Society*, *98*(12), 100246. https://doi.org/10.1016/j.jics.2021.100246

Ge, Q., Tian, Q., Hou, R., & Wang, S. (2022). Combing phosphorus-modified

hydrochar and zeolite prepared from coal gangue for highly effective immobilization of heavy metals in coal-mining contaminated soil. *Chemosphere*, *291*(P2), 132835. https://doi.org/10.1016/j.chemosphere.2021.132835

Geng, R., Yuan, L., Shi, L., Qiang, S., Li, Y., Liang, J., Li, P., Zheng, G., & Fan, Q. (2022). New insights into the sorption of U(VI) on kaolinite and illite in the presence of Aspergillus niger. *Chemosphere*, *288*(P1), 132497. https://doi.org/10.1016/j.chemosphere.2021.132497

Gougazeh, M. (2018). Removal of iron and titanium contaminants from Jordanian Kaolins by using chemical leaching. *Journal of Taibah University for Science*, *12*(3), 247–254. https://doi.org/10.1080/16583655.2018.1465714

Hamidi, R., Khoshbin, R., & Karimzadeh, R. (2021). A new approach for synthesis of well-crystallized Y zeolite from bentonite and rice husk ash used in Ni-Mo/Al2O3-Y hybrid nanocatalyst for hydrocracking of heavy oil. *Advanced Powder Technology*, *32*(2), 524–534. https://doi.org/10.1016/j.apt.2020.12.029

Hao, R., Li, X., Xu, P., & Liu, Q. (2022). Thermal activation and structural transformation mechanism of kaolinitic coal gangue from Jungar coalfield, Inner Mongolia, China. *Applied Clay Science*, *223*(March), 106508. https://doi.org/10.1016/j.clay.2022.106508

He, Y., Tang, S., Yin, S., & Li, S. (2021). Research progress on green synthesis of various high-purity zeolites from natural material-kaolin. *Journal of Cleaner Production*, *306*, 127248. https://doi.org/10.1016/j.jclepro.2021.127248

Hernández, A. C., Sánchez-Espejo, R., Meléndez, W., González, G., López-Galindo, A., & Viseras, C. (2019). Characterization of Venezuelan kaolins as health care ingredients. *Applied Clay Science*, *175*(April), 30–39. https://doi.org/10.1016/j.clay.2019.01.003

Hu, T., Gao, W., Liu, X., Zhang, Y., & Meng, C. (2017). Synthesis of zeolites Na-A and Na-X from tablet compressed and calcinated coal fly ash. *Royal Society Open Science*, *4*(10). https://doi.org/10.1098/rsos.170921

Hudaib, B. (2021). Treatment of real industrial wastewater with high sulfate concentrations using modified Jordanian kaolin sorbent: batch and modelling studies. *Heliyon*, *7*(11), e08351. https://doi.org/10.1016/j.heliyon.2021.e08351

Iannicelli, J., & Pechin, J. (1997). Magnetic separation of kaolin clay using a high temperature superconducting magnet system. *IEEE Transactions on Applied Superconductivity*, *7*(2 PART 1), 1061–1064. https://doi.org/10.1109/77.614706

Ibrahim, M. M., El-Zawawy, W. K., & Nawwar, G. A. M. (2012). Modified kaolin and polyacrylic acid-g-cellulosic fiber and microfiber as additives for paper

properties improvements. *Carbohydrate Polymers*, *88*(3), 1009–1014. https://doi.org/10.1016/j.carbpol.2012.01.048

Jaramillo, E., & Chandross, M. (2004). Adsorption of Small Molecules in LTA Zeolites. 1. NH3, CO2, and H2O in Zeolite 4A. *The Journal of Physical Chemistry B*, *108*(52), 20155–20159. https://doi.org/10.1021/jp048078f

Jin, X., Chen, L., Chen, H., Zhang, L., Wang, W., Ji, H., Deng, S., & Jiang, L. (2021). XRD and TEM analyses of a simulated leached rare earth ore deposit: Implications for clay mineral contents and structural evolution. *Ecotoxicology and Environmental Safety*, *225*, 112728. https://doi.org/10.1016/j.ecoenv.2021.112728

Jin, Y., Li, L., Liu, Z., Zhu, S., & Wang, D. (2021). Synthesis and characterization of low-cost zeolite NaA from coal gangue by hydrothermal method. *Advanced Powder Technology*, *32*(3), 791–801. https://doi.org/10.1016/j.apt.2021.01.024

Jin, Y., Liu, Z., Han, L., Zhang, Y., Li, L., Zhu, S., Li, Z. P. J., & Wang, D. (2022). Synthesis of coal-analcime composite from coal gangue and its adsorption performance on heavy metal ions. *Journal of Hazardous Materials*, *423*(March 2021). https://doi.org/10.1016/j.jhazmat.2021.127027

Kantarcı, M. D. (2017). *VII. ULUSAL HAVA KİRLİLİĞİ VE KONTROLÜ SEMPOZYUMU TRAKYA'DA VİZE, SARAY VE ÇERKEZKÖY KÖMÜRLERİ İLE ÇALIŞTIRILACAK TERMİK SANTRALLARIN ÇEVREYE YAPACAĞI KÜMÜLATİF ETKİLER ÜZERİNE EKOLOJİK BİR DEĞERLENDİRME*.

Karayigit, A. I., Oskay, R. G., & Çelik, Y. (2021). Mineralogy, petrography, and Rock-Eval pyrolysis of late Oligocene coal seams in the Malkara coal field from the Thrace Basin (NW Turkey). *International Journal of Coal Geology*, *244*(June). https://doi.org/10.1016/j.coal.2021.103814

Kasneryk, V., Shamzhy, M., Zhou, J., Yue, Q., Mazur, M., Mayoral, A., Luo, Z., Morris, R. E., & Opanasenko, M. (n.d.). *for the synthesis of new zeolites*. *2019*, 1–8. https://doi.org/10.1038/s41467-019-12882-3

Kirdeciler, S. K., & Akata, B. (2020). One pot fusion route for the synthesis of zeolite 4A using kaolin. *Advanced Powder Technology*, *31*(10), 4336–4343. https://doi.org/10.1016/j.apt.2020.09.012

Kithome, M., Paul, J. W., Lavkulich, L. M., & Bomke, A. A. (1999). Effect of pH on ammonium adsorption by natural zeolite clinoptilolite. *Communications in Soil Science and Plant Analysis*, *30*(9–10), 1417–1430. https://doi.org/10.1080/00103629909370296

Kloprogge, J. T. (2018). *Spectroscopic methods in the study of kaolin minerals and their modifications*.

Koohsaryan, E., Anbia, M., & Maghsoodlu, M. (2020). Application of zeolites as

non-phosphate detergent builders: A review. *Journal of Environmental Chemical Engineering*, *8*(5), 104287. https://doi.org/10.1016/j.jece.2020.104287

Kosinov, N., Gascon, J., Kapteijn, F., & Hensen, E. J. M. (2016). Recent developments in zeolite membranes for gas separation. *Journal of Membrane Science*, *499*, 65–79. https://doi.org/10.1016/j.memsci.2015.10.049

Kostinko, J. A. (1982). Factors Influencing the Synthesis of Zeolites a, X, and Y. *American Chemical Society, Division of Petroleum Chemistry, Preprints*, *27*(2), 487–450. https://doi.org/10.1021/bk-1983-0218.ch001

Kovo, A. S., Hernandez, O., & Holmes, S. M. (2009). Synthesis and characterization of zeolite y and ZSM-5 from Nigerian Ahoko Kaolin using a novel, lower temperature, metakaolinization technique. *Journal of Materials Chemistry*, *19*(34), 6207–6212. https://doi.org/10.1039/b907554b

Krol, M. (2020). Natural vs. Synthetic Zeolites. *Crystals*, *10*(622), 1–8.

labcompare. (2019). Laser Particle Size Analyzer (Laser Diffraction) | Labcompare. In *Labcompare*. https://www.labcompare.com/Laboratory-Analytical-Instruments/247-Laser-Particle-Size-Analyzer-Laser-Diffraction/

Li, C., Zhong, H., Wang, S., Xue, J., & Zhang, Z. (2015). A novel conversion process for waste residue: Synthesis of zeolite from electrolytic manganese residue and its application to the removal of heavy metals. *Colloids and Surfaces A: Physicochemical and Engineering Aspects*, *470*, 258–267. https://doi.org/10.1016/j.colsurfa.2015.02.003

Li, J., & Wang, J. (2019). Comprehensive utilization and environmental risks of coal gangue: A review. *Journal of Cleaner Production*, *239*, 117946. https://doi.org/10.1016/j.jclepro.2019.117946

Li, Y., Xia, W., Wen, B., & Xie, G. (2019). Filtration and dewatering of the mixture of quartz and kaolinite in different proportions. *Journal of Colloid and Interface Science*, *555*, 731–739. https://doi.org/10.1016/j.jcis.2019.08.031

Li, Z., Gao, Y., Zhang, J., Zhang, C., Chen, J., & Liu, C. (2021). Effect of particle size and thermal activation on the coal gangue based geopolymer. *Materials Chemistry and Physics*, *267*(February), 124657. https://doi.org/10.1016/j.matchemphys.2021.124657

Lima, P. E. A., Angélica, R. S., & Neves, R. F. (2018). Dissolution kinetics of Amazonian metakaolin in nitric acid. *Ceramica*, *64*(369), 86–90. https://doi.org/10.1590/0366-69132018643692179

Lin, D. C., Xu, X. W., Zuo, F., & Long, Y. C. (2004). Crystallization of JBW, CAN, SOD and ABW type zeolite from transformation of meta-kaolin. *Microporous and Mesoporous Materials*, *70*(1–3), 63–70.

https://doi.org/10.1016/j.micromeso.2004.03.003

Lin, Y. J., & Chen, J. C. (2021). Resourcization and valorization of waste incineration fly ash for the synthesis of zeolite and applications. *Journal of Environmental Chemical Engineering*, *9*(6), 106549. https://doi.org/10.1016/j.jece.2021.106549

Liu, M., Zhu, Z., Zhang, Z., Chu, Y., Yuan, B., & Wei, Z. (2020). Development of highly porous mullite whisker ceramic membranes for oil-in-water separation and resource utilization of coal gangue. *Separation and Purification Technology*, *237*(December 2019), 116483. https://doi.org/10.1016/j.seppur.2019.116483

Liu, Y., Lei, S., Huang, T., Ji, M., Li, Y., & Fan, Y. (2017). Research on mineralogy and flotation for coal-series kaolin. *Applied Clay Science*, *136*, 37–42. https://doi.org/10.1016/j.clay.2016.11.010

Liu, Y., & Ling, T. C. (2018). Potential Use of Calcined Kaolinite-Based Wastes as Cement Replacements in Concrete - An Overview. *IOP Conference Series: Materials Science and Engineering*, *431*(3). https://doi.org/10.1088/1757-899X/431/3/032006

Liu, Y., Wang, G., Wang, L., Li, X., Luo, Q., & Na, P. (2019). Zeolite P synthesis based on fly ash and its removal of Cu(II) and Ni(II) ions. *Chinese Journal of Chemical Engineering*, *27*(2), 341–348. https://doi.org/10.1016/j.cjche.2018.03.032

Liu, Y., Zhang, H., Zhang, F., Zhu, M., Hu, N., & Chen, X. (2020). *Facile synthesis of low-silica zeolite erionite by ultrasonic-assisted method*. *260*, 1–4. https://doi.org/10.1016/j.matlet.2019.126934

Luz, A. B., Yildirim, I., & Yoon, R. H. (2000). *Purification of Brazilian Kaolin Clay by Flotation*. *13*, 79–83. https://doi.org/https://doi.org/10.1016/S0167-4528(00)80078-2

Ma, D., Duan, H., Liu, J., Li, X., & Zhou, Z. (2019). The role of gangue on the mitigation of mining-induced hazards and environmental pollution: An experimental investigation. *Science of the Total Environment*, *664*, 436–448. https://doi.org/10.1016/j.scitotenv.2019.02.059

Mackinnon, I. D. R., Millar, G. J., & Stolz, W. (2010). Low temperature synthesis of zeolite N from kaolinites and montmorillonites. *Applied Clay Science*, *48*(4), 622–630. https://doi.org/10.1016/j.clay.2010.03.016

Marsh, A., Heath, A., Patureau, P., Evernden, M., & Walker, P. (2018). Alkali activation behaviour of un-calcined montmorillonite and illite clay minerals. *Applied Clay Science*, *166*(February), 250–261. https://doi.org/10.1016/j.clay.2018.09.011

Martínez-Luévanos, A., Rodríguez-Delgado, M. G., Uribe-Salas, A., Carrillo-

Pedroza, F. R., & Osuna-Alarcón, J. G. (2011). Leaching kinetics of iron from low grade kaolin by oxalic acid solutions. *Applied Clay Science*, *51*(4), 473–477. https://doi.org/10.1016/j.clay.2011.01.011

Mathur, S. (2002). Kaolin flotation. *Journal of Colloid and Interface Science*, *256*(1), 153–158. https://doi.org/10.1006/jcis.2002.8271

Meftah, M., Oueslati, W., & Ben Haj Amara, A. (2009). Synthesis process of zeolite P using a poorly crystallized kaolinite. *Physics Procedia*, *2*(3), 1081–1086. https://doi.org/10.1016/j.phpro.2009.11.066

Meftah, M., Oueslati, W., Chorfi, N., & Ben Haj Amara, A. (2017). Effect of the raw material type and the reaction time on the synthesis of halloysite based Zeolite Na-P1. *Results in Physics*, *7*, 1475–1484. https://doi.org/10.1016/j.rinp.2017.04.013

Melo, C. R., Riella, H. G., Kuhnen, N. C., Angioletto, E., Melo, A. R., Bernardin, A. M., Da Rocha, M. R., & Da Silva, L. (2012). Synthesis of 4A zeolites from kaolin for obtaining 5A zeolites through ionic exchange for adsorption of arsenic. *Materials Science and Engineering B: Solid-State Materials for Advanced Technology*, *177*(4), 345–349. https://doi.org/10.1016/j.mseb.2012.01.015

Morante-Carballo, F., Montalván-Burbano, N., Carrión-Mero, P., & Espinoza-Santos, N. (2021). Cation exchange of natural zeolites: Worldwide research. *Sustainability (Switzerland)*, *13*(14), 1–26. https://doi.org/10.3390/su13147751

Moshoeshoe, M., Nadiye-Tabbiruka, M. S., & Obuseng, V. (2017). A review of the Chemistry, Structure, Properties and Applications of Zeolites. *American Journal of Materials Science*, *7*(5), 191–221. https://doi.org/10.5923/j.materials.20170705.12

Mostafa, N. Y., Garib, R. A., Heiba, Z. K., Abd-Elkader, O. H., & Al-Majthoub, M. M. (2015). Synthesis of pure zeolite P2 from calcium silicate hydrate; tobermorite. *Oriental Journal of Chemistry*, *31*(2), 1051–1056. https://doi.org/10.13005/ojc/310254

Murray, H. H. (2000). *Traditional and new applications for kaolin , smectite , and palygorskite : a general overview*.

Németh, T., Máthé, Z., Pekker, P., Dódony, I., Kovács-Kis, V., Sipos, P., Cora, I., & Kovács, I. (2016). Clay mineralogy of the Boda Claystone Formation (Mecsek Mts., SW Hungary). *Open Geosciences*, *8*(1), 259–274. https://doi.org/10.1515/geo-2016-0024

Novembre, D., Gimeno, D., & Del Vecchio, A. (2021). Synthesis and characterization of Na-P1 (GIS) zeolite using a kaolinitic rock. *Scientific Reports*, *11*(1), 1–11. https://doi.org/10.1038/s41598-021-84383-7

Oskay, R. G., Inaner, H., Karayigit, A. I., & Christanis, K. (2013). Coal deposits of Turkey: properties and importance on energy demand. *Bulletin of the Geological Society of Greece*, *47*(4), 2111. https://doi.org/10.12681/bgsg.11106

Otieno, S. O., Kengara, F. O., Kemmegne-Mbouguen, J. C., Langmi, H. W., Kowenje, C. B. O., & Mokaya, R. (2019). The effects of metakaolinization and fused-metakaolinization on zeolites synthesized from quartz rich natural clays. *Microporous and Mesoporous Materials*, *290*(August), 109668. https://doi.org/10.1016/j.micromeso.2019.109668

Pabst, W., Kuneš, K., Havrda, J., & Gregorovà, E. (2000). A note on particle size analyses of kaolins and clays. *Journal of the European Ceramic Society*, *20*(9), 1429–1437. https://doi.org/10.1016/S0955-2219(00)00016-9

Panda, A. K., Mishra, B. G., Mishra, D. K., & Singh, R. K. (2010). Effect of sulphuric acid treatment on the physico-chemical characteristics of kaolin clay. *Colloids and Surfaces A: Physicochemical and Engineering Aspects*, *363*(1–3), 98–104. https://doi.org/10.1016/j.colsurfa.2010.04.022

Perinçek, D., Ataş, N., Karatut, Ş., & Erensoy, E. (2015). GEOLOGICAL FACTORS CONTROLLING POTENTIAL OF LIGNITE BEDS WITHIN THE DANIŞMEN FORMATION IN THE THRACE BASIN. *Bulletin of the Mineral Research and Exploration*, *150*, 77–108. https://doi.org/10.19111/bmre.65462

Purna Chandra Rao, G., Satyaveni, S., Ramesh, A., Seshaiah, K., Murthy, K. S. N., & Choudary, N. V. (2006). Sorption of cadmium and zinc from aqueous solutions by zeolite 4A, zeolite 13X and bentonite. *Journal of Environmental Management*, *81*(3), 265–272. https://doi.org/10.1016/j.jenvman.2005.11.003

Quartz R040031 - RRUFF Database: Raman, X-ray, Infrared, and Chemistry. (n.d.). https://rruff.info/quartz/display=default/R040031

Rahman, A. U., Khan, F. U., Rehman, W. U., & Saleem, S. (2018). Synthesis and characterization of zeolite 4A using swat kaolin. *Journal of Chemical Technology and Metallurgy*, *53*(5), 825–829.

Ramaswamy, S., & Raghavan, P. (2011). Significance of Impurity Mineral Identification in the Value Addition of Kaolin – A Case Study with Reference to an Acidic Kaolin from India. *Journal of Minerals and Materials Characterization and Engineering*, *10*(11), 1007–1025. https://doi.org/10.4236/jmmce.2011.1011077

Reed, T. B., & Breck, D. W. (1956). Crystalline Zeolites. II. Crystal Structure of Synthetic Zeolite, Type A. *Journal of the American Chemical Society*, *78*(23), 5972–5977. https://doi.org/10.1021/ja01604a002

Roque-Malherbe, R. (2000). Complementary approach to the volume filling theory

of adsorption in zeolites. *Microporous and Mesoporous Materials*, *41*(1–3), 227–240. https://doi.org/10.1016/S1387-1811(00)00296-1

Roy, S., Kar, S., Bagchi, B., & Das, S. (2015). Development of transition metal oxide-kaolin composite pigments for potential application in paint systems. *Applied Clay Science*, *107*, 205–212. https://doi.org/10.1016/j.clay.2015.01.029

Rozhkovskaya, A., Rajapakse, J., & Millar, G. J. (2021). Process engineering approach to conversion of alum sludge and waste glass into zeolite LTA for water softening. *Journal of Water Process Engineering*, *43*(April), 102177. https://doi.org/10.1016/j.jwpe.2021.102177

Rožić, M., Cerjan-Stefanović, Š., Kurajica, S., Vančina, V., & Hodžić, E. (2000). Ammonical Nitrogen Removal From Water by Treatment With Clays and Zeolites. *Water Research*, *34*(14), 3675–3681. https://doi.org/https://doi.org/10.1016/S0043-1354(00)00113-5

Rubtsova, M., Smirnova, E., Boev, S., Kotelev, M., Cherednichenko, K., Vinokurov, V., Lvov, Y., & Glotov, A. (2022). Nanoarchitectural approach for synthesis of highly crystalline zeolites with a low Si/Al ratio from natural clay nanotubes. *Microporous and Mesoporous Materials*, *330*(November 2021), 111622. https://doi.org/10.1016/j.micromeso.2021.111622

Sachan, A., & Penumadu, D. (2007). Identification of microfabric of kaolinite clay mineral using x-ray diffraction technique. *Geotechnical and Geological Engineering*, *25*(6), 603–616. https://doi.org/10.1007/s10706-007-9133-8

Scanning electron microscopy (SEM). (2017). https://serc.carleton.edu/research_education/geochemsheets/techniques/SEM.html

Şengüler, İ. (1982). *Ergene (Trakya) HavzasiniJeolojisi Ve KömüPotansiyeli*. 109–114. http://www.mta.gov.tr/v3.0/sayfalar/hizmetler/kutuphane/ekonomi-bultenleri/2013_16/109.pdf

Shi, Q. (2021). Molecular dynamics simulation of diffusion and separation of CO2/CH4/N2 on MER zeolites. *Ranliao Huaxue Xuebao/Journal of Fuel Chemistry and Technology*, *49*(10), 1531–1539. https://doi.org/10.1016/S1872-5813(21)60095-6

Shi, Y., Ren, X., Zheng, H., Zhang, Y., & Zuo, Q. (2022). Hierarchical 13X zeolite/reduced graphene oxide porous material for trace Pb (II) capturing from drinking water. *Microporous and Mesoporous Materials*, *329*(October 2021), 111540. https://doi.org/10.1016/j.micromeso.2021.111540

Sowunmi, A. R., Folayan, C. O., Anafi, F. O., Ajayi, O. A., Omisanya, N. O., Obada, D. O., & Dodoo-Arhin, D. (2018). Dataset on the comparison of synthesized and commercial zeolites for potential solar adsorption

refrigerating system. *Data in Brief*, *20*(August), 90–95. https://doi.org/10.1016/j.dib.2018.07.040

Survey, B. G. (2002). British Geological Survey. *Structural Survey*, *20*(1), 21–33. https://doi.org/10.1108/ss.2002.11020aab.002

Toprak, S. (2009). Petrographic properties of major coal seams in Turkey and their formation. *International Journal of Coal Geology*, *78*(4), 263–275. https://doi.org/10.1016/j.coal.2009.03.006

Torkian, N., Bahrami, A., Hosseini-Abari, A., Momeni, M. M., Abdolkarimi-Mahabadi, M., Bayat, A., Hajipour, P., Amini Rourani, H., Abbasi, M. S., Torkian, S., Wen, Y., Yazdan Mehr, M., & Hojjati-Najafabadi, A. (2021). Synthesis and characterization of Ag-ion-exchanged zeolite/TiO2 nanocomposites for antibacterial applications and photocatalytic degradation of antibiotics. *Environmental Research*, *207*(86), 112157. https://doi.org/10.1016/j.envres.2021.112157

Tuncalı, E. (2002). *Chemical and technological properties of Turkish tertiary coals*. General Directorate of Mineral Research and Exploration.

Tuncuk, A., Ciftlik, S., & Akcil, A. (2013). Factorial experiments for iron removal from kaolin by using single and two-step leaching with sulfuric acid. *Hydrometallurgy*, *134–135*, 80–86. https://doi.org/10.1016/j.hydromet.2013.02.006

Ugal, J. R., Hassan, K. H., & Ali, I. H. (2010). Preparation of type 4A zeolite from Iraqi kaolin: Characterization and properties measurements. *Journal of the Association of Arab Universities for Basic and Applied Sciences*, *9*(1), 2–5. https://doi.org/10.1016/j.jaubas.2010.12.002

USGS OFR01-041: Illite Group Minerals. (n.d.). http://pubs.usgs.gov/of/2001/of01-041/htmldocs/clays/illite.htm

Üzer, M. (2001). *İstanbul ili maden ve enerji kaynaklari*.

Veglio', F. (1997). Factorial experiments in the development of a kaolin bleaching process using thiourea in sulphuric acid solutions. *Hydrometallurgy*, *45*(1–2), 181–197. https://doi.org/10.1016/s0304-386x(96)00078-3

Velde, B., & Meunier, A. (2008). The origin of clay minerals in soils and weathered rocks. In *The Origin of Clay Minerals in Soils and Weathered Rocks*. https://doi.org/10.1007/978-3-540-75634-7

Visa, M. (2016). Synthesis and characterization of new zeolite materials obtained from fly ash for heavy metals removal in advanced wastewater treatment. *Powder Technology*, *294*, 338–347. https://doi.org/10.1016/j.powtec.2016.02.019

Wang, G., Xue, Q. G., & Wang, J. S. (2016). Effect of Na2CO3 on reduction and

melting separation of ludwigite/coal composite pellet and property of boron-rich slag. *Transactions of Nonferrous Metals Society of China (English Edition)*, *26*(1), 282–293. https://doi.org/10.1016/S1003-6326(16)64116-X

Wang, P., Sun, Q., Zhang, Y., & Cao, J. (2019). Hydrothermal synthesis of magnetic zeolite P from fly ash and its properties. *Materials Research Express*, *7*(1). https://doi.org/10.1088/2053-1591/ab609c

Wang, P., Sun, Q., Zhang, Y., & Cao, J. (2020). Effective removal of methane using nano-sized zeolite 4A synthesized from kaolin. *Inorganic Chemistry Communications*, *111*(November 2019), 107639. https://doi.org/10.1016/j.inoche.2019.107639

Wang, W., Cong, J., Deng, J., Weng, X., Lin, Y., Huang, Y., & Peng, T. (2018). Developing effective separation of feldspar and quartz while recycling tailwater by HF pretreatment. *Minerals*, *8*(4), 1–15. https://doi.org/10.3390/min8040149

Wang, Y., Zhou, W., Li, Y., Liang, L., Xie, G., & Peng, Y. (2021). The role of polyvinylpyrrolidone in the selective separation of coal from quartz and kaolinite minerals. *Colloids and Surfaces A: Physicochemical and Engineering Aspects*, *626*(April), 126948. https://doi.org/10.1016/j.colsurfa.2021.126948

Weaver, C. E., & Pollard, L. D. (1973). *Developments in Sedimentology 15- The Chemistry of Clay Minerals*.

Wilson, I., & Hart, F. (2019). *Positive outlook for kaolin in ceramics*. *April*, 28–32.

Wood, N. (2021). An AAS study of Chinese imperial yellow porcelain bodies and their place in the history of Jingdezhen's porcelain development. *Advances in Archaeomaterials*, *2*(1), 49–65. https://doi.org/10.1016/j.aia.2021.09.002

Wu, W., & Tian, L. (2013). Formulation and morphology of kaolin-filled rubber composites. *Applied Clay Science*, *80–81*, 93–97. https://doi.org/10.1016/j.clay.2013.06.025

X-Ray Fluorescence (XRF). (2013). In *Encyclopedia of Biophysics* (pp. 2781–2781). https://doi.org/10.1007/978-3-642-16712-6_101129

Xie, M., Liu, F., Zhao, H., & Ke, C. (2021). Mineral phase transformation in coal gangue by high temperature calcination and high-efficiency separation of alumina and silica minerals. *Journal of Materials Research and Technology*, *14*, 2281–2288. https://doi.org/10.1016/j.jmrt.2021.07.129

Yang, R. T. (2003). Zeolites and Molecular Sieves. *Adsorbents: Fundamentals and Applications*, *1862*, 157–190. https://doi.org/10.1002/047144409x.ch7

Yaoli, P., Chao, N., Guangxi, M., Wei, W., & Guangyuan, X. (2017). Removal of organic carbon in coal-series kaolin using gravity separation. *Energy Sources,*

Part A: Recovery, Utilization and Environmental Effects, *39*(11), 1153–1158. https://doi.org/10.1080/15567036.2017.1307885

Yildirm, I., Smith, M. D., & Pruett, R. J. (2009). *Methods for purifying kaolin clays using reverse flotation, high brightness kaolin products, and uses thereof* (Issue WO2009114404 A2). http://www.google.com/patents/WO2009114404A2

Yin, X., Long, Z., Wang, C., Li, Z., Zhao, M., & Yang, S. (2019). Ultrasonics - Sonochemistry A time- and cost-e ff ective synthesis of CHA zeolite with small size using ultrasonic-assisted method. *Ultrasonics - Sonochemistry*, *58*(December 2018), 104679. https://doi.org/10.1016/j.ultsonch.2019.104679

Yoon, R. H., Nagaraj, D. R., Wang, S. S., & Hildebrand, T. M. (1992). Benefication of kaolin clay by froth flotation using hydroxamate collectors. *Minerals Engineering*, *5*(3–5), 457–467. https://doi.org/10.1016/0892-6875(92)90225-X

Zamani, F., Rezapour, M., & Kianpour, S. (2013). Immobilization of L-Lysine on zeolite 4A as an organic-inorganic composite basic catalyst for synthesis of α,β-unsaturated carbonyl compounds under mild conditions. *Bulletin of the Korean Chemical Society*, *34*(8), 2367–2374. https://doi.org/10.5012/bkcs.2013.34.8.2367

Zegeye, A., Yahaya, S., Fialips, C. I., White, M. L., Gray, N. D., & Manning, D. A. C. (2013). Refinement of industrial kaolin by microbial removal of iron-bearing impurities. *Applied Clay Science*, *86*, 47–53. https://doi.org/10.1016/j.clay.2013.08.041

Zhang, K., Zhang, H., Liu, L., Yang, Y., Liu, L., & Liu, Q. (2021). Dispersibility of kaolinite-rich coal gangue in rubber matrix and the mechanical properties and thermal stability of the composites. *Minerals*, *11*(12). https://doi.org/10.3390/min11121388

Zheng, H., Han, L., Ma, H., Zheng, Y., Zhang, H., Liu, D., & Liang, S. P. (2008). Adsorption characteristics of ammonium ion by zeolite 13X. *Journal of Hazardous Materials*, *158*, 577–584.

Zheng, Y., Li, X., & Dutta, P. K. (2012). Exploitation of unique properties of zeolites in the development of gas sensors. *Sensors*, *12*(4), 5170–5194. https://doi.org/10.3390/s120405170

Zhou, C., Liu, G., Wu, S., & Lam, P. K. S. (2014). The environmental characteristics of usage of coal gangue in bricking-making: A case study at Huainan, China. *Chemosphere*, *95*, 274–280. https://doi.org/10.1016/j.chemosphere.2013.09.004

Zhu, Y., Zhu, Y., Wang, A., Sun, D., Liu, K., Liu, P., & Chu, Y. (2021). Valorization of calcined coal gangue as coarse aggregate in concrete. *Cement*

and Concrete Composites, *121*(December 2020), 104057. https://doi.org/10.1016/j.cemconcomp.2021.104057

Zimmermann, N. E. R., & Haranczyk, M. (2016). History and Utility of Zeolite Framework-Type Discovery from a Data-Science Perspective. *Crystal Growth and Design*, *16*(6), 3043–3048. https://doi.org/10.1021/acs.cgd.6b00272